L , - OF RADIO
WAVES IN THE IONSPHERE
10 JANUARY 1980 BY A. G. SHIONSKIY (FOUO) 1 OF 2

JPRS L/8860

10 January 1980

Translation

Long-Distance Propagation of Radio Waves in the Ionsphere

By

A. G. Shionskiy

FBIS FOREIGN BROADCAST INFORMATION SERVICE

NOTE

JPRS publications contain information primarily from foreign newspapers, periodicals and books, but also from news agency transmissions and broadcasts. Materials from foreign-language sources are translated; those from English-language sources are transcribed or reprinted, with the original phrasing and other characteristics retained.

Headlines, editorial reports, and material enclosed in brackets [] are supplied by JPRS. Processing indicators such as [Text] or [Excerpt] in the first line of each item, or following the last line of a brief, indicate how the original information was processed. Where no processing indicator is given, the information was summarized or extracted.

Unfamiliar names rendered phonetically or transliterated are enclosed in parentheses. Words or names preceded by a question mark and enclosed in parentheses were not clear in the original but have been supplied as appropriate in context. Other unattributed parenthetical notes within the body of an item originate with the source. Times within items are as given by source.

The contents of this publication in no way represent the policies, views or attitudes of the U.S. Government.

For further information on report content call (703) 351-2938 (economic); 3468 (political, sociological, military); 2726 (life sciences); 2725 (physical sciences).

APPROVED FOR RELEASE: 2007/02/08: CIA-RDP82-00850R000200040027-6

JPRS L/8860

10 January 1980

LONG-DISTANCE PROPAGATION OF RADIO WAVES IN THE IONOSPHERE

Moscow DAL'NEYE RASPROSTRANENIYE RADIOVOLN V IONOSFERE in Russian 1979 signed to press 24 Apr 79 pp 1-152

Book by A. G. Shlionskiy, "Nauka" Publishers, 850 copies

CONTENTS

CONTENTS (Continued)

PUBLICATION DATA

English title	:	LONG-DISTANCE PROPAGATION OF RADIO WAVES IN THE IONOSPHERE
Russian title	:	DAL'NEYE RASPROSTRANENIYE RADIOVOLN V IONOSFERE
Author (s)	:	A. G. Shlionskiy
Editor (s)	:	
Publishing House	:	Nauka
Place of Publication	:	Moscow
Date of Publication	:	1979
Signed to press	:	24 Apr 79
Copies	:	850
COPYRIGHT	:	Izdatel'stvo "Nauka", 1979

LONG-DISTANCE PROPAGATION OF RADIO WAVES IN THE IONOSPHERE

Moscow DAL'NEYE RASPROSTRANENIYE RADIOVOLN V IONOSFERE in Russian 1979 signed to press 24 Apr 79 pp 1-152

[Monograph by Aleksandr Grigor'yevich Shlionskiy, Nauka, 850 copies, 152 pages]

[Text] Annotation

Conditions and characteristics of ultra long-range (around-the-world, inverse, antipodal) and long-range propagation of short radio waves in ionospheric channels when the emitter is on the Earth's surface and in the ionosphere.

Results of analysis and interpretation of experimental data and a theoretical consideration of the relationship of characteristics of ionospheric radio waveguides as a function of key-points of the ionosphere are presented.

The book is of interest to radiophysicists, radio engineers, graduate and other students specializing in the field of long-range ionospheric propagation of radio waves.

Table 2, illustrations 66, references: 118 titles.

Foreword

Both experimental and theoretical research of long-range and ultra long-range propagation of decameter radio waves have revealed the important role of waveguide ionosphere modes possessing extremely favorable energy and other characteristics. In a still greater measure, the role of these modes is increased when the emitter is placed in the ionosphere and even more so if the receiver is located in near space. Therefore the results of experimental, theoretical and applied research of conditions of ionospheric waveguide propagation of radio waves in long-range and ultra long-range routes for emitter placement on the Earth's surface and in the ionosphere have not only a scientific but also a tremendous practical significance.

Problems in this field were rather complex, and research begun in the 1920's and especially actively conducted in recent decades are continuing in both the

experimental and theoretical planes. Still, now the need has matured for a certain systematization and generalization of the results obtained. In solving this problem, the author mainly relied on the results of those studies which were carried out with his participation and set the goal of completely capturing various existing theoretical approaches and experimental findings. Some review information in different trends of research have been cited in the introductory portions of each chapter and the corresponding studies are included in the bibliography.

Underlying the book is the extremal-parametric method (EPM) for determining a complex of characteristics of ionospheric radio waves. This method is based on analytic relationships of waveguide characteristics as a function of extremes of altitude variation of the modified index of refraction and of these extremes as a function of extremes of the vertical gradient of eletron concentration. Key ionospheric points (predicted critical frequencies, geometric parameters, etc.) can be used as initial data to determine certain properties of waveguides.

In Chapter 1 are presented the results of experimental research on propagation of ultra long-range signals when an emitter is placed on the Earth's surface. Different properties of ultra long-range signals are considered; observable variations are interpreted, allowing for the effect of azimuth anisotropy of the ionosphere and orientation of ultra long-range routes with respect to the terminator line.

In Chapter II are investigated the results of experimental research of propagation of long-range signals when the emitter is located in the ionosphere. Interpretation was done to allow for the global distribution of electron concentration in the ionosphere of distinctive features affecting optimum conditions and other properties of long-range signals.

In Chapter III are analyzed conditions of radio wave refraction in the ionosphere, initial assumptions of EPM are presented and the bases of its mathematical apparatus, models of altitude profiles of electron concentration and modified dielectric permeance are justified. Materials are adduced on calculating limiting boundaries and channel axes, frequencies of degeneration, etc.

In Chapter IV are considered the refraction properties of capture and escape of radio waves from channels for varied emitter position (on the Earth's surface, in the ionosphere), several integral characteristics (intervals of oscillation of beams in a duct, cluster, phase paths, absorption, etc.), spatial attenuation of radio waves in a channel, etc.

Mathematical and graphical relationships adduced in the book can be used both for analysis of experiments and for prediction of conditions and characteristics of ultra long-range and long-range propagation of decameteter radio waves for ground-based or ionosphere-based emitters.

The authors are deeply grateful to the following persons for reading and criticizing the book: Yu. N. Cherkashin and T. S. Kerblay, as well as V. V.

Kuryatnikovaya and L. I. Shlionskaya for their aid in preparing the manuscript.

Chapter I

Propagation of Ultra Long-Range Radio Signals

In the initial period of use of short radio waves for long-range radio communication in the 1920s, radio signals were detected with large time lags corresponding to the curvature of the Earth (world-wide radio echo) or propagation through a long inverse route 20,000 to 40,000 kilometers in length (inverse radio echo)[1-4]. Long-range radio echos detected in several operating radio lines connecting different continents on the Earth were first considered mainly as interference in radio station reception. But it soon became clear that the emission of echo signals was very interesting. So, in the late 1920s the effect of "inverse echo" began being used for long-range communication through the reverse route between England and Australia.

In addition to world-wide and reverse signals, signals have been recorded from sensors situated near the antipodes of a receiver at a distance of about 20,000 kilometers (antipodal signals), as well as signals with delays ranging from units to tens of seconds, whose origin is most difficult to explain [5-12].

Because many distinctive features of long-range echos could not be explained as skip modes, various hypotheses were then advanced on the possible mechanics of propagation [13, 14] and special experiments were run [15-19].

Because several distinctive features of ultra long-range signals can appear in shorter routes, on the order of 10,000 to 17,000 kilometers, the results obtained can be used to investigate long-range propagation as a whole for ground-based and ionosphere-based emitters.

§1. Around-the-World Radio Echo

When circumterrestrial radio signals (KS) are received the largest amount of experimental data is obtained at medium-latitude points (Western Europe, North America, eastern and European parts of USSR). KS reception was also done in the Arctic, near-equatorial region and in Antarctica.

From 1926 through 1934, world-wide signals were recorded in Berlin from a number of North American, South American and Asiatic commercial radio broadcasters [1-3]. From 1927 through 1929, the USA recorded world-wide signals from European radio broadcasters [4].

From 1941-1944, in Denmark world-wide radio signals were received from broadcasters situated on all continents of the globe [15-18]. In the post-war period, special experiments have been conducted using powerful transmitters and highly directional transmitting and receiving antennas. In the winter of 1958-1959, KS observations were made in Sweden on a transauroral radio line running

between the geographic and geomagnetic poles [20]. From 1960 to 1970, intensive KS research was done in the USA [21-23].

World-wide radio signals were detected in the USSR in the 1950s in reception of signals of backward sloping probing (VNZ)[24].

Since 1967, KS research has been conducted in Antarctica at the Molodezhnaya Soviet station with reception of the Moscow transmitter in the transauroral quasi-meridional direction [25, 26]. In 1970 to 1971, KS observations were made in the eastern part of the USSR [27-32]. Some KS observation results have been obtained in Cuba [31]. In 1974-1975, KS reception was also done in the middle latitudes of the USSR [29, 30, 38].

The experiments which have been conducted permit us to judge the variations in diverse KS characteristics: time of curvature of the globe, attenuation, pulse distortion, optimum periods of reception and directions, etc.

When KS is received in middle latitudes of eastern USSR, the transmitting and receiving points were almost superposed (distance between them was about 0.05 percent of the world-wide path). The azimuth of the maximum of the narrow directionality of the receiving antenna system rotated in a 360° sector. Emission of signals was done into non-directional antennas of type VGDSh-2U and directional antennas of type RGD 65/4 I. Azimuthal characteristics of KS, seasonal and diurnal and frequency variations were investigated.

Estimates of probability (in percentages) were derived for passage of KS as a function of time of day (LT) and season, characterized by the amount of cases of KS reception in a period of observation (Fig. 1.1).

Working frequencies and KS reception time intervals are indicated in Fig. 1.2 by straight lines and in the 360° sector by little circles. The data adduced correspond mainly to emission into a non-directional antenna of type VGDSh-2U. KS have well expressed seasonal and diurnal variations. In the winter, KS reception was only during the day, from 9:00 a.m. to 7:00 p.m. local time (LT) and in the summer, only at night from 8:00 p.m. to 4:00 a.m. The best KS reception conditions occurred in the winter (2:00 p.m. to 4:00 p.m. with almost 100 percent probability). In summer, probability of reception reached 80 percent (11:00 p.m. to midnight, LT). The worst KS reception was during the equinox. So, KS in April and September, 1971 were not recorded. In October, 1971, KS reception was noted only in directional emission.

Furthermore, diurnal variation of KS in October is similar to winter.

Some seasonal and diurnal asymmetry of KS reception probability has been noted. So, KS reception in winter is better than in summar, and in the second half of the day it is better than in the first. We should indicate the possible connection of this KS asymmetry in KS with the seasonal and diurnal asymmetry of ionization of the F-region of the ionosphere. In most cases, world-wide radio routes were reversibly independent of azimuth, time of day and season and frequency [32].

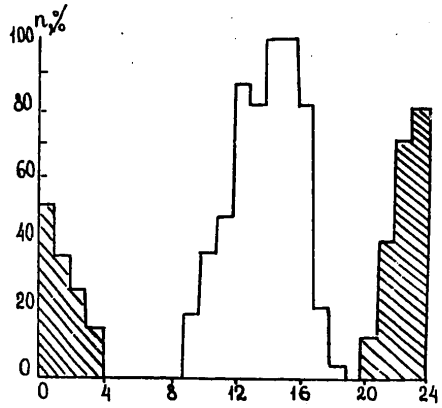

Fig. 1.1.

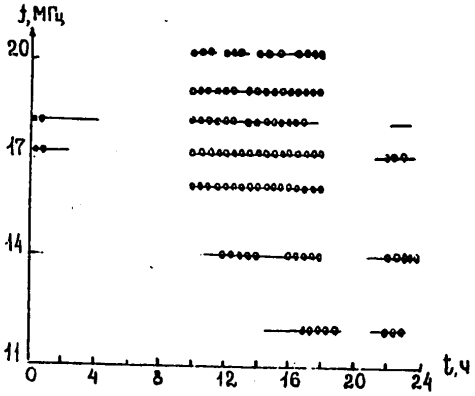

Fig. 1.2.

Figure 1.3. shows the measured bearings of optimum directions of KS reception for winter, summer and equinox (points, triangles and circles, respectively). The calculated diurnal variation of bearings A are also plotted; they form minimum angles with the terminator and values of these angles α_{min} for the same seasons (winter—solid lines; summer—dashes; equinox-dots and dashes). Variation of α_{min} is shown by smooth curves with noon peak. Other curves show variation of A. Straight lines indicate bearings 40 and 140° (their inverses 220 and 320°), corresponding to boundaries of the sector of non-polar routes.

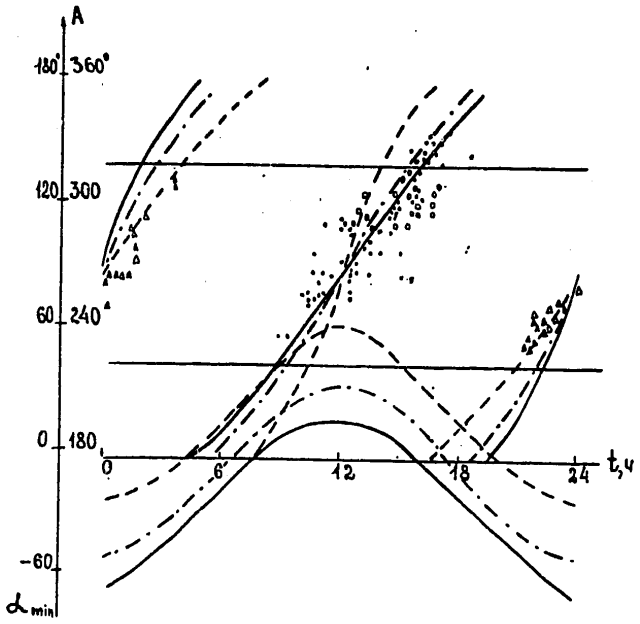

Figure 1.3

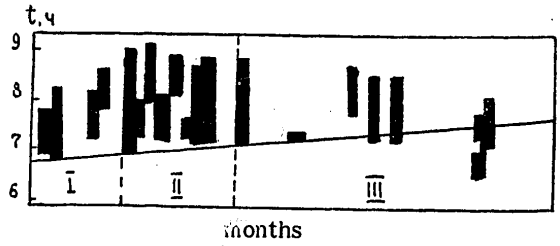

Figure 1.4

In all seasons, measured optimum bearings are close to calculated A. Best KS reception was in both summer and winter at α min = 10-20°. KS were not observed in periods where α min reached 50-65°.

KS reception bearings deviated from calculated A usually in the direction of polar routes. Only in rare cases did optimum bearings of KS reception drop behind the auroral zones.

Improved KS receiving conditions usually involve broadening of a signal arrival sector and range of working frequencies.

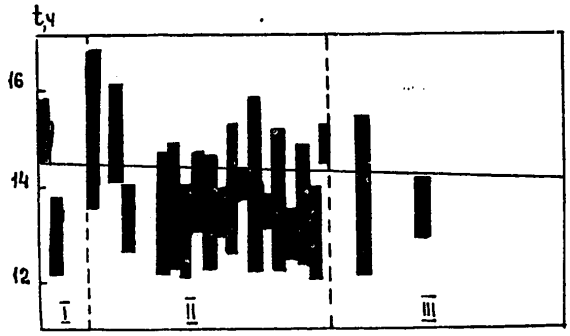

Figure 1.5

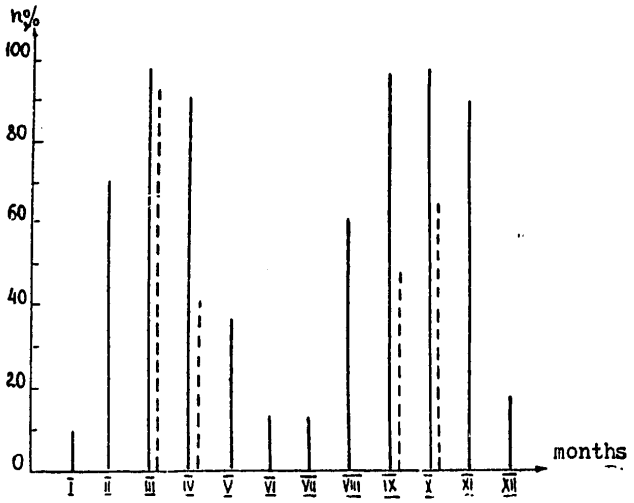

Figure 1.6

The probability of KS reception greated increased in direct proportion to emitted signal power, e.g. when highly directional transmitting antennas were used or if the sensitivity of the receiving equipment was increased. However the nature of the seasonal-diurnal and other patterns does not depend on technical parameters.

In December 74-March 75, in middle latitudes of European Russia, KS observations were made in two fixed directions with transmitter and receiver positions at one point. Emission and reception were done using highly directional transmitting and receiving antennas. The power of the standard transmitter was about 100 kW [28]. Observation results are shown in Figures 1.4 and 1.5. Figure 1.4 corresponds to bearing 22°, Figure 1.5—to bearing 309°. Along the vertical

line is shown local time (LT) at the observation point. Blackened area is time intervals when KS were received in different months and days. In direction with bearing 22°, KS at a frequency of 11 MHz were received mainly in the morning at 6:30 a.m. to 9:00 a.m.; with bearing of 309° at a frequency of 19 MHz--in the latter half of the day at 12 noon to 5:00 p.m. Straight lines in Figures 1.4 and 1.5 indicate approximate theoretical variation of moments of coincidence of fixed direction with bearing A (α min) from winter solstice to equinox. Reception of KS was mainly noted in periods + 1-2 hours from moment of coincidence of the route bearing with theoretical bearing A (with slight asymmetry). In this context, α min usually was more than 10°, reaching 19° at equinox at bearing 22° and 35° at bearing 309°.

Thus despite the great discrepancy in longitude from other middle latitude points, the main quantitative characteristics of optimum KS reception were preserved. From Figure 1.4 and 1.5 it can be seen that daily variations in KS in both directions are significant. In routes with bearing 309°, the probability and duration of time intervals of KS reception are much greater than in a route with bearing 22°. For a whole series of days, KS reception in route 309° was present and in route 22° was absent. Differences can be explained by the fact that in a route with bearing 309°, because of great values of the coefficient of antenna gain, the output of sounding pulses was several times greater than in the route with bearing 22°. Furthermore, integral attenuation in the route with bearing 309° not intersecting the auroral regions and with emission at higher frequencies of 19 MHz were apparently lower.

In experiment [29], study and reception of signals were done at a middle latitude point in the transauroral direction with a bearing of 30 and 210° during a two-year period from August 1972 through September 1974 under conditions of gradual (non-monotonous) subsidence of solar activity (Zurich numbers W of sunspots changed from 80 to 20). Probability of KS reception (expressed in percents of ratio of the number of days of KS reception to the total number of days of observation in a given month) changed from 34 to 100 percent. In periods close to solstices, KS were received almost daily. Probability of KS reception on a winter day was about 83 percent, on a summer night about 70 percent. When W is greater than 50, KS were received two times with attentuation averaging 10-13 dB in seven cases.

KS were received at frequencies of 12-21 MHz, mainly above the muf skip modes. Experiments showed that with reduced W, KS can pass through the transauroral world-wide route with high probability.

In experiment [30], measurements were made of the angular characteristics of KS. The transmitter was located in Irkutsk and KS reception was done 100 kilometers from there using a broad-band phase direction finder. Pulses in the 18-20 MHz range were studied with pulse width of 1-20 ms and pulse repetition rate of 5 MHz. In December, emission was done through a VGDSh antenna with maximum in the N-S direction; on other days--using a rhombic antenna with bearing 302°. Measured bearings of KS arrival were within 117.5-127.5°, and angles of KS arrival in the vertical plane were 4-10°. Errors in measurement

of bearing and angle of KS arrival were no more than 0.5 and 2.5°, respectively.

In the near-equatorial region, observations were made in Guam (13°30 N. Lat., 145° E. Long.) with placement of transmitter on Okinawa, 2,250 to the NW of Guam on 14-23 February, 1963 [22].

Studies were carried out on near and world-wide inverse routes 37,750 kilometers long. Bearing of the inverse route from Guam was 132°. Power of the transmitter was about 0.7 kW, with emission through a rhombic antenna. Broadcasts were in the 14.5-21.8 MHz range. Greatest duration of reception and field strength were at a frequency of 18 MHz. Optimum conditions for reception (100 percent of days) were in the 10 a.m. to 4 p.m. period LT, wherein about 1 p.m., field strength was at a maximum. Theoretical moment of coincidence of route bearing with the direction forming the minimum angle α min with the terminator corresponds to 1-2 p.m. LT at α greater than 42°. KS reception at significant angles of the route with the terminator indicates the existence in the equatorial region of factors which improve their characteristics. In 1973 (June-October), in the Cuba-USSR route, KS were observed using the VNZ method. Transmitter power in the pulsed mode was about 80 kW, rhombic antenna, width of radio pulses 1 ms with repetition rate of 12.5 and 6.25 Hz. Sounding from Havana was done in a direction with bearing 39° at a frequency of 16.2; 14.9; 12.2; and 10.7 MHz from 5:30 p.m. to 11:30 p.m. Havana time (60° West Longitude)[31].

KS reception occurred only in June and early July at frequencies of 16.2; 14.9; and 12.2 MHz. Most favorable for reception was the evening period in the summer, which corresponds to convergence of routes with the twilight zone. Appearance of KS at these frequencies and those periods when there is a large number of signals from back scattering, indicates the possible role of scattering in ionospheric irregularities as a factor of channel capture of KS.

In Antarctica, at the Molodezhnaya station, KS received from the Moscow transmitter have been observed since 1967. The length of the direct quasi-meridional route was 13,700 kilometers. A 20 kW transmitter operating in a pulsed mode was used with a rhombic antenna aimed at the Molodezhnaya station. Emission was done every three hours at 10 working frequencies in the 4.5-23 MHz range. At the Molodezhnaya station, reception was accomplished using an omnidirectional antenna. At each frequency were measured field strength and relative delay time of pulsed signals received.
KS were mainly observed in periods near the equinox. Seasonal variation of the ratio of the number of days when KS were observed to the entire number of days of reception in a given month (in percents) is shown in Fig. 1.6 by dashes. In periods near the equinox (March, April, September, October), KS were received almost daily only in the evening from 6 p.m. to 7:30 p.m., within $\pm$ 20 days from the moment of equinox. Two-time direct echoes were observed only in March at evening twilight. Therefore, KS appeared in periods when the route passed through the evening (twilight) and morning (post-sunrise) zones, i.e., when it forms the smallest angle with the terminator. Direct KS pass better when the direct route is found in the evening, twilight zone. KS were observed at frequencies of 11-23 MHz. Optimum frequencies correspond to the least

attenuation and lie in the range of 16-21 MHz. The upper limit of frequencies can be much higher than the standard maximum usable frequencies (muf) of the route.

KS observations in the transauroral direction were made from December, 1957 through February, 1958 at the high latitude Swedish point of Kirun (67.8° NLat, 20.4° ELong). A 4kW transmitter was located in Coolidge, Alaska (64.8° NLat, 147.8° WLong). Emission was done through a three-element Yagi antenna. The length of the direct route was 5,200 kilometers. Reception bearing was 312° [20]. Of the three working frequencies used, 12.18 and 21 MHz, KS reception only occurred at 18 MHz. KS were received in a period 1-1.5 hours after coincidence of the route with a bearing near the terminator, these moments being extremely close to the moments of maximum probability of KS reception (see Fig. 1.7).

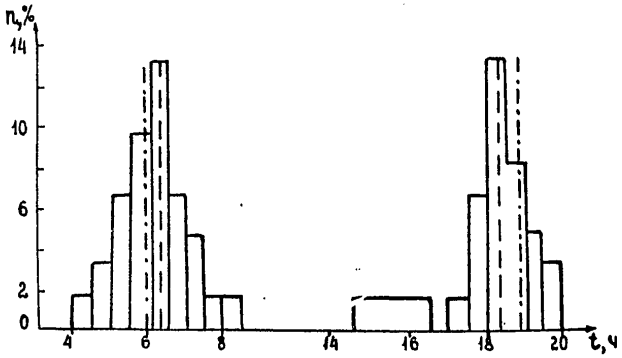

Figure 1.7

Experiments showed that rounding-the-globe time τ is extremely stable. The difference in various experiments is within 5 percent. According to [2], τ = 136.05 to 137.60 ms. Averaged value of τ = 137.788 ms corresponds to the active path which is 1,300 kilometers larger than the Earth's circumference, or average altitude of the world-wide path equal to about 200 kilometers. Slight greater values of τ were obtained in [25]: 0.1367 to 0.1393 sec, with 0.1382 sec most probable. In practice, the spread of values of τ lies within measurement error which does not exceed $\pm$ 1 ms. Variations of τ as a function of time of day, season and solar activity are not revealed. Frequency variations of τ are also small. A negligible increase in τ is noted in direct proportion to frequency (by 1-2 ms in the entire frequency range), and it is difficult to exclude the possible effect of various equipment factors and measurement errors.

With world-wide propagation of pulses, high stability of their shape is observed in many cases regardless of the time of day, season and frequency when transmitting and receiving points are separated by various distances. No substantial distortions were noted in repeated KS. Distortions of KS shape were often less than in direct signals running much shorter paths. In addition, cases of substantial change in KS shape were observed, in all likelihood due to the presence of multipath emission [23]. KS primarily propagate in the plane of the

great circle. Deviations from it in 90 percent of the cases do not exceed + 30 [21]. Individual measurements of the angles of KS arrival in the vertical plane yielded values of 15-25° to the horizon in some cases. For the existing corpus of observations, the range of frequencies fo KS is constrained below about 10 MHz and above about 40 MHz, whereas 15-22 MHz was often optimum. KS reception is noted in many cases at frequencies much high than muf and with substantially less attenuation per unit path length than in direct signals.

Reception of KS usually improves somewhat when solar activity is increased.

In all experiments, attraction of favorable routes toward the twilight zone was noted. Analysis of KS observations in middle latitude points of various longitudes, at high latitude points and in transpolar routes and the near-equatorial region yields close quantitative characteristics of optimalness associated with the relative juxtaposition of the route and the terminator.
Bearing anisotropy of KS routes occurs. Optimum directions usually form a 10-20° angle with the terminator. Some deterioration is noted in KS reception conditions in transauroral directions and during magnetic ionospheric disturbance. In [27], for reception in middle latitude points was fixed the deviation of optimum bearing of KS reception from the direction which forms a minimum angle with the terminator toward a direction which does not intersect the auroral regions.

In experiment [20] in the transpolar route, KS were received with low magnetic activity. During disturbances with KS reception in middle latitude points in routes of varying orientation, a decrease was noted in the probability of KS reception, duration of reception during the day, signal levels and range of working frequencies (reduction of upper limit and rise of lower limit of frequencies) with a rise in the planetary index of magnetic activity $\leq$Kp. At very high values of the index, KS completely vanished for several days. Deterioration of KS reception with a rise in magnetic activity shows up more clearly in the twilight zone, because it passes near the geomagnetic poles [21]. Conclusions derived from analysis of experimental data permit us to recommend the use of quantitative characteristics of relative juxtaposition of the route and terminator (see Chapter 1 §6.4)
as empirical prognosis of optimum conditions of KS reception. It is necessary, however, to bear in mind that even with optimum conditions there can be no KS reception if field strength level—which depends on emitted power, working frequency and integral attentuation in the route—is below threshold.

KS reception will not occur (regardless of emitted power) if the working frequency exceeds the limiting frequency of reflection of radio waves on the ionosphere (frequency of degeneration of the ionospheric channel). In this connection, substantial differences in KS characteristics can occur under optimum conditions (signal level, frequency range) in different seasons, time of day, solar activity, during ionospheric magnetic disturbances, etc.

§2. Inverse Radio Echo

Propagation of radio waves through a large arc of the great circle (R > 20,000 kilometers) was recorded in the 1920s during the initial period of assimilation of the SW range. A large number of inverse signals (OS) were recorded, for example, during reception in 1927-1934 (during half-cycle of solar activity W) in Berlin from a number of North American (New York, Mexico), South American (Venezuela, Rio de Janeiro, Buenos Aires, Santiago) and Far Eastern (Shanghai, Bangkok, Java, Nagoya, Mukden, Manila) transmitters.

IS passed primarily in directions firming minimum angles with the terminator, in some cases at working frequencies above the muf of the inverse route with attenuation lower than in the direct route [1-3].

Use of the "inverse echo" effect to raise reliability of communication, i.e. for practical purposes, was begun back in the late 1920s in the commercial rote connecting England and Australia: Grimsby (55°33' NLat, 0°05' WLong) to Melbourne (37°40' SLat, 145°08' WLong). Length of the direct route was 16,850 kilometers and the inverse route was 23,150 kilometers. The short route passed through Europe, India, Indochina; the long one—through the Atlantic Ocean, South America and the Pacific Ocean. Receiving and transmitting stations at both points are identical. The antennas had high directionality in the horizontal plane and could be reversed. Change of emitting direction was done in Melbourne 1.5 hours after sunrise to the inverse route and about 3 hours after sunset to the direct route. In the short path, audibility at Grimsby improved as the terminator moved away from Melbourne towards Grimsby and reached its highest values when the path was in total darkness. After sunrise in Melbourne, audibility in the direct route began to drop sharply and after a short interval of time vanished completely. In the long path, the maximum audibility in Grimsby corresponded to total illumination of the direct route. Therefore, the darkened part of the Earth was best. Fixed working frequencies about 11.6 MHz were used. Audibility in the direct and inverse routes was comparable in the corresponding periods. Because of reverse, assured communication was provided about 70 percent of the day [33].

From 1941 to 1944, OS (and KS) observations were intensively carried out for reception of the world network of transmitters in Denmark in the frequency range from 10 to 20 MHz [15-17]. From 14 to 23 February, 1963 in the inverse (almost world-wide) Okinawa-Guam route, a special experiment was run [22]. The Okinawa transmitter, which emitted in the direction of the inverse route 37,750 kilometers in length, was picked up in Guam and simultaneously at intermediate points in Salonica and Malta. Reception of signals at the end point observed at specific periods (when absent from the intermediate points on the route nearer to the emitter) was interpreted as direct experimental proof of propagation without intermediate reflections from the Earth under conditions of assured input and output of energy from the ionospheric channel with ground-based emitter and receiver because of the horizontal inclindes of the ionosphere.

In 1967, OS observations from the Moscow transmitter were begun at the Molodezhnaya station [25, 26]. The large circle was oriented almost along the helographic meridian and intersects, thereby, the polar regions. The length of the direct route was 13,700 kilometers and the inverse route was 26,300

kilometers. Reception was achieved in the 4.5-23 MHz range at 10 working frequencies.

The seasonal variation of OS obtained in 1967 is shown in Figure 1.6 by solid lines. In contrast to non-meridional routes, the most favorable season for OS was during the day of equinox from 6:00 a.m. to 5:30 p.m. LT. During this period (March, April, September, October), OS were picked up almost daily. Probability of OS detection sharply dropped during solstices ($\lesssim$ 10-15 percent).

Optimum conditions of OS reception were when: a) the inverse route coincided with the evening (twilight) and morning (post-sunrise) zones. In some cases reception even of two-fold OS; b) the sun was located at the middle point of the direct route. The bulk of inverse route passed in the darkened region and its end points were identically removed from the boundaries of the darkened region. In the first half of the day, including noon, OS were observed in the 10-23 MHz range, after noon and in the evening twilight--primarily at frequencies of 11-15 MHz. Frequency relationships of OS attenuation were much less expressed than in ordinary direct signals. In practice, the amplitude of OS was almost unchanged with frequency and time and day. Despite the doubly long length of the inverse route (intersecting the northern and southern polar regions), and the emission one order lower in the inverse direction, during daylight hours of equinox only OS passed at 10-16 MHz and there were no direct signals, apparently because of high attenuation. At 18-20 MHz, amplitudes of the basic signals and OS at that time were identical. At higher frequencies, amplitude of the basic signal was much higher and OS had decreased somewhat. OS passed at frequencies above muf of skip modes of the inverse route by 5-8 MHz. So, at midnight during the entire year, muf in the direct route even on specific days did not exceed 18 MHz. However at noon in periods near the equinox, OS were often passed through the midnight zone at frequencies up to 23 MHz.

The cited OS characteristics indicate the high probability of the non-skip mechanism.

In 1969-1970, observations were made in Leningrad of inverse echo-signals from ham radio transmitters situated on various continents of the globe, at various distances and in various directions [34, 35]. OS reception was done at frequencies of 7-7.1, 14-14.35, 21-21.45, 28-29.5 MHz. Experimental values of bearings of OS arrival for September, January, May and July were derived as a function of time of day and working frequency. Medians of experimental bearings were compared with theoretical azimuths of directions forming a minimum angle with the terminator. As a result, good correspondence between them was attained. At the same time, there was some relationship between the difference in said azimuths and the working frequency. As the latter increased, at frequencies of 21-29.5 MHz was recorded a slight delay of the experimental azimuth from the theoretical. For example, in January and July it deviated by 5-10°. For the lower frequencies, 7-14.35 MHz, both azimuths vanished completely. OS reception occurred when the theoretical azimuth was closest to the terminator. So, in January, OS were picked up only during the day, while in July it was primarily at night. However during the equinox, in the hours of sunrise and sunset, the difference in azimuths was even noticeable at low

frequencies 7 to 14.35 MHz (up to 45 and 20°, respectively). The direction of OS arrival deviates toward the non-polar routes from the theoretical azimuth which intersects the auroral zones. In May, there is a shift from the day conditions of OS reception to nighttime conditions. The width of the OS reception sector contains two peaks: morning and evening. The peak for low frequencies slightly outstrips the peak for high frequencies, similar to measured azimuths.

In September, at about 12:00 noon LT at a frequency of 7 to 14.35 MHz there is a deep valley in sector width which is apparently due to the significant influence of ionospheric absorption. In September at high frequencies in the evening, the width of the sector is slightly greater than at low frequencies. In January, on the other hand, sector width is greater at the low frequencies. Sector width of OS is maximum in twilight periods for low frequencies. In equinox, sector width at high frequencies is greater than at low frequencies and vice versa during solstice days. Some possible deviation in direct proportion to a rise in working frequencies of the optimum OS azimuth from the direction intersecting the terminator at a minimum angle is associated with the need to assure reflection of radio waves on the ionosphere.

In 1971-1972 (from October 14 through February 29), OS observations were made aboard the Borovichi scientific-research ship in the water landing area of the Atlantic Ocean [36]. Reception of signals from the 20 kW Moscow transmitter was done virtually around the clock. Pulses of 300 mcs in width and frequency of 12.5 Hz were emitted to an antenna isotropic in the azimuthal plane at 10 fixed frequencies in the 5-23 MHz range. In the period from 9:20-10:30 am and 12:20-1:30 p.m. LT, in almost 60 sessions, OS were received mainly at high frequencies of 16-23 MHz. Duration of OS was close to that of the emitted pulse. Probability of receptionof OS grew in direct proportion to the length of the direct route. OS intensity in some sessions was the same as in direct signals or even 1-3 dB higher. There were cases where at frequencies 20-23 MHz only OS were received, although the direct signal passed at the lower frequencies. OS had low dispersion, possibly due to the low-mode structure and smaller contribution of the scattered component. Optimum OS routes passed near the twilight zone. In addition to the direct signals, OS were recorded at frequencies near the muf of the inverse route. In the near-noon period LT, when the inverse route was removed from the twilight zone and was more uniform and working frequencies were much higher than muf, OS reception deteriorated. In a direction perpendicular to the twilight zone, only weak isolated pulses were received which were difficult to identify.

Results of experiments on OS reception indicate attraction of optimum inverse routes toward the twilight zone. Many characteristics of OS indicate the important role of non-skip modes in their propagation.

§3. Attenuation of Circumterrestrial and Inverse Echo Signals

Based on current measurements of world-wide and inverse echo signal levels, we can assess their attenuation. Results of KS and OS measurements made at the Molodezhnaya station in reception of the Moscow transmitter in a meridional direction during years of high and average solar activity were used for that

purpose; OC received in middle latitudes of the northern hemisphere in routes of different orientation, during a period near the minimum of solar activity, were employed likewise [37].

Results of the first experiment are given in Figures 1.8, 1.9; the second experiment results are shown in Fig. 1.10.

In Figure 1.8 are presented the amplitude-frequency characteristics of OS and KS for one of the most probable periods of detection (equinox, March 1967) in various intervals of local time. The solid curves are monthly medians of measured field strength of E signals in decibels with respect to 1 microvolt per meter. Vertical fragments characterize the spread of field strength values on various days, if the reliability of OS detection at a given frequency is at least 30 percent.
Individual cases of detection are indicated by dots. The frequency with the greatest reliability of detection at a given time of day is noted by the figure which indicates the percentage of detection. In cases where reliability of detection is less than or equal to 50 percent, the monthly median was determined in terms of the smallest measured value. The dotted curves correspond to the theoretical field strength E for skip modes of radio wave propagation allowing for additional absorption in polar regions. The length of the inverse route was 26,300 kilometers. The length of the KS path in the direct direction was 53,700 kilometers. Calculation of E for KS yields about -100 dB. The measured KS attenuation with respect to the level of the unabsorbed field E_H comprises 20-30 dB. The measured OS attenuation averaged about 20 dB with respect to E_H or 30-50 dB less than the value predicted for the skip mode 9F 2 (dotted line). OS and KS passed at frequencies of 12-23 MHz (with a measurement frequency ragne of 4.5 to 23 MHz). Maximally observable frequency of OS and KS is almost double the theoretical muf. The relationship of OS AND KS amplitude as a function of working frequency is weak. It has a flat peak in intermediate optimum frequencies. Variations in OS amplitude with time of day are also negligible.

In Figure 1.9 are shown the limits of amplitude measurements for OS and KS in various equinox months (March and September) of 1967-1972 with a change in solar activity W = 110-60 at fixed frequencies: OS—12.8 MHz (at noon and transitional hours LT), KS--18.2 MHz (evening hours). The horizontal dashes are the monthly medians of field strength.

The best conditions for OS and KS propagation relate to 1967, a period of increased W. OS were regularly observed for six years, and periods of reception showed no pronounced changes in amplitude, although reliability of detection was changed.

After 1967, conditions of KS propagation deteriorated and only in 1972 did they improve again. Measured KS attenuation for the distance D = 53,700 kilometers with respect to E_H at working frequencies f_w = 18-21 MHz comprised 20-30 dB in 1967 and 30-35 dB in 1972. (see Figure 1.8). In other years (1968-1971), integral attenuation of KS exceeded 40 dB (with this attenuation, the KS level is below the threshold of equipment sensitivity).

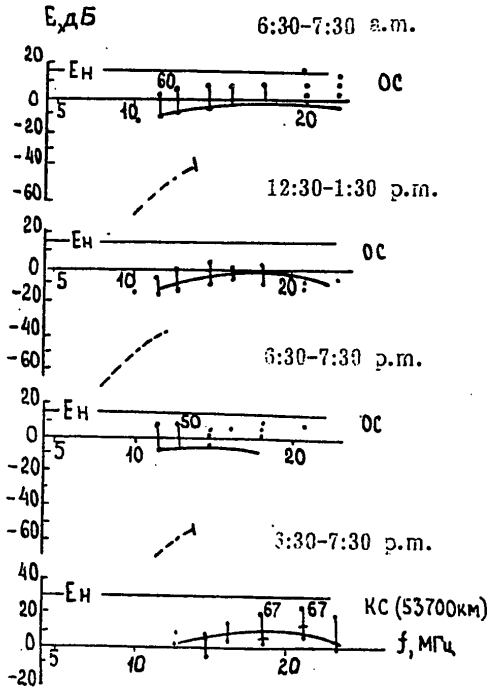

Figure 1.8

Reiterated KS were recorded in March, 1967 from 7:10-7:40 p.m. LT at f_w = 18-23 MHz with a reliability of detection of 35 percent. Their attenuation with respect to the first KS was 8-20 dB.

According to published data, attenuation sometimes did not exceed 5-10 dB [18]. When the emitter is situated on an artificial earth satellite, KS attenuation changed with respect to attenuation of the direct signal at a frequency of 34.3 MHz within 3-18 dB.

In Figure 1.10 are cited the results of OS observations in a period of low level in routes having different orientation: north-east (N-E), south-east (S-E), west (W) and south-west (S-W) extending 25,000-38,000 kilometers. Observations were made at frequencies of 6.5 to 22 MHz. The most complete measurements in various seasons were obtained at frequencies of 12.5 to 17 MHz, for which Figure 1.10 is plotted. At other frequencies of the selected range, OS were only detected in a small number of cases in individual months. Routes with the greatest volume of field strength measurements were selected for analysis (average of 200-250 measurements per month). Averaging was done for the month period within the sector of azimuthal angles no greater than 10° and 1000 kilometers in distance. In the observations made, OS were recorded only under optimum conditions of propagation along the evening (twilight) and morning (post-sunrise) bands.

Figure 1.10 shows the seasonal variations of OS attenuation with respect to E_H for routes of different orientation and extension. For most directions, seasonal variations of attenuation were small. Only for the north-east direction in some months was attenuation noticeably higher than average. The relationship of attenuation as a function of route orientation was also extremely weak. The frequency dependence of attenuation is also very weak. When working frequency was changed, maximum attenuation drop did not exceed 6 dB.

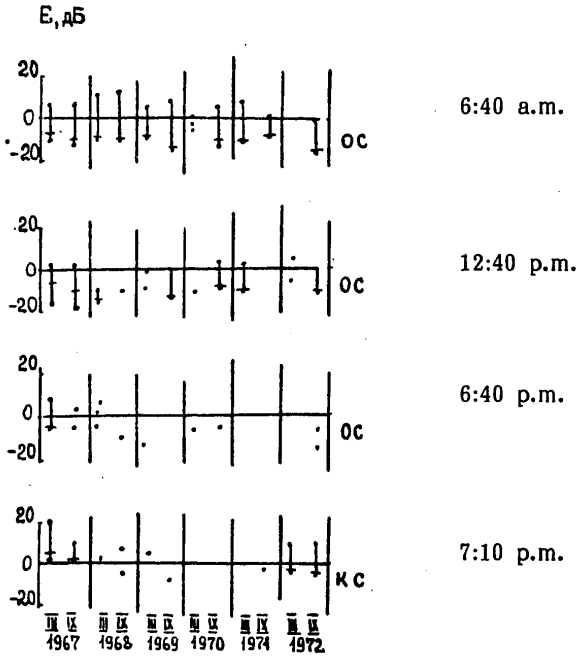

Figure 1.9

Some rise in OS attenuation with a decrease in level W may be caused, in particular, by the passage of radio waves of the lower frequencies. According to [3], at middle latitudes during a high level of W there occurred OS reception under both optimum conditions and with great deviations in the route from the terminator and even normally to it. At low values of W, OS were received only under optimum conditions. Propagations of ultra long-range signals at frequencies exceeding standard muf, reduced attenuation with weakly expressed frequency dependence, small variations and weak depend on route orientation indicate the important role of non-skip modes.

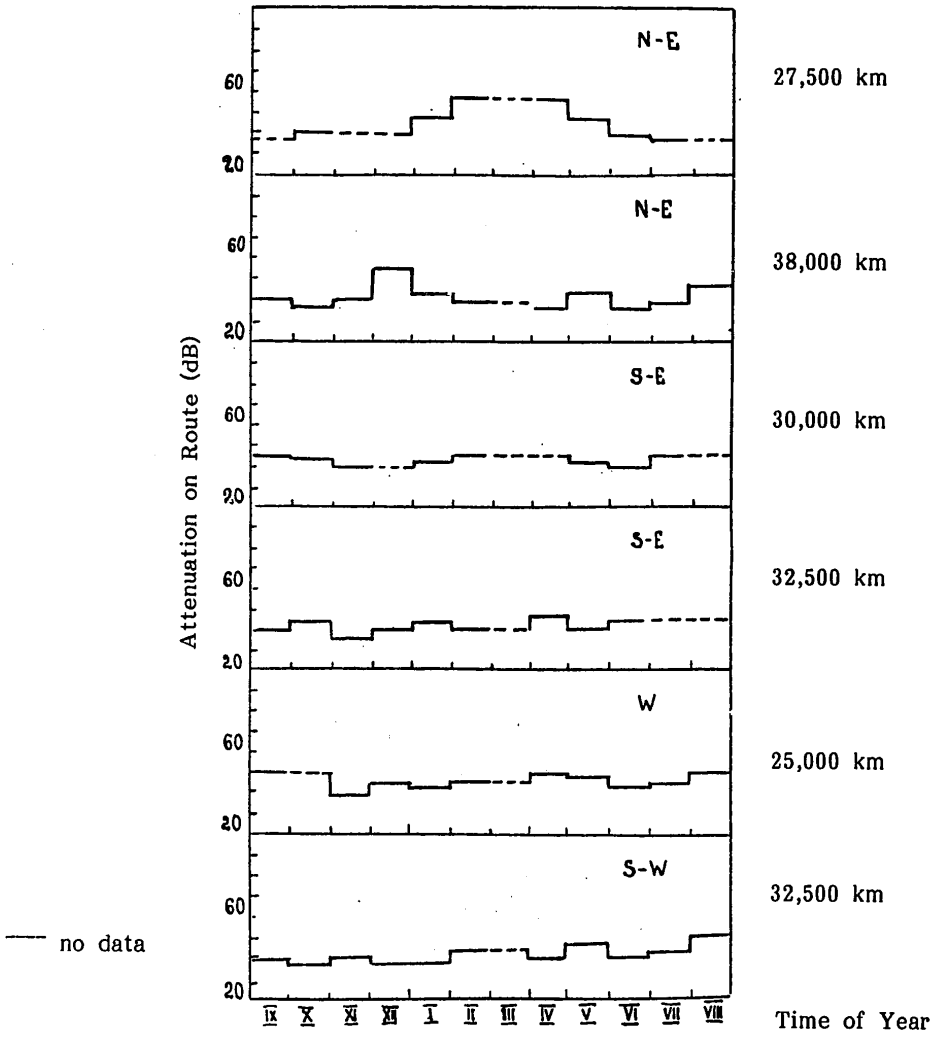

Figure 1.10

§4. Effect of Azimuthal Anisotropy of Ionosphere on Propagation of Ultra Long-Range Signals

Variations observed in optimum directions and periods of reception of ultra long-range signals are a consequence of the space-time changes in the ionosphere and its azimuthal anistropy. Variations in the structure of the ionosphere alter the configuration and parameters of ionospheric waveguides and thereby the conditions and characteristics of radio wave propagation.

However various aspects of this interrelationship and the relative role of various parameters of the ionosphere in the formation of azimuthal-time characteristics of signals have been insufficiently investigated. This kind of analysis is necessary to reveal the relative role of various factors of radio wave propagation (conditions of refraction, absorption, etc. in different sections of routes) and the physical interpretation of the observable interrelationship of optimum conditions with the terminator.

Underlying one of the possible variants of analysis used in this study is the comparison of several characteristic ionospheric parameters for optimum and unfavorable conditions of reception of ultra long-range signals [38, 39]. A waveguide mechanism of propagation is possible in a significant portion of the ultra long-range route. It is natural to consider that an important role should be placed by ionospheric conditions in both the waveguide, i.e., mainly in the F-region and in sections of the possible capture-release where beams intersect the absorbing D/E-region and refract in the F-region.

Typical ionospheric parameters must be selected to allow for relationships appearing in the extremally-parametric method of channel characteristics versus ionosphere parameters.

The channel closest to degeneration in a section where f_{max} is the upper limit of frequencies of radio wave reflection has a minimum value (and also the transverse cross section and volume). This section is most critical for refraction of beams in the ultra long-range route

$$f_{max} = f_0F2 \sqrt{\varphi(r_0) + \frac{r_0}{2} \frac{d\varphi(r_0)}{dr}} .$$

Because the quantities f_{max} and f_0F2 are directly related and change of the second multiplier is much less than f_0F2, we can roughly consider that $(f_0F2)min$ corresponds to $(f_{max})min$. Let us take $(f_0F2)min$ in the route as one typical ionospheric parameter. Necessary angles of rotation of refracting beams for capture-release by the channel are functionally associated with f_0F2 in the appropriate sections. The channel can be either completely world-wide or partially world-wide. In the first case, capture and release must be realized in a region of end points with a radius of 1,500-2,000 kilometers. Integral absorption in the route and in capture-release sections when intersecting the D/E regions can be characterized respectively by the parameters $(f_0E)cp$ (assuming skip modes) and f_0E [51].

Let us take (fE)cp as a typical parameter of ultra long-range routes. It is assumed that this choice is justified for channels passing in the lower part of the F-region and F/E-valley, i.e., closer to the altitude of the maxmum layer E ($h_{max}E$), than to $h_{max}F2$. According to observations, optimum world-wide routes primarily corresponded to the smallest change along the route of zenith angles of the sun, which should be tantamount to a minimum value of $(f_0E)cp$. Absorption in channels having an upper boundary along $h_{max}F2$ we can roughly characterize by the second parameter f_0F2cp. All selected typical ionospheric

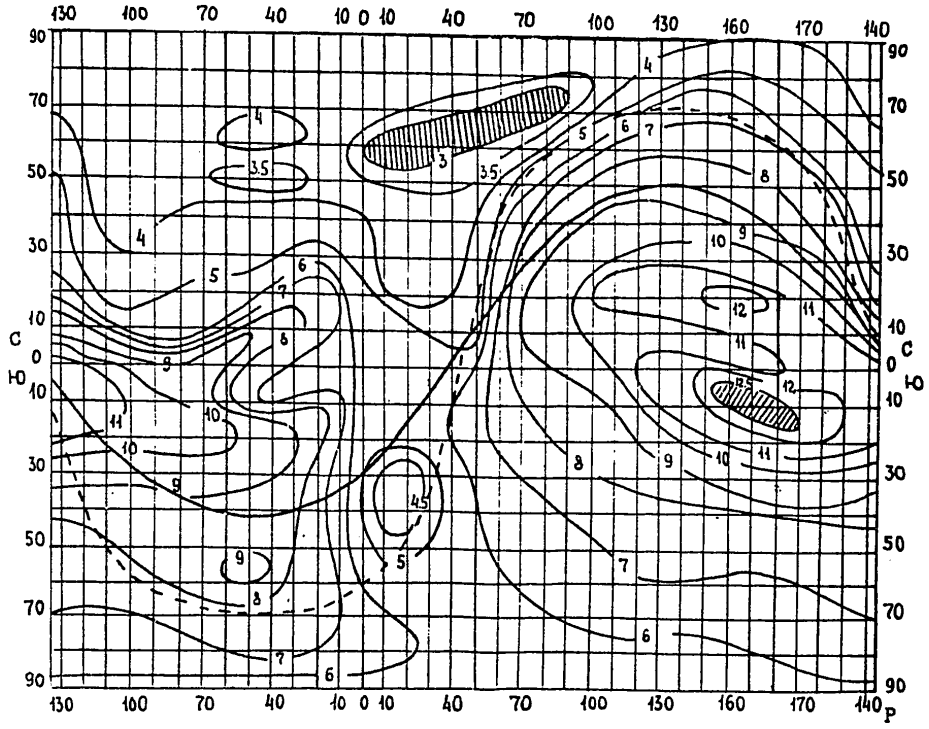

Figure 1.11

parameters can be rather easily determined using global ionospheric maps, which can, for example, be found in weather forecasting publication. In view of the appearance of the geomagnetic longitudinal effect in the F2 layer, global distributions f_0F2 and f_0E differ substantially at the same physical instants of time. Especially typical are differences in the position of the extremes of distribution of f_0E and f_0F2. For the regular E-layer $(f_0E)max$ is located in the subsolar point, while $(f_0E)min$ is at its nadir. Both extremes are geographical antipodes with respect to one another.

In the F2-layer, the region $(f_0F2)max$ located in the near-equatorial region is displaced with respect to the nadir and is located primarily in the polar latitudes. High latitude minimums in ionization of the F-layer occupy many thousand kilometers in latitude and longitudie and are arranged above the low latitutde boundaries of the auroral zones of the northern and southern hemispheres. The deepest minimums of ionization of the F-layer are arranged in the northern hemisphere in winter (Fig. 1.11), and in summer are in the souther, while in equinox there are ionization minimums close in magnitude in both hemispheres at the same time.

An example of the global distribution of critical frequencies of the F2 layer in Figure 1.11 corresponds to December, 1971 at 6:00 a.m. LT. The solid line

denotes the large circle of direction nearest the terminator which is plotted with a dotted line.

Lines of the ground-based terminator sink in the polar regions, reaching the geographic poles during equinox, i.e., 90° latitude; in periods of the winter and summer solstice, about 67° latitude; therefore, they intersect regions of minimum ionization.

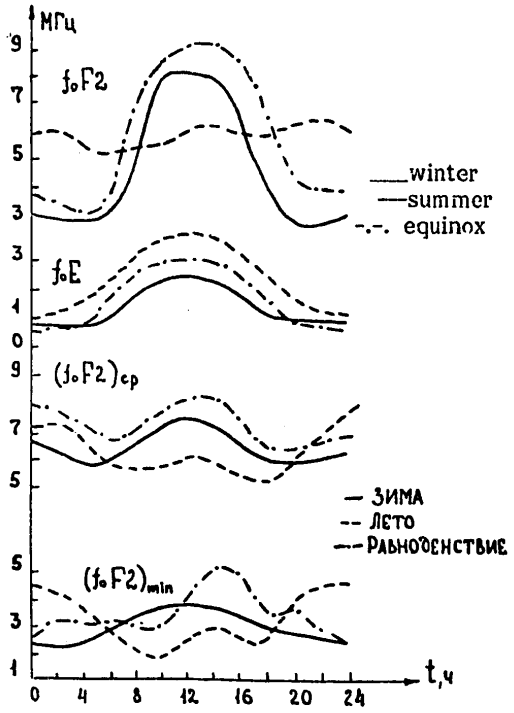

Figure 1.12

Both extremes f_0F2 in the general case are not antipodes because of considerable differences in absolute values, etc.

Directions from a prescribed point, corresponding to the minimum (f_0E)cp (in a route intersecting the terminator at a minimum angle) and the maximum (f_0F2)min, should occupy an intermediate position between directions to extremes of the global distributions. In the general case, both typical directions can change according to point coordinates and the period of observation. Let us adduce the results of variation analysis of typical ionospheric parameters for both optimum periods of time and direction and for unfavorable ones, for the reception of KS in a combined receiving and transmitting point.

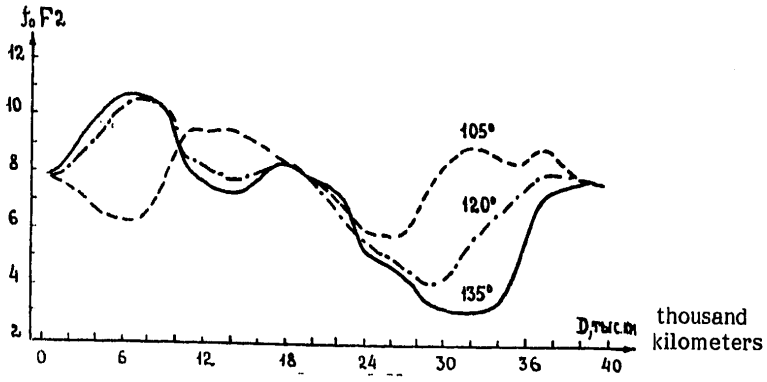

Figure 1.13

Daily changes in parameters in directions forming a minimum angle with the terminator for three seasons in 1971 calculated in terms of predictions of IZMIRAN are shown in Figure 1.12.

Figure 1.13 shows variations in f_0F2 for winter, 2:00 p.m., along world-wide routes corresponding to a direction of 120°; forming a minimum angle with the terminator and deflected 15° toward higher and lower latitudes.

In optimum periods, there were favorable conditions for capture-release (low absorption in the D/E-region with comparatively low values of f_0E, high f_0F2). So, on a winter day f_0E are small, but f_0F2 are great. On a summer night f_0E are slightly lower and much lower than f_0F2 (by two MHz). During the equinox day, f_0E are higher than on a winter day, by some 0.5 MHz; and on a summer night—by two MHz, with a value of f_0F2 greater than in the winter (up to 1 MHz).

Increased values of (f_0F2)min correspond to optimum receiving conditions.

Boundaries of change in typical parameters during the season and the year are shown in Table I.

The indexes 1.5 and 1 correspond to the distance, in thousands of kilometers, from the section observation point where the parameter was determined. KS(opt) are optimum conditions for signal reception, KS(| opt) is KS reception in a direction perpendicular to optimum where KS have not passed through. The last column corresponds to the direction nearest the terminator in the absence of KS. The most perceptible differences between optimum and unfavorable conditions of KS reception are in the parameter (f_0F2)min. KS were recorded only at values of (f_0F2)min greater than 4.5 MHz and were not observed at lower values (2.5 to 4.4 MHz). Figure 1.14 plots the values of several typical ionospheric parameters as a function of (f_0F2)min.

To the left of the vertical line drawn through the value 4.5 MHz, parameters correspond to unfavorable conditions, while to the right of the line they indicate optimum conditions of KS reception. The combination of the following parameter values were favorable:

(f_0F2)min	4.5 MHz,	$(f_0F2)_{1.5}$	6.8 MHz,
(f_0E)cp	1.9 MHz,	$(f_0E)_1$	2.8 MHz.

Values of (f_0E)cp and $(f_0E)_1$ under optimum conditions are basically lower than under unfavorable ones, while $(f_0F2)_{1.5}$ are much higher than conditions where there was no KS reception at all. Values of (f_0F2)cp were not noticeably lower under optimum conditions, which can be explained by the attraction of the channel toward the region of minimum absorption lying closer to $h_{max}E$.

Table I

Parameter, MHz	Season	KS(opt)	KS(lopt)	No KS
	winter	4.6-4.8	3.0-3.2	3.3
	equinox	4.6-5.9	4.3-4.4	3.6
(f_0F2)min	summer	4.5-5.0	2.6-3.0	3.3
	year	4.5-5.9	2.6-4.4	3.3-3.6
	winter	6.9-7.2	6.2-6.8	6.6
	equinox	7.2-8.3	7.4-7.6	7.2
(f_0F2)cp	summer	6.9-7.8	5.7-6.4	6.2
	year	6.9-8.3	5.7-7.6	6.2-7.2
	winter	7.4-8.8	9.0-9.8	3.8
	equinox	10.0-10.4	10.7-11.6	8.0
$(f_0F2)_{1.5}$	summer	6.8-8.2	7.1-8.3	7.6
	year	6.8-10.4	7.1-11.6	3.8-8.0
(f_0E)cp	winter	1.5-1.6	1.7-2.0	1.8
	equinox	1.6-1.7	1.9-1.9	1.8
	summer	1.6-1.9	2.0-2.0	1.9
	year	1.5-1.9	1.7-2.0	1.8-1.9
$(f_0E)_1$	winter	1.7-2.2	2.2-2.6	0.6
	equinox	2.3-2.8	2.8-3.2	2.4
	summer	1.1-1.2	0.9-1.1	3.8
	year	1.1-2.8	0.9-3.2	0.6-3.8

In addition, for optimum directions the absence of substantial inclines is typical near the point of observation ($\partial f_0F2/\partial D$ less than 0.5 MHz/thousand kilometer) which probably favors the KS reversibility observed in most cases. In optimum routes in the winter period there are favorable inclines of the ionosphere near intersections with the terminator. This seems to favor improved energy characteristics of KS which are better in winter than in summer. In the general case, in the region of an observation point the line of the ionospheric incline rises or decreases; continuously ; this can make it possible for capture or release

in the direction of the rise in level with fixed value of electron concentration N, but it can not assure capture and release simultaneously. Inclines of the ionosphere in the region of the observation point can not assure the KS route reversibility observed in most cases and thereby their reception in a wide sector (up to 360°). Inclines can appear as a factor in capture and release in a route with partially world-wide channel having sections with very great longitudinal gradients of ionization.

With capture and release in the vicinity of the observation point, deflection of beams from the direction of ordinary refraction can be caused by ionospheric irregularities of various form and dimensions located at various altitudes and evoking quasirefraction and scattering of radio waves. Changes in the regular and fine structure of the ionosphere in the region of the observation point must affect observable KS variations. The results of analysis mainly confirm the assumptions made on the effect of conditions in the channel and in capture/release sections on KS propagation.

In optimum directions, favorable conditions of refraction and absorption of radio waves are combined in the ionospheric waveguide ground-based channel. Conditions required for propagation of ultra long-range signals are determined by refraction, while adequate conditions are defined by the set of energy factors which guarantee a signal level above threshold at a given working frequency. One of the most important required conditions is an adequately large quantity (f_0F2)min in the route. The general tendency observed toward improvement of KS passage when ionization in the route is elevated, including the region (f_0F2)min and the region of the observation point, permits interpretation of observable features.

A reduction in the values of (f_0F2)min can serve as an explanation of deterioration of KS propagation in transpolar routes.

The observed deviation of optimum routes from the terminator by 10-20° towards the lower latitudes corresponds to an increase in the quantity (f_0F2)min in the route, as well as the greater uniformity of ionization distribution along the route.

When solar activity W is increased, depth of (f_0F2)min must decrease, i.e. its absolute magnitude increases, which leads to an improvement in KS reception. A reduction of (f_0F2)min during the negative phase of ionosphere-magnetic disturbances can explain the observed deterioration in KS passage. There should be a particularly strong decrease in f_0F2 in high latitude regions, which can lead to degeneration of the channel. The presence of a pre-morning minimum in the daily variation of f_0F2 and winter anomaly indicates the possible higher values of (f_0F2)min in the evening than in the morning and winter than in the summer which agrees with the observable seasonal/diurnal asymmetry of KS.

With an increase in W, critical frequencies of all layers increase; on one hand, this improves refraction characteristics of the channels and capture/release; on the other hand, it increases absorption. It would appear that some partial compensation for both effects can explain the not very sharply pronounced passage of KS in direction proportion with an increase in W.

Discovery of the appropriate optimum bearing requires a choice of several directions for a prescribed period and the presence of f_0F2 maps (or for a fixed bearing, the choice of several periods of time to determine the optimum). A more correct modification of this method would be the analysis of the direction corresponding to the highest of the smallest values of f_{max} in various routes. The magnitude of the latter, in addition, yields the upper limits of radio wave frequencies capable of refracting in the ionospheric channel.

Another, also approximate, method which is much simpler to determine optimum conditions consists in the use of materials which let us find direction A which forms a minimum angle with the terminator α min and perpendicular to the direction to the subsolar point or nadir.

By using the formula of spherical trigonometry, we find:

$$\alpha_{min} = \arcsin\left[\sin\varphi \sin\delta + \cos\varphi \cos\delta \cos 15^\circ(t-12)\right], \qquad (1.1)$$

$$A = \arccos\left[\frac{\cos\delta \sin 15^\circ (t-12)}{\cos\alpha_{min}}\right], \qquad (1.2)$$

where φ is the geographical latitude of the observation point, δ is declination of the Sun, t is local time at the observation point.

It is now advantageous to use global maps of isolines A and α min for analysis of experimental data and practical, empirical prediction of optimum conditions (Fig. 1.15-1.17, solid lines and dotted line, respectively). These maps of isolines of azimuths from various points on the globe to the point with fixed latitude were calculated earlier [40]. In contrast to them, maps (Figs. 1.15-1.17) were calculated for fixed latitudes of subsolar points, unambiguously determined by the Sun's declination for a given season. Global maps can be used with any position of the point of observation (it suffices to know its latitude), for any season (winter, equinox, summer) and required local time. When determining a favorable time of reception in a given season, it suffices to know the latitude of the observation point and the azimuth from it to the point of emission [28, 39].

Experiments conducted on reception of inverse echo signals, antipodal signals also indicate improvement of their propagation when the route approaches the twilight zone. A route lying in the evening, post-sunset regions is more optimum.

Global maps can thus be used for empirical prediction of optimum conditions not only of world-wide, but also inverse and antipodal signals.

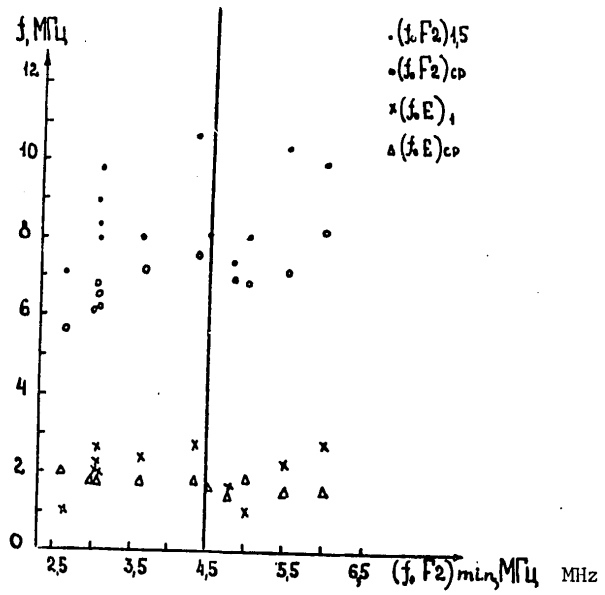

Figure 1.14

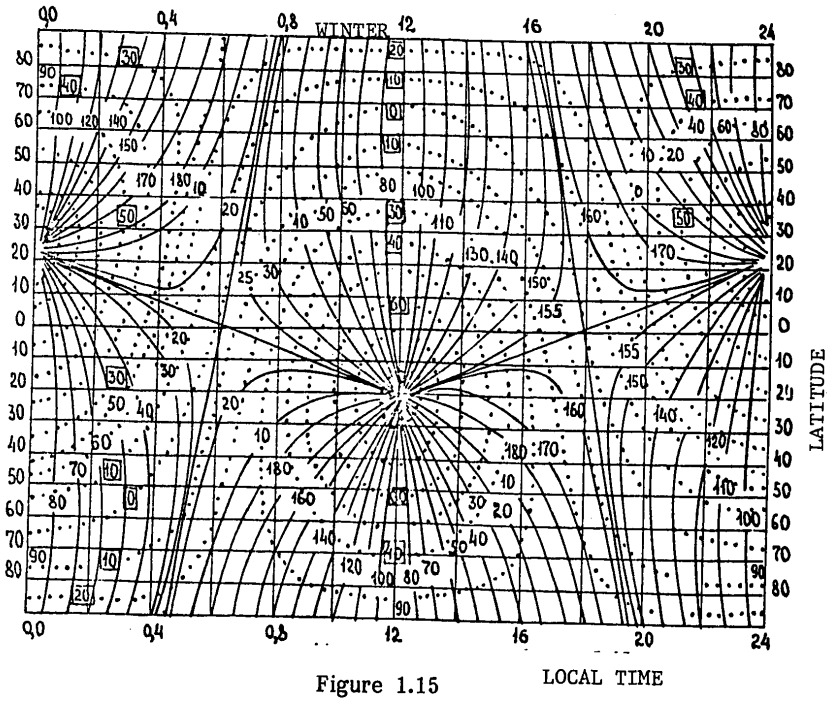

Figure 1.15

EQUINOX

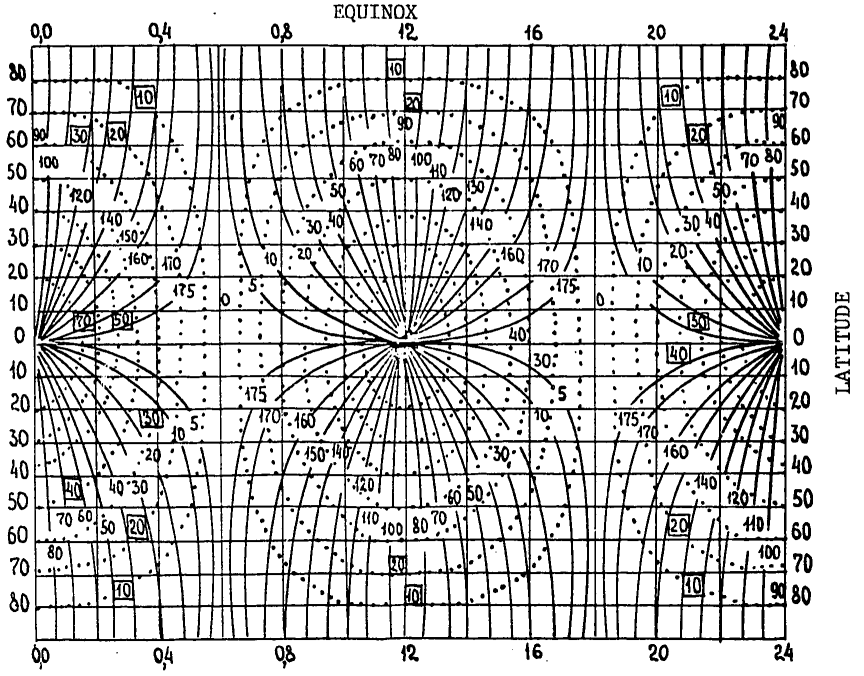

Figure 1.16

SUMMER

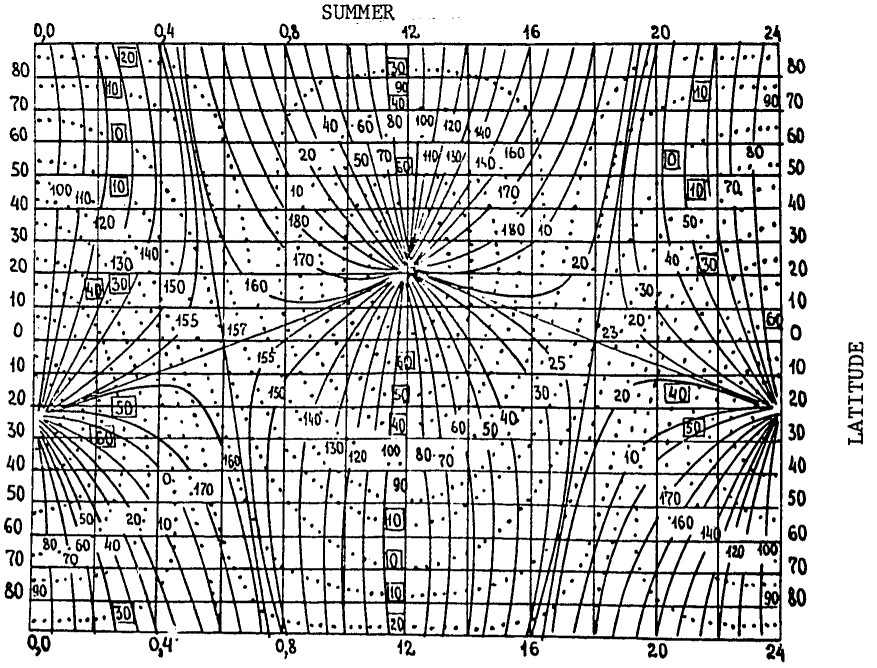

Figure 1.17

The use of the empirical method in the first stage of calculations to obtain the first approximation permits us to substantially simplify the problem of stricter theoretical methods which can be used to obtain absolute values of several features (attenuation, frequency range, etc.) for optimum conditions.

§5. Antipodal Propagation of Radio Waves

When emitter and receiver are separated by about 20,000 kilometers, where they are at diametrically opposed points on the globe (geographic antipodes), extremely diverse directions of radio wave arrival become possible. In other words, at antipodal locations, there is a qualitative change in conditions of radiowave propagation whose study is of considerable interest.

Antipodal signals have been observed in the SW range under various conditions in different regions of the globe. Let us cite some of these observations as an example.

In 1930 radio communication was established between Arctic and Antarctic expeditions (Hooker Island in Franz Josef Land, 80° NLat, Ross Ice Barrier, 78° SLat). Duration of communication at 7.5 MHz and 250 W output at noon on January 12 was 1.5 hours and continued the next day. In 1954, from November 14 through 17, at midnight local time, duplex radio communications were established between the floating station "Severnyy Polyus-3" and the "Slava" whale slaughtering flotilla cruising in the Antarctic. The results of a number of experiments have been published in [41].

A special experiment was run in 1964 in September and October when in the region of the antipode of Moscow were recorded signals on the "Kovrov" steamship [42]. Duplex round-the-clock communications were accomplished even with the low output of the marine transmitter (about 0.25 kW), with omnidirectional emission at a frequency of 8.0 MHz. Some ships with similar radio equipment located much closer to Moscow (14,000-16,000 kilometers) did not have regular duplex communications.

Figure 1.18 shows the diurnal variation of monthly median levels of field strength E at frequencies 8.0 and 12.6 MHz, obtained in the Moscow antipodal region with omnidirectional (1) and directional (2) emission using a double rhombus type RGD 65/4 I with a bearing of 290-310°. In omnidirectional emission at 8.0 MHz, E was rather high during the day, while at 12.6 MHz reception was from 4-11 a.m. and 5 p.m. to 1 a.m., local time, i.e., mainly inthe morning and evening hours. Maximums of E in these periods correspond to the position of both antipodes in the twilight zone. Minimum of E occur at midnight and noon, wherein at 12.6 MHz, E fell rather sharply or was not recorded at all.

In directional emission toward a bearing of about 300°, maximum of E at 8.0 MHz occurs at 6-8 a.m. local time and corresponds to radio reception in the direction of the unilluminated region. The value of maximum E is somewhat higher than in omnidirectional emission and apparently, it would be greater if the emission azimuth lay closer to the direction of the terminator (boundary of day and night). Daily variation of E sig has a valley at 4 p.m. to 11 p.m. local

time. At 12.6 Mhz, E is negligible and reception was irregular (about 10 percent of the entire observation period), mainly from 2 p.m to 9 p.m. LT from the illuminated direction.

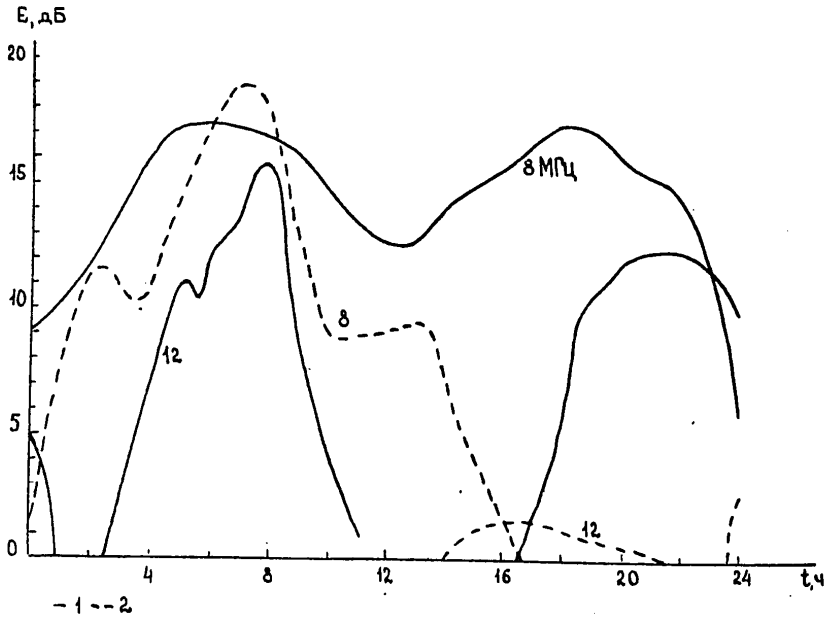

Figure 1.18

Observations showed that maximum values of E in most cases do not coincide with the geometric antipode, but are displaced from it, sometimes up to 1400 kilometers. The most likely boundaries of "antipodal drift" (with different velocity) are located within 400 to 800 kilometers. This effect is due to the deflection of beams from the planes of the great circles under the influence of lateral inclines of the ionosphere, scattering, etc. As we approach the region of the antipode at distances greater than 15,000 kilometers, there is an increase in E because of focusing of beam energy in the horizontal plane, as well as increase in the number of possible paths of radio propagation affecting the net E. When approaching the antipode, signal fading also increases. The mean square deviation in the antipodal region is 13 dB. An increase in both fast (3-5 min. interval) and slow (from day to day) fading can be explained by the complex structure of the field with polyvariant arrival of beams to the receiving point. The overall state of the ionosphere in this period of minimum solar activity was comparatively calm, if we ignore some local ionospheric disturbances.

Over the course of a two year period (1960-1961) in Bermuda (32°15' NLat; 64°50' WLong), antipodal signals (AS) were received from the Perth, Australia transmitter (32° SLat; 116° ELong)[41]. The receiver was located at a distance

of 19,920 kilometers from Perth and 80 kilometers from its antipode (a shift in the limits of one degree in latitude and longitude). To compare the results, two other stations from America were picked up situated 1700 kilometers closer to the transmitter. Emission energy at frequencies: 5.050; 15.905; 30.005; 45 and 60 MHz. Emitted power was 5 kW for the first three frequencies and 250 W for the last two. The transmitting and receiving antennas: quarter-wave vertical vibrator, omnidirectional. During the two-year period of observation, from January, 1960 to December, 1961, the number of sunspots changes significantly from 146.3 to 39.9 (Zurich number).

The basic results of observations were as follows.

Reception at the antipode was better (longer duration and higher intensity) than at two stations 1700 kilometers from the antipode for all frequencies. The frequency 15.905 MHz was best; reception at 45 and 60 MHz was not clearly recorded.

At about 16 MHz, duration of reception at 48 percent level changed from 25 hours near the winter solstice to 8 hours near the summer soltice. Reception at all frequencies was greatly improved in the near-sunrise and near-sunset periods (4-5 hours each). The average monthly percent of reception at these hours exceeded 50 percent by 5-25 percent at 30 MHz and more than 70 percent at 16 MHz. Reception deteriorated 30-70 minutes before the winter sunrise (i.e. during sunrise at ionospheric altitude). Less than one half hour after the winter sunrise there was a post-sunrise maximum of reception. Similar but less clear variations were noted near the sunset. Reception was better in winter than in summer. During solstices, at 16 and 30 MHz it was better during hours when one point was located in the summer night hemisphere, and in 1960 was somewhat better than in 1961, especially during the first half of the year. In other words, with a decrease in W there was some deterioriation in reception of antipodal sgnals at 16 and 30 MHz.

The directions of arrival of antipodal signals were also determined in this experiment. A three-element Yagi antenna with a directionality pattern width in the horizontal plane of about 70^{o}, was rotated through 360^{o} for 15 and 45 minutes each hour. Field strength of the signal was recorded as a function of the bearing. The antenna was rotated twice through 360^{o} in the course of two minutes. The average signal strength in each azimuthal sector of 15^{o} was obtained by calculating quantities recorded during both rotations; this reduced to the minimum all short-periodic polarization changes.

Measurements of the dominant direction of emission arrival at 16 MHz were made in September through December, 1961 (Figure 1.19).

The sector $+ 90^{o}$ with respect to the direction to the subsolar point was unfavorable for arrival of antipodal signals. The sector $+ 90^{o}$ with respect to the direction to the nadir of the subsolar point was favorable. In the near-sunset and near-sunrise periods, the reception sector expanded greatly. The optimum receiving sector for antipodal signals was mainly limited to directions forming the minimum angle with the terminator (perpendicular to the bearing to the

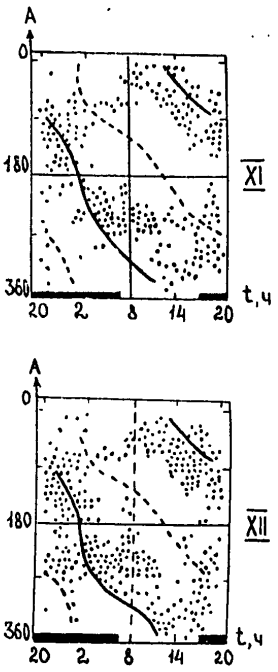

Figure 1.19

subsolar point). The direction to the nadir of the subsolar point lies inside the optimum sector.

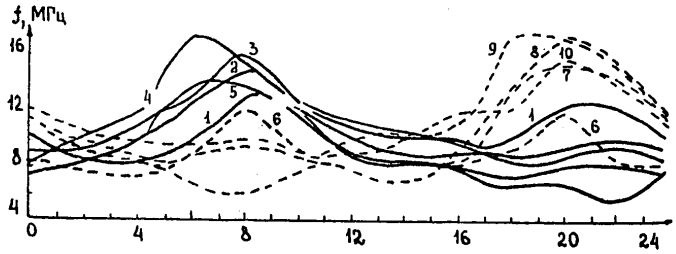

Figure 1.20

As Figure 1.19 indicates, variations in the optimum azimuth from day to day are extremely insignificant. This is due to changes in ionospheric conditions leading to displacement of the maximum in the spatial distribution of field strength relative to the geometric antipode. Reception of signals from directions passing through the auroral zone and the region of the polar cap was poor, while in routes with dominance of the sea it was better than in dry land routes.

In order to interpret the experiment described above on reception of antipodal signals from the Moscow transmitter, diurnal variations in muf for various directions were calculated (Figure 1.20). In morning hours, muf increases in eastern routes (2-5), while in evening hours—in the western (7-10). Minimums at noon and midnight are the result of the descent of one of the end points of the route into the shaded region. Minimum values of muf were no less than 6-8 MHz. When the antipodes were located in the twilight zone, there is a clearer separation of routes touching the illuminated and shadowed parts of the globe. Radio waves of low frequencies can pass through the shaded side, while high frequencies pass through the illuminated side. In the twilight zone, passing near the meridian of the end points (routes 1 and 6) and comparatively uniformly illuminated, there seems to be favorable conditions for radio wave ricochet in the ionospheric channel. Morning and evening maximums of muf did not exceed 12.6 MHz. Radio waves in this frequency passed in the morning and evening primarily above muf in the twilight zone, but below the upper envelope of muf in illuminated regions. But attenuation in illuminated routes of skip modes is extremely great and E must be below threshold values. Thus we can assume that some energy was propagated to the antipodal region at 12.6 MHz above standard muf through the twilight zone by non-skip means with comparatively little attenuation. A direction in which, first of all, the condition of reflection of radio waves on the ionosphere is satisfied and secondly, attenuation is lowest, is optimum for fixed frequency. With an increase in working frequency, the optimum direction can displace from the midnight to the twilight zone and then to the noon direction. The sector of radio wave conduction of a given frequency is limited to two directions corresponding to threshold E. With a decrease in emitted power, the sector of conduction narrows and may become commensurate with the width of the antenna directionality pattern. Consequently, the advisability of using directional antennas increases at emission power is reduced.

As power increases, the ratio of conduction sector width to emission directionality pattern aimed on the optimum azimuth of the antenna increases, within whose limits there occurs a concentration of beam energy. In the general case, the conduction sector lies on both sides of the direction closest to the day-night boundary, i.e., it includes the twilight zone.

Some effect on the position of the optimum direction can also be exerted by the "underlying" surface, because attenuation in long routes on the ground can be twice as great as on sea water.

When weakly directional antennas with comparatively wide lobes are used, we can expect the effect of horizontal focusing within the optimum sector. Emission toward the optimum sector is especially advantageous when small transmitters are used, since in omnidirectional emission, must of the energy will be absorbed in the illuminated zone without reaching the receiving point.

There is a great deal of practical interest in such features of antipodal routes as the substantial increase in field strength, expansion of the frequency range as compared with shorter routes, lower susceptibility to ionospheric magnetic

disturbances and absorption in the polar zones, high probability of radio wave ricochet in ionospheric channels.

The use of the antipodal effect is especially vital to increase communications reliability with moving objects (marine vessels, artifical Earth satellites, etc.) which usually utilize emitters of limited output.

To determine the boundaries of the optimum sector, we can use a global map of azimuths intersecting the terminator at a minimum angle (Chapter 1, §4) allowing for the fact that the direction to the nadir of the subsolar point lies within the optimum sector.

§6. Ionospheric Radio Echo with Multisecond Delays

Among the various types of echo signals, radio echoes have been detected with delays many times in excess of that of world-wide signals (about 1/7 sec.) and reaching the tens of seconds. The first observations date back to late summer 1927 when weaker echo signals with a three-second delay were received in Oslo along with KS. Observations were then made at different periods in various regions of the globe and special research on this type of echo was done. Unusually great delays of radio echo in conjunction with relatively low attenuation and distortion and other aspects have yet to receive generally accepted explanations. The earliest hypotheses emerging from the propagation of these echo signals outside of the Earth, in space, are inconsistent with modern data. The most likely is the propagation of echo signals in the ionosphere below the main ionization maximum. Therefore, instead of the term "world" echo, we should use another, such as LDE (long delay echoes), adopted in foreign literature of recent years.

Basic experimental research on LDE was done in Norway and Holland in 1928-1929 [5, 6, 8], in Indochina in 1929 [10, 11], in England in 1929 [7, 9], 1934 [12] in 1947-1949 [19], in the USA in 1967 [43-46]. After the first observations in Oslo of echo signals from the transmitter at Eindhoven (15 kW), a special experiment was arranged. In 1928-1929, signals were transmitted from Hilversum on a 31.4 meter wave in the form of three dashes of an overall length of 1.5 to 2 seconds with 20-second intervals. Regular observations began in March, 1928 and not until October 11 after noon were LDE received in Oslo with 3-15 second delays. The received LDE, like those transmitted, consisted of three dashes. The modulation frequency was unchanged, though sometimes the width of the signals received was slightly greater. In some cases several LDE were recorded which corresponded to the same transmitted signal (dittoes). On the same evening many LDE were received at Eindhoven with 3-15 second delays. Signals were transmitted from three points. LDE received often consisted of three dashes, in addition to LDE with a three-second delay. The working frequency of the received signals was not displaced from the transmitted frequency. On October 11, 1928, a series of LDE with various delays was obtained:

15, 9, 4, 8, 13, 8, 12, 10, 9, 5, 8, 7, 6;
12, 14, 14, 12, 8;

12, 5, 8;
12, 8, 14, 14, 15, 12, 7, 5, 5, 13, 8, 8, 8, 13, 9, 10, 7, 14, 6, 9, 5, 9;
8, 11, 15, 8, 13, 8, 8, 8, 12, 15, 13, 8, 8 seconds.

On October 24th, several dozen LDE were again received in Oslo (4-5 pm Greenwich Mean Time) with 3-30 second delays. Some of them were simultaneously received at two separated receivers in Eindhoven. In February, 1929 LDE were again recorded. In Oslo, they were received on February 14, 15, 18 and 19. On February 18, near the northern polar circle, 5 echoes from Eindhoven were received with a 12-13 second delay. On February 19, London received LDE with delays of up to 25 seconds and width of more than 2 seconds from the Eindhoven transmitter. In Oslo, LDE were then received on February 20 (with delays of 2 and 18 seconds), and also on February 28 and April 23, 1929.

In May, 1929 LDE observations were made by a French marine expedition in Indochina on Pouleau-Condor Island. Two-point signals were transmitted by a 500 W transmitter every 30 seconds at 12 MHz. During May 8, 9 and 10 many LDE were received with 1-32 second delays.

In England, during the period from May 30 through July 8, 1934, over 70 echoes with delays of 1-60 second were recorded. Distribution of delays had peaks of 8-10 seconds and about 25-30 seconds [12].

In 1947-1949, in England, a special experiment was run in which transmission was effected in almost a vertical direction at working frequencies of 13.5 and 20.7 MHz. LDE reception in this experiment was not recorded [19]. However in vertical transmission of radio waves of the lower frequencies under f_0F2, LDE were recorded in the USA in 1970 with delays of 15-20 seconds [46]. A transmitter with 20 kW output and 13-element log periodic antenna with vertical beam pattern were used.
A series of two pulses 0.1 wide each separated by 1.5 seconds were transmitted at intervals of 30 seconds. LDE were received: 1) on January 22 at 10:38 a.m. Mean Atlantic Time at 11.02 MHz (which was 0.5 MHz lower than f_0F2) with a 15 second delay. The pulses received were similar to those transmitted, but the working frequencies were 55 and 65 Hz lower and the interval between pulses was compressed to 1.1 seconds, i.e. 25 percent. 2) on February 14 at 1:57 p.m. at 10.65 MHz (which was 1 MHz lower than f_0F2) with a 20 second delay. Working frequency was almost 100 Hz higher and interval compression was about 35 percent. 3) on February 14 at 3:20 p.m. at 10.62 MHz (almost equal to f_0F2) with a delay of 20 seconds. Working frequency was 100 Hz higher and the interval was coompressed about 50 percent. Aside from these first LDE observations, by September, 1972 about 20-30 recordings had been received which could be LDE. No large series or more than two echoes per day were recorded.

According to [43-45], 46 American observers reported cases of LDE reception in the period from 1932-1969 in routes of different length and direction. Observations relate to all seasons, different time of day, range of working frequencies mainly from 3.5 to 28 MHz. Frequencies of about 14 MHz were optimum. Delays ranged within wide limits, but did not exceed 10 seconds in

most cases. In many instances (about 60 percent), observers were listening to their own signals. Existing experimental data indicate several features of LDE which can be summarized as follows.

The geography of LDE reception is extremely variegated. Observations were made in middle and near-equatorial latitudes (Norway, Holland, England, Indochina, USA). LDE signals were recorded both with separation of transmitter and receiver (about 1,000 kilometers or more) and with matching, for example with vertical transmission. They were observed comparatively rarely (an average of less than one percent of transmitted pulses), but on some days much more often. The most likely were isolated echoes, but in some cases a series of LDE were received for several minutes (up to 30 minutes). More often, reception was at frequencies of about 14 MHz, mainly in the 7-28 MHz range. Attenuation of LDE was comparatively low, perhaps three times greater than in the main signal. Signal dispersion (distortion) in most cases was not substantial, although it was sometimes significant. The Doppler shift of working frequencies was usually unremarkable and increased only in vertical transmission. LDE pass well when ordinary and ultra long-range signals pass well along the direct route(world-wide, inverse). Apparently, ionospheric conditions corresponding to high solar activity, low geomagnetic activity and transauroral directions were most favorable for LDE reception.

Hypotheses advanced at various times concerning the origin of LDE can be arbitrarily divided into two groups. One includes hypotheses based on the porpagation of LDE beyond the Earth, in space. Remaining hypotheses are based on the possible propagation of LDE in the ionosphere. One of the first was the assumption about reflection of LDE with three-second delays on the surface of the Moon. After reception of LDE with a wide spectrum of delays, the hypothesis was advanced concerning reflection of LDE at great distances from Earth on bands of charged particles formed by solar wind [5]. In terms of modern ideas on radiation bands and interplanetary plasma, this hypothesis has been found to be inconsistent, since the delays would be much shorter (less than one second) and attenuation would be much gerater than observed. It was also assumed that LDE can be channelized through very long curvilinear trajectories around ionized formations of prolate form appearing beyond the Earth and rotating with it [19].

The possible guiding of echos along bands of charged particles associated with the circular current around the Earth in the plane of the geomagnetic equator was also indicated, since LDE were often observed when the Earth-Sun line lay in the plane of the circular current [9].

These hypotheses, however, could not explain the set of features observed. For example, LDE attenuation would be much greater than observed, even if it only passed through the thickness of the ionosphere.

The hypothesis was advanced on world-wide propagation of LDE with a large number of revolutions (7, 70 and 210 with delays of 1, 10, 30 seconds, respectively). Low attenuation might be due to repeated focusing near the antipode of the transmitter and the transmitter per se [12].

It was also assumed that the signal slides along ionized regions having a refraction index near zero, where group velocities are low [19]. When these regions are found above $h_{max}F2$, where the number of collisions of charged particles is small, attenuation should diminish. But in this case it will be much greater than that observed. Long-term propagation of a signal in a medium with near-zero index of refraction leads to considerable expansion and diffusion. But observable LDE usually represent rather clear, undistorted signals.

Attempts have been made in recent years (mainly qualitative) to use the concepts of modern plasma physics to explain LDE.

So in [46] it is indicated that strong retardation of signals in the reflective region of the ionosphere can be associated with the transition of some energy to longitudinal plasma waves which do not undergo substantial attenuation. The signal frequency shift can correspond to displacement of the reflective region about 1.5 kilometers per second and change in group velocity may yield the observable effect of interval compression between pulses. Because of the plasma-beam interaction in the presence of the reflective region of the traveling electron flux (associated primarily with solar activity), transmission of part of its energy to the wave is possible and in consequence, some neutralization of its attenuation [47]. These effects can appear not only in vertical sounding of the ionosphere, but also in inclined reflection on it. In long routes there may be intensification by natural electron fluxes in several sections. Passage of LDE in transauroral directions may be associated with intense electron fluxes in these regions and possible effects of plasma-beam interaction. In view of the great manifestation of plasma effects in the environment of $h_{max}F2$, conditions of LDE appearance can be extremely favorable.

In our view, assumptions concerning the appearance of plasma effects in propagation of LDE are more acceptable than some others mentioned above. The most likely is propagation of LDE by means of reflection of radio waves on the ionosphere below $h_{max}F2$, as in the case of vertical and inclined propagation [48].

Attention should be paid to the following. There is no clear tendency toward increase in time delays of LDE in direct proportion to route length, for example, in routes 200, 950 and 1,150 kilometers long in the Norway-Holland experiments. Time delays rapidly and significantly changed in a short time interval. With discrete transmission of signals with on-off time ratio of 20-30 seconds, delays at this time suddenly change several seconds in absolute magnitude (in some cases, up to 9 seconds). The summary time of reception of several LDE with rapidly changing delays reached tens of minutes.

These features of time delays of LDE indicate the important role of ionospheric parameters distinct from f_0, h_{max}, Y_m which characterize its regular structure and change much more slowly. We can assume that delays are greatly affected by rapidly changing factors of the ionosphere such as vertical ionization gradients, wave-like ionospheric disturbances and small-scale irregularities near the region of wave transformation. Specific paths of LDE appear to be extremely diverse.

In a significant number of cases, LDE reception was observed with combined emitter and receiver in one place at extremely high working frequencies, exceeding f_0F2 and f_0E_s, which precludes vertical reflection of radio waves in the ionosphere.

Without completely excluding the possibility of reverse incline reflection of these signals in the ionosphere near an observer, it may be assumed that LDE, like KS, have rounded the globe. In favor of this possibility are the existing cases of simultaneous LDE and KS reception and the similarity of favorable conditions for reception of both type of signals. Interpretation of LDE observations with separated and matched receiving and transmitting media is extremely complicated. LDE can propagate via ionospheric reflection in the direct route (skip mode), reverse-incline on the ionosphere near an observer, and world-wide propagation of LDE in the ionospheric channel. In this last case, at close to optimum (resonance) working frequencies and under favorable conditions of capture/release, emissions from the ionospheric channel can be small.

It is also impossible to exclude the possibility of antipodal focusing of emission which can provide additional compensation for signal attenuation. Reduction of attenuation can be promoted by resonant effects associated with reaction to electron flux and the transmission of some energy to the propagating wave. However, a fundamental physical factor leading to great LDE delays, despite the diversity of various modes, seems to be the plasma effects [49, 50] in irregularities in reflective regions of the ionosphere. In long routes, these effects can appear simultaneously in some sections, leading to integral growth of LDE delays. That means, in the general case, that LDEs can be a multiplanar complex effect, where the total action of several effects of different physical nature are manifested. The relative role of these effects under different conditions can be substantially altered.

Chapter II

Long-Range Propagation of Radio Waves with Emitter in the Ionosphere

In this chapter, the basic results of observations and special experiments in the study of propagation of radio waves with an emitter located in the ionosphere are discussed. This type of research first became possible after the launch of an artificial Earth satellite (October 4, 1957) with an on-board radio transmitter and antenna-emitting system. The characteristics of signals from the satellite with ground-based reception beyond the zone of direct radio line-of-sight at distances over 6,000 kilometers were found to be quite similar to those of ultra long-range ground-based transmitters. This indicated the important role of non-skip modes, increasing with transfer of the emitter from the Earth's surface to the ionosphere. Despite the usually small output of an emitter situated in the ionosphere, a significant number of cases of long-range reception was recorded, up to an including the region of the satellite's antipode. Of particular interest is an experiment concerning satellite reception of radio waves broadcasted from another satellite. The results can be seen as experimental proof of the ricochet mechanism of radio waves in an ionospheric waveguide.

Based on comparison of several experimental characteristics of long-range reception of satellite signals with theoretical data, the effect of global properties of the ionosphere and orientation of the route with respect to the terminator were considered. Several conclusions were drawn on the possibility of predicting optimum conditions of long-range propagation of radio waves with an emitter located in the ionosphere.

§1. Experimental Study of Long-Range Radio Signals

Experimental research on long-range propagation of radio waves emitted in the ionosphere was begun after the October 4, 1957 launch of the first artificial Earth satellite. Even the initial observations of signals from the first, second and later satellites revealed several important features of long-range propagation of radio waves (at distances over 6,000-8,000 kilometers) with an emitter located in the ionosphere as compared to emission from the Earth's surface. Attenuation of signals was much less and they often passed at frequencies above the muf of skip modes. These features (and some others)indicated the possibility of non-skip (most likely waveguide) mechanisms of propagation akin to that commonly appearing in ultra long-range propagation of signals transmitted by a ground-based transmitter. The appearance of typical features in routes of much shorter length suggested the increased role of richochet modes when an emitter is placed in orbit.

Recording of orbital signals was done to obtain information not only on the characteristics of propagation of radio waves (long-range and within the zone of direct radio line-of-sight), but also about parameters of the ionosphere: to solve the inverse problem.

Let us consider published data on observations and experiments and some results of analysis related to various space-time ionospheric and initial conditions of radio wave escape.

Measurements of field strength at 20 MHz from the first artificial Earth satellite on October 5-7, 1957 in Moscow and Khabarovsk, and from the second artificial Earth satellite on November 3, 7, and 8, 1957 in Moscow were analyzed in study [51]. It is noted that the average field strength decreases much more slowly with increased distance than in ground-based routes. Absolute values of field were slightly greater than those calculated for ground-based routes and even exceeded the theoretical unabsorbed field in free space. The range of reception reached 16,000 kilometers or more. The antipodal and world-wide signals were also detected.

The results of observations in several high-latitude stations of the Soviet Arctic (Chelyuskin, Tikhaya, Dikson, Tiksi) of signals from the third artificial Earth satellite on May 16-June 6, 1958 at 20 MHz are presented in [52]. The maximum range of reception reached 8,500 kilometers, with displacement of the satellite from the equator to 65°NLat, when it was below $h_{max}F2$. Median intensity outside of the zone of direct radio line-of-sight reached 0.4 and 0.3 mcV/m with the artificial Earth satellite located above and below $h_{max}F2$, respectively.

The duration of radio reception (from radio rise to radio set of the satellite) was directly proportional to the moment of artificial Earth satellite location in direct line-of-sight. The median of durations of artificial Earth satellite signal detection is inversely proportional to the geomagnetic latitude of the receiving point. The duration of radio reception depends on the position of the artificial Earth satellite with respect to the polar region. The duration of radio reception is affected not only by the position of the geomagnetic pole with respect to the receiving point, but also by the geographic distribution of the geomagnetic field.

Some results of comparison of ground-based signal reception from the artificial Earth satellite Vostok-1 and Vostok-6 for the summer period 1961-1963 at 20 MHz are cited in [53] with the muf values. These data relate to the location of an artificial Earth satellite below $h_{max}F2$, beyond the zone of direct line-of-sight. In this period of subsidence of solar activity, in the summer, muf were under 20 MHz in most cases. Excess of working frequencies of received signals over muf in some cases reached very high magnitudes (up to 8-10 MHz), which can not be explained by errors in calculating muf. When the radio of f_w/MPCh was reduced, the percentage of reception at different times increased somewhat; the probability of signal reception from an artificial Earth satellite did not drop in direct proportion to solar activity (and consequently, MPCh), and stayed at roughly an identical level of about 50 percent. When MPCh near the reception point located in an illuminated hemisphere were greater than 20 MHz, and were small near the artificial Earth satellite, conditions of reception are extremely favorable. The probability of geat deviations of f_w-muf is significant when reception points are illuminated. A rise in illumination toward the receiver corresponds to horizontal gradients of ionization (ionospheric incline) favorable for re-entry of ricochet beams to Earth without additional signal attenuation.

Several special experiments were also done [54-61] to study long-range propagation of signals from artificial Earth satellites (see Table 2). Launchings of artificial Earth satellites were done in periods of different solar activity and seasons, into orbits having different perigees, apogees and angles of inclination to the equator (middle latitudes, equatorial, polar). Reception of artificial Earth satellite signals transmitted with different outputs was done during experiments at several stations (middle latitude, equatorial, polar) in a certain range of working frequencies.

As a result of experimentation, the basic features of long-range propagation of artificial Earth satellite transmissions were confirmed with the reception of signals from the first artificial Earth satellite. The set of features revealed indicates the high probability of a ricochet mechanism in long-range propagation of artificial Earth satellite signals.

In all experiments it was noted that when an artificial Earth satellite is situated above $h_{max}F2$, reception conditions are much less favorable than when it is below $h_{max}F2$.

In December, 1970, signals received from the artificial Earth satellite Kosmos-381 were utilized to experimentally study the possibility of long-range

propagation of radio waves along magnetic force lines: in magnetospheric waveguides. It is assumed that when an emitter is located above $h_{max}F2$, the probability of passage of this type of mode should be raised, especially into a magnetically-coupled region.

Table 2

Satellite	Period of observation	Orbital Inclination	Apogee/Perigee km	Working freq.	Emitted power, W
Orbis [54,55]	1964 Nov 19-Dec 2	70.02°	368/188	10.0040	0.75
San Marco 1 [56]	1965 Jan 1-13	37.8°	753/203	20.0050	0.20
OV4-1 [57,58]	1966 Nov 3-Dec 27	30°	300/250	20.7500 34.3000 46.8000	600.00
San Marco 2 [59,60]	1967 Jun 26-Jul 15	2.9°	635/213	20.0050	0.60
Orbis-Kol [61]	1969 Mar 19-24	99°	419/184	8.9825 13.2525	2.00

On board artificial Earth satellites (altitude range 985-1025 kilometers, orbital inclination 74°) were established ionospheric stations with the following parameters: pulsed transmitter output 100 W, duration of sounding pulse 150 mcs, pulse repetition rate 48 Hz. The following fixed frequencies were used: 2.0; 3.2; 5.6; 10.4; and 12.8 MHz. Out of 13 sessions, the signal from the artificial Earth satellite was received from a magnetically-coupled region once in Moscow for 20 seconds at 12 MHz and twice in Gorky for 0.25-0.5 second. In five cases, no signal could be detected because of strong interference. In other cases, there was no reception of orbital satellite signals in the magnetically-coupled region. Test data can prove the possibility of magnetospheric modes and their variability in space and time [62].

With orbital satellite signal reception, experimental research was done on fluctuations of amplitude and duration of interference fading. Results of this type of measurements in the northern polar cap and auroral zones, on the floating stations Severnyy Polyus 16 and 19, with reception of signals from the artificial Earth satellites Kosmos-321, Kosmos-356, Kosmos-381 at 20 MHz are presented in [63, 64]. Observations of artificial Earth satellites Kosmos 321 (altitude 280-507 kilometers, orbital inclination 71°) were done in Feb-Mar 1970; Kosmos 356 (altitude 240-600 kilometers, orbital inclination 82°) in Aug-Sep 1970 and Kosmos 381 (altitude 970-1030 kilometers, orbital inclination 74°) in Dec 1970/Jan 1971. The distribution of signal levels permits us to assess the

stability of radio line operation (duration of field drop below the noise level of the receiver) and also the mechanics of radio wave scattering in ionospheric irregularities. To limit the polyvalence of trajectories, only cases where the artificial Earth satellite was in the direct line-of-sight zone were considered. It is noted that intersection of the ratio route by the terminator did not affect the spectra of distribution of fading duration. During magnetic storms there is an increase in fluctuations of signal amplitudes and a change in the distributive pattern. It is assumed that great fluctuations are the result of interference of several beams passing thorugh various irregularities. Small fluctuations are the result of partial scattering of beams in irregularities ("winking") and small changes in the angle of wave arrival to the antenna ("quivering").

The results of measurements of the Doppler spectrum of artificial Earth satellites in the Moscow region in June, 1970 at frequencies 15, 18 and 20 MHz are cited in [65]. The Doppler spectrum of a signal in a vague way contains a large amount of information about the state of the propagation channel. According to the spectrum of a received signal we can determine angles between the vector of the velocity of motion of the artificial Earth satellite and lines normal to the wavefront. In the general case, the Doppler spectrum of an artificial Earth satellite signal reflects its multiple beam structure. The width of the signal spectrum very often had a band of 30-100 Hz. In routes 7,000-10,000 kilometers long, the spectrum sometimes narrowed to 6-18 Hz. The spectrum always expanded, sometimes to a maximum of 300 Hz, in transpolar routes or with reflection of radio waves on large mountain chains. The spectrum noticeably narrows for routes with smooth underlying surfaces (valleys, ocean) and especially under conditions of ricochet modes. When an artificial Earth satellite travels perpendicular to the direction toward the observer, one would expect a narrowing of the spectrum to a minimum of 6 Hz. Indeed, there was expansion to 50 Hz, which can be explained by lateral deviations up to 8-17°. This may explain displacements in time of the maximum of the signal level envelope from an artificial Earth satellite with respect to receiving antennas, e.g., in transpolar routes. The Doppler spectrum of artificial Earth satellite signals were observed for 20 orbits.

An important trend in experimental research is the observation of artificial Earth satellite signals at ground-based stations to determine certain parameters of the ionosphere.

So, by observing moments of radio rise and radio set of an artificial Earth satellite when situated above $h_{max}F2$, variations N(h) above $h_{max}F2$ were determined, as approximated by exponents. For this purpose, from the derived experimental limited range of reception of the artificial Earth satellite is substracted the term computed for the refraction section below $h_{max}F2$ [66].

Determination of the electron concentration in different sections of satellite orbit is possible from observations of Doppler and Faraday effects [67]. Some results of measurement of these effects in receiving of the orbital satellite beacon from Interkosmos 8 at frequency of 20 and 30 MHz in Dec 72-Jan 73 at two high-latitude points (68 and 65°NLat) are cited in [68]. Ninety-nine sessions of measurement were done in the radio line-of-sight zone. Under ionospheric

disturbances, these effects yield an irregular picture because of the influence of irregularities. Their rates of motion and parameters may be determined by measuring Doppler and Faraday effects at receiving points having separated bases.

§2. Effect on Characteristics of Long-Range Signals of Global Properties of the Ionosphere

The results of analysis of test data obtained from reception of artificial Earth satellite data beyond direct radio line-of-sight at several points in the USSR are presented.

The goal of analysis was to assess the effect of orientation of long-range routes with respect to the terminator, variations in signal levels as a function of distance, ionospheric conditions, orbital satellite position with respect to $h_{max}F2$ favoring occurrence of certain mechanisms of propagation of radio waves on the maximum range of signal reception. The effect of route orientation with respect to the terminator on the propagation of long-range signals (range D = 10,000-20,000 kilometers) was analyzed using test data obtained from reception of long-range signals from low-flying artificial Earth satellite in middle latitudes in the summer, during a period of low solar activity [69]. The presence of directional receiving antennas with large active length made it possible to produce a signal detection threshold of about 50 dB (with respect to 1 mcV/m) and systematically record signals at great distances at a working frequency of 20 MHz. An automatic plotter with logarithmic attachment was used for recording.

Figure 2.1 cites the relationship of maximum detection range D_{max} of an artificial Earth satellite signal as a function of the angle between the direction of reception and the terminator α. Orbits were primarily used where the artificial Earth satellite passed near the observation point and the direction of signal reception near that of the artificial Earth satellite travel through its orbit had little variation over large intervals of distance. The dots indicate test values and the straight line is plotted by the method of least squares. As the angle α decreases (when the route approaches the terminator), D_{max} increases and the number of cases of long-range reception grows. The smallest angle α at which long-range signals were received was 15°. A considerable number of long-range signals (D_{max} = 13,000-18,000 kilometers) was received at α = 15-30°. Therefore, for long-range signals of artificial Earth satellites, as in ultra long-range signals of a ground-based transmitter, conditions of propagation improve at the route approaches the twilight zone and this tendency is intensified with an increase in distance to the transmitter. The test data given in Fig. 2.2 are compared with the calculated relationships of optimum directions of reception A_{opt} as a function of local time, using methods found in [39, 26]. The figures in circles denote measured D_{max}. The solid line corresponds to [39], the dotted line to [26]. The x's denote the calculated moments in time of best reception during the day. Test data, as seen in Fig. 2.2, agree well with theoretical estimates; differences between them are small in favorable periods and are slightly greater during unfavorable ones. This is because [39] uses a direction which forms a minimum angle with the terminator as the optimum direction at

a given point at a given time, while [26] uses a direction toward an equatorial point through which the terminator had passed one hour prior. It is worth noting that the methods in [39] are more acceptable for fixed frequencies, while those in [26] are for higher optimum frequencies. So, in [34] it is experimentally proven that as working frequencies are increased, the actual time of occurrence of optimum conditions in the desired direction if often delayed by about one hour from the calculated time.

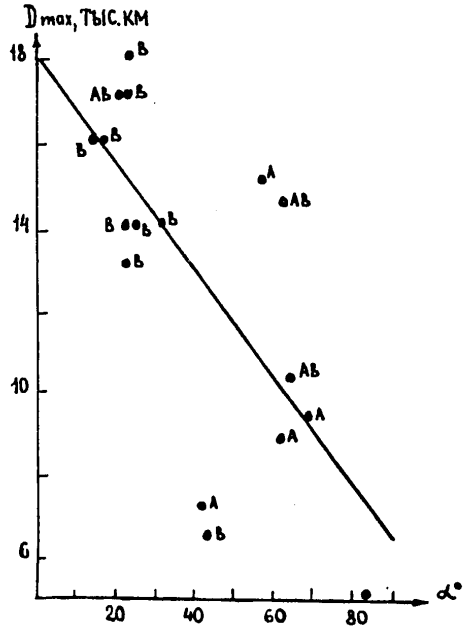

Figure 2.1

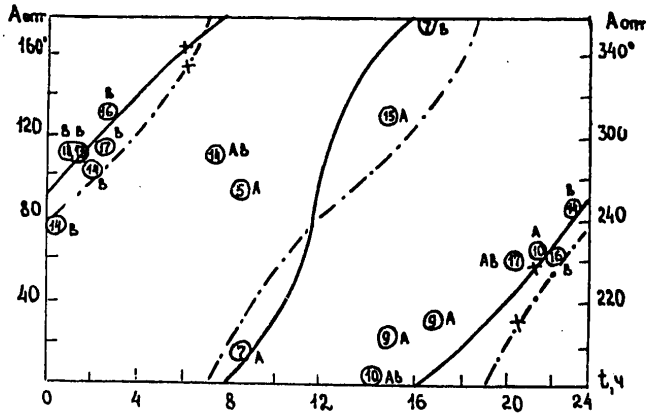

Figure 2.2

Results indicate the possible use of semi-empirical methods [26, 39] to determine optimum periods and lines of long-range routing from artifical Earth satellites. Predictions are employed to determine minimum muf values of 4000 kilometers corresponding to the upper limit of skip mode frequency in order to analyze the relative role of various modes in artifical Earth satellite routes. Variations in altitudes of equal electron concentrations are calculated for the same routes on the basis of prediction of f_0F2 and geometric parameters of the F2 layer [70]; this permits us to assess the presence or absence of inclinations favoring escape of enegy from the duct channel to the Earth. Routes having favorable inclinations for the entire expanse are denoted by the index A in Figures 2.1 and 2.2; unfavorable inclinations are denoted by B and inclinations favorable over half the route are denoted AB. Average values of muf in A routes are about 12 MHz, i.e., 40 percent below working frequencies equal to 20 MHz. Non-skip duct modes are most likely for these routes. In type B routes having ionospheric inclinations not favoring escape of energy from the duct and extremely high maximum usable frequency (muf) near working frequencies, skip modes are more likely. In type AB routes, a hybrid mode including ducts is possible with escape of energy to Earth in the intermediate sector, shifting to skip modes in the rest of the route. Routes of types A and AB, where duct propagation of artifical Earth satellite signals is possible, may intersect the terminator at angles greater than type B routes.

Attraction of long-range routes having par excellence skip modes to the terminator can be attributed to the fact that comparatively low absorption and high upper limit of radio wave reflection (muf) are simultaneously assured near the terminator because of the most uniform distribution of ionization along the twilight zone. Lower attraction of long-range routes having par excellence duct modes to the terminator can be explained as follows.

When transmitter output is low, there is an increase in the limiting role of energy losses in the duct and in its energy escape sector. With comparativelylow absorption in the duct (weak directional dependence), a decisive role is played by the presence of conditions for energy escape from ducts due to the ionospheric inclination, which is not connected with additional energy losses.

Test values of field strength E at various ranges of artifical Earth satellites from the receiving point are indicated by the points in Figure 2.3. The solid line indicates averaged relationships of E as a function of D. The dotted line plots the theoretical relationship of field strength as a function of free space $E_0(D)$.

A drop in the field primarily occurs with an increase in range recorded in other experiments [51].

Measured results of field strength were used in estimating damping with respect to field strength in free space. In Figure 2.4, solid lines plot satellite-Earth route sectors corresponding to those satellite revolutions where the azimuth to it from the receiving point barely undergoes variation. Dots and dashes show the terminator. Estimates of OS, KS and two-time KS damping are cited for similar orientation of routes with respect to the terminator in [37]: 4.8; 2.4-3.6; 0.5-2.9

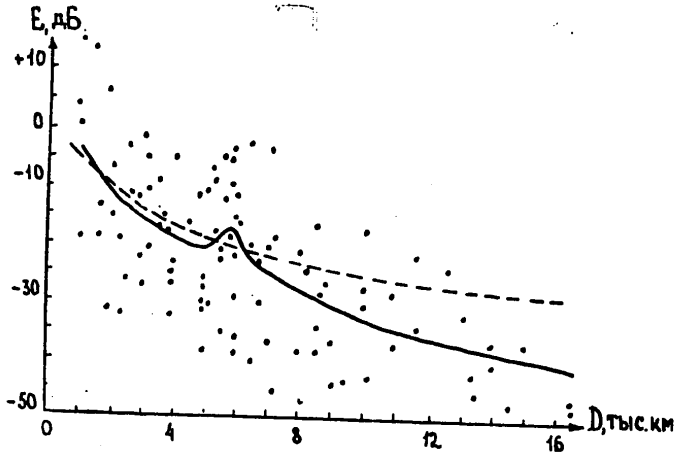

Figure 2.3

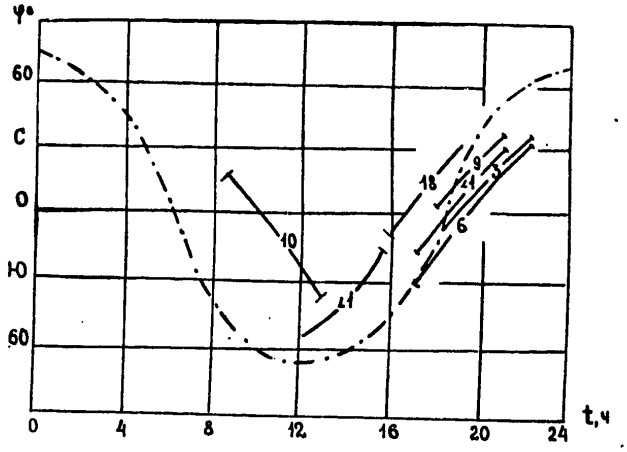

Figure 2.4

dB/rad. Let us compare these estimates with those of damping shown in numerical form in Figure 2.4. In these routes, and also in some route sectors, there are extremely different magnitudes of damping (1-18 dB/rad). Damping less than 3 dB/rad apparently indicates non-skip mechanisms of propagation in corresponding routes from satellite to Earth and their sectors.

Results of analysis of another experiment on reception of long-range satellite signals at three middle-latitude points widely spaced in longitude are shown in

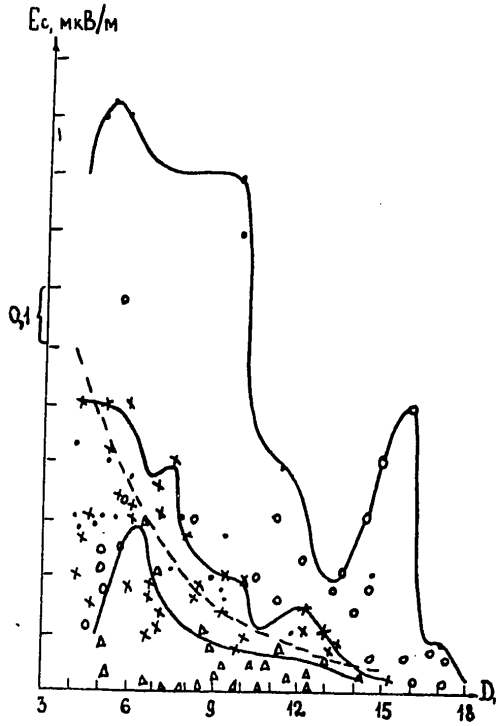

Figure 2.5

Figures 2.5 through 2.8 [71]. Observations pertain to a period of low solar activity, under summer and autumn conditions (Fig. 2.6). Highest signal levels (envelopes in Figs. 2.5-2.6) were reached in routes as muf increased toward the receiver (A) with the satellite positioned below $h_{max}F2$ and above $h_{max}F2$ (dots and circles, respectively). In most cases, there are ionospheric inclinations in these routes toward the receiver which favor escape of beams ricocheting in the ionospheric channel toward the Earth. Slightly lower is the highest level of signals in routes having reduced muf toward the receiver when the artifical Earth satellite is positioned above $h_{max}F2$ (C). Thus the highest signal level is reached in routes having possible ricocheting (A) and almost one order lower in routes where ordinary skip modes are most likely (B). The lowest signal levels are in type C routes where skip modes are possible with deflection of refracting beams passing below $h_{max}F2$ by such factors as scattering on the Earth's surface and in the ionosphere, involving significant energy losses. For all types of routes, there is a clear reduction in signal levels as range is increased. Abatement is slower in routes having possible ricocheting, where there is some increase in the signal level attained at long range. Differences in signal levels for routes of various types increase in direct proportion to range. In signal levels attained, they mainly correspond to calculations for skin modes (dotted line in figure). In routes with possible ricocheting, the highest signal level is reached in most cases at working frequency f_{opt} above muf near the satellite, but below muf_n near the ground-based receiving point (Fig. 2.7). This working frequency, in most cases, is near muf_n when the satellite is positioned below or above $h_{max}F2$ (Fig. 2.8).

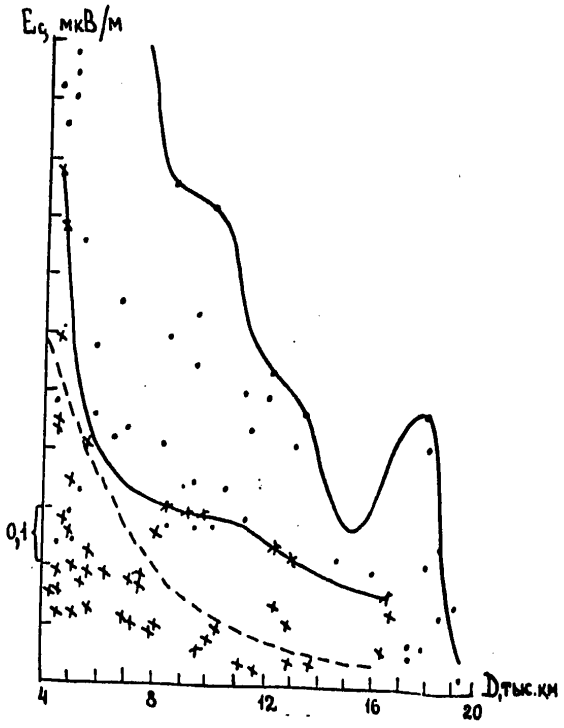

Figure 2.6

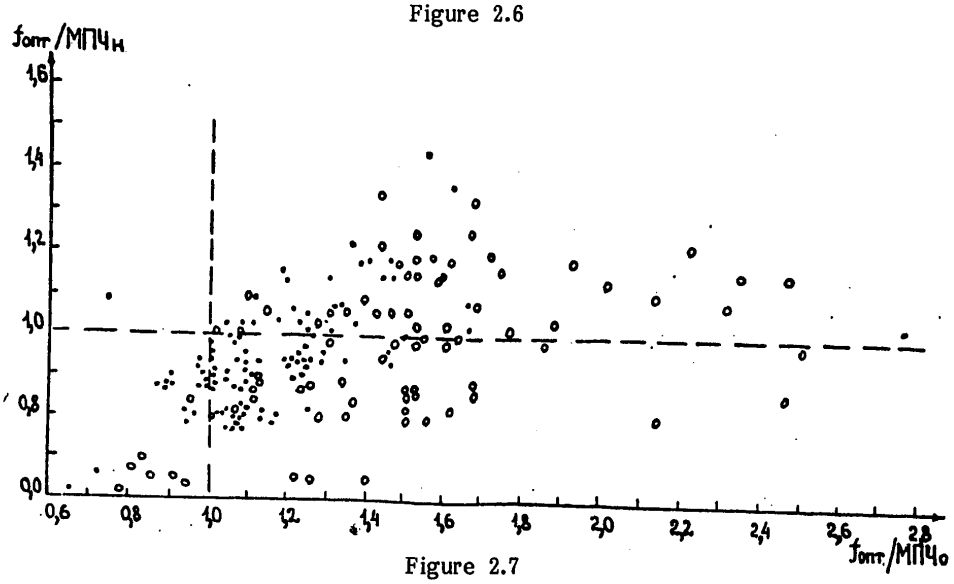

Figure 2.7

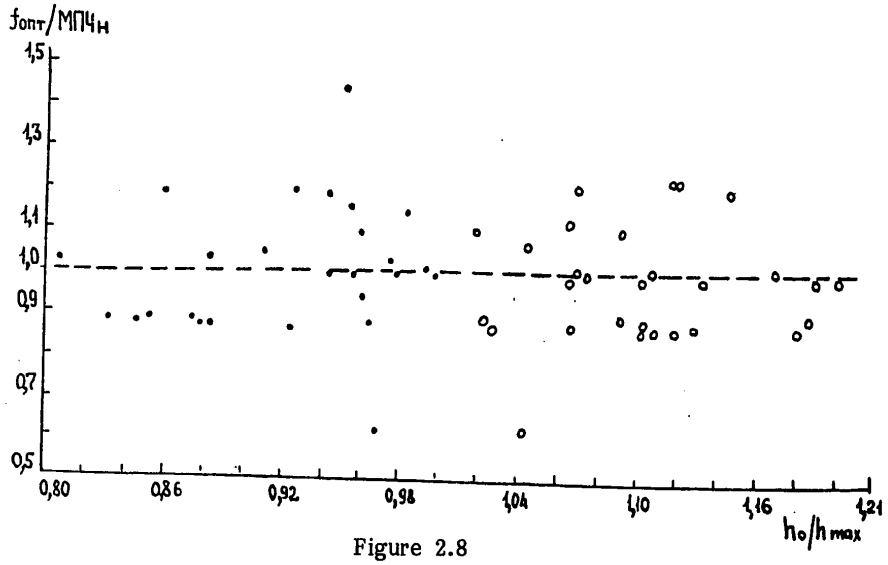

Figure 2.8

§3. "Antipode Effect" in Reception of Signals Transmitted in the Ionosphere

3.1. Reception of Antipodal Signals at Mirnyy (Antarctica) from the First Sputnik

Signals were first recorded from the first sputnik on October 6, 1957 at the Mirnyy station in the Soviet Antarctic at a frequency of 20.005 MHz and continued through October 10th [72]. A VINP direction finder with bidirectional loop antenna was used for reception: its direction could be changed to obtain maximum signal level. Recording of field strength was done on tape using an automatic recorder running at 120 mm/hr. The tape clearly shows alternating high and low maximums of intensity corresponding to the longest and shortest ranges of the satellite from Mirnyy (Figure 2.9).

On October 6th were recorded four cases in a row; on October 7th another four, and on October 8th, three cases in a row. Low maximums were displaced from high ones by about 1/2 period of satellite revolution around the Earth (about 48 minutes).

Data have been obtained in reception at Mirnyy of satellite signals at short-range and long-range up to and including the antipodal region. Short-range signals correspond to ranges up to about 6000 kilometers; antipodal ranges are 16,000 to 19,500 kilometers. Maximum field strength in short-range signals ran from 1.0-12.5 mcV/m, and antipodal—from 0.2-0.8 mcV/m.

When the satellite approaches the geometric antipode of Mirnyy, E_{sig} level increased slightly. The duration of short-range signals was 6-17 min. and antipodals were 6-11 minutes.

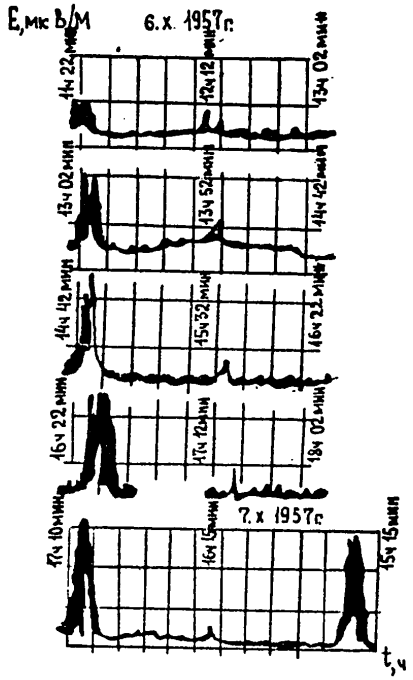

Figure 2.9

Several cases of very long-range reception (10,000-15,000 kilometers) were recorded, generally preceding antipodal signals. These signals showed an abrupt rise and fall in amplitude within 5-10 minute periods. For example, on October 8th at 5:25 p.m., i.e., 17 minutes for detection of AS, there was a case of long-range propagation (31st minute after satellite passed over Mirnyy), corresponding to a range of about 15,000 kilometers. After October 10th, signals from the first sputnik were so weak at Mirnyy that they were almost inaudible. Signals from the second sputnik were also very weak. In connection with the fact that Mirnyy's latitude and its antipode are 66°36' while the plane of the satellite's orbit has an inclination of 65° to the equator, the satellite was displaced at least 1°36' north of Mirnyy and south of its antipode (170 kilometers). In fact, minimum displacement was greater (500 to 1,000 kilometers). The satellite flew by above $h_{max}F2$ throughout the southern hemisphere about 30° SLat, including the Mirnyy region. The radius of the zone of direct radio line-of-sight from Mirnyy was capable of reaching higher values--4,000 to 6,000 kilometers. High maximums of intensity correspond to direct radio line-of-sight reception.

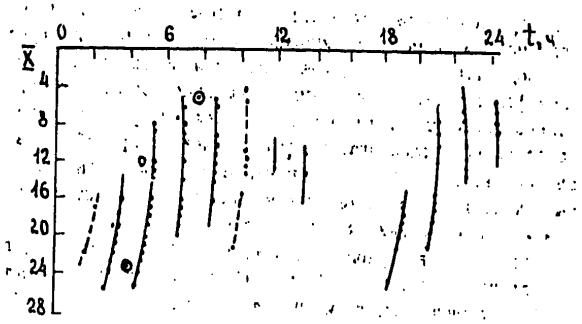

Figure 2.10

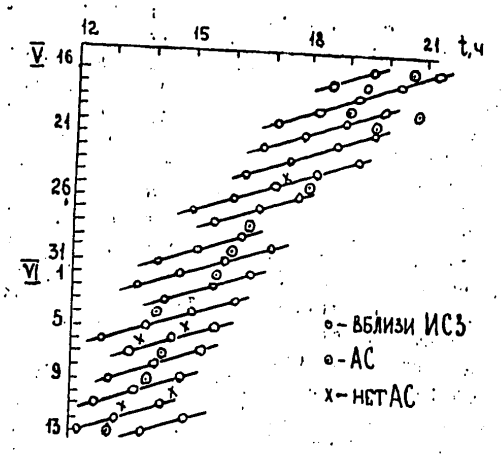

Near the satellite
Antipodal signal
No antipodal signal

Figure 2.11

Variations in these maximums are associated with diurnal change in the state of the ionosphere as well as changes in the angle of beam arrival to Earth in conformity with the range of the artificial Earth satellite from Mirnyy.

In almost all cases, when the artificial Earth satellite passed by Mirnyy on October 6-8, in the direct radio line-of-sight zone its signals were recorded. The duration of reception was 6-17 min., corresponding to the time of passage in the short-range zone. At ranges larger than the radius of the direct radio line-of-sight zone, especially from 6,000-16,000 kilometers, cases of reception are rare.

Reception of signals usually is restored at a range of 16,000-19,500 kilometers from Mirnyy. Duration of antipodal signals of 6-11 min. roughly corresponds to the time of passage of the artificial Earth satellite in the zone of the antipode at a radius less than 4,000 kilometers.

AS were received at Mirnyy in daylight hours (local daylight-saving time), when the antipode to Mirnyy was in the darkened zone and all Mirnyy-to-antipode routes intersected the day-night line. Basically, cases of antipodal reception correspond to very high values of muf over 20 MHz, in direct routes with the shortest range. There are cases, however, where muf in such routes were under 20 MHz. The loop antenna of the direction finder did not unambiguously determine the direction of the beam arrival in the horizontal plane. It was noted that the direction of beam arrival par excellence was near the NW/SE line.

Short-range reception at Mirnyy (1,000-6,000 kilometers range) corresponds to artificial Earth satellite position in the northern sector of azimuths (270-90°). Longest ranges of reception in the short-range zone relate to the eastern and western lines to the satellite and the shortest ranges--to the northern lines (330-30°) with the satellite travelling both to the NE on ascending revolutions and to the SE on descending revolutions. Long-range reception (16,000-19,500 kilometers) corresponds to a line to the satellite on the shortest routes 60-120° (NE, partially SE) and 180-300° (SW, partially NW). We can assume that the direction of signal arrival from antipodal zones in many cases differed from the direction of the shortest direct route. In particular, this is true of ranges of 1,500 kilometer from the antipode, where the antipodal effect could occur. At long ranges from the antipode, 1,500-4,000 kilometers, where the field intensifies because of horizontal focusing, we can anticipate propagation through an inverse, slightly longer route, if conditions of propagation happen to be more favorable there than in the direct route. Comparatively small damping of AS as compared to short-range signals (15-35 dB) also indicate signifciant probability of ground-based ricocheting in some sectors of the routes.

From observations at Mirnyy it follows that the antipodal effects, whose duration reaches 6-11 min. (2,500-5,000 kilometers) in a revolution, i.e. about 10 percent of the time that the satellite is located within the direct radio line-of-sight zone, is of real interest.

3.2. Reception of Antipodal Signals from Artificial Earth Satellites at Middle-Latitude Points

Antipodal signals were recorded after the launch of the first sputnik and later at several points in the US, Japan, Italy, England and other places around the world [73,-77].

In Derwood, Maryland, just outside Washington, D.C., signals were received from the first sputnik from October 4-25, 1957 at 40.005 MHz. AS were received on October 5 about 8 a.m., then on October 12 at 4:30 am and on October 24 at 4 a.m., local time (Figure 2.10); they were also received from the second sputnik, except for one week in early November. Dispersion of AS were much less than in skip propagation. In Stanford, California, antipodal signals were

received from the third sputnik in the summer of 1958 at 20.005 MHz (Figure 2.11). In the period from May 16 through June 13, 1958, the artificial Earth satellite passed over Stanford and its antipode mainly after noon and in the evening. Altitude of the artificial Earth satellite at this time was about 800 kilometers above the receiver and 1,100 kilometers in the region of the antipode, i.e., it was above the primary ionization maximum. Antipodal reception occurred in 13 cases out of 20. In the morning, the altitude of the artificial Earth satellite was 220 kilometers above the receiver and 1,800 kilometers (at apogee) above the antipode. At that time, there were only two clear cases of antipodal reception out of 17. In this experiment, an attempt was made to determine the azimuth of AS artrival.

After noon, signals came from the SE, before noon from the SW. Directions of arrival were situated in a comparatively narrow sector between SE and E and did not vary during this antipodal passage. In the period from June 14 through August 217, in 53 cases the artificial Earth satellite was near the antipode, but there was no signal reception. From August 28 through September 20, 1958, AS were received four times. On August 28, they were received early evening from the SE. In the signal spectrum, some traces correspond to different paths of passage. Best conditions for AS reception in the summer afternoon were from SE. They were received at other reception points at both 40 MHz and 20 MHz. In Japan, observations of signals from Soviet artificial Earth satellites were begun on October 5, 1957. Antipodal reception occurred when the artificial Earth satellite was at a range of 1,000-3,500 kilometers from the receiver's antipode and the duration of these signals reached 8 minutes. Sputnik I was much higher than the ionization maximum in the southern hemisphere. Reception at the antipode from Sputnik IV was noted in Florence, Italy. Long-range propagation at 20 MHz of signals from Sputnik I were noted in Bedford, Massachusetts and signals were received from Sputnik III near Boston.

In broadcasts from Sputnik I on October 8, 1957 at the Great Beddowe station in England (51°45' NLat, 0°30' ELong) at half-past midnight to 12:33 a.m. (Zulu Time), there was a world-wide echo.

3.3. Observations of Antipodal Signals from Artificial Earth Satellites in the Near-Equatorial Region

In the summer, June 16-July15,1967, an experiment was run on reception of AS from an artificial Earth satellite with a near-equatorial orbit (inclination to the plane of the equator 2.91°), at three ground-based stations situated near the equator. Because the San Marco 2 artificial Earth satellite was situated successively in regions of antipodes of the ground-based stations in each revolution, favorable opportunities for observing the antipodal effect were available. In continuation of 162 orbital revolutions of the experiment, reception at a range greater than 17,500 kilometers was recorded 115 times:

Nairobi (01°19' SLat, 36°50' ELong, Kenya)--61 times
Quito (00°37' SLat, 78°35' WLong, Ecuador)--24 times
Lima (11°46' SLat, 77°09' WLong, Peru)--30 times.

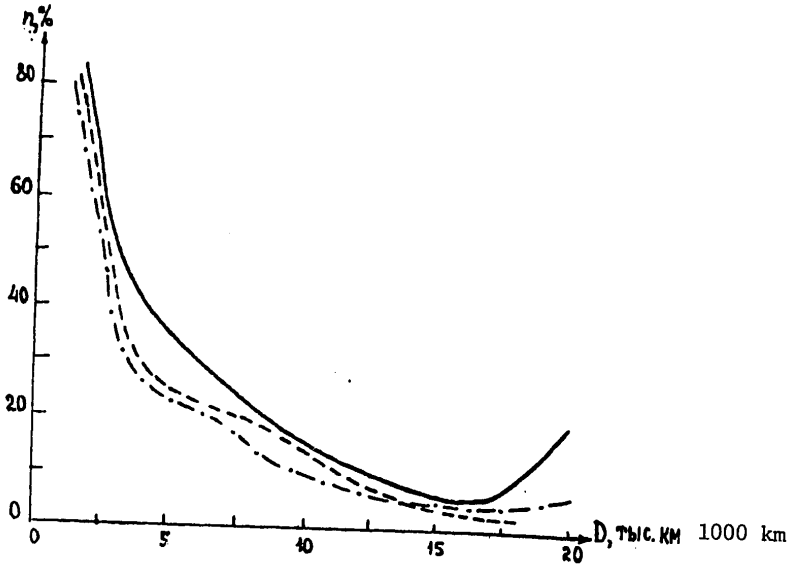

Figure 2.12

The apogee of the artificial Earth satellite was 630 kilometers, perigee was 204 kilometers. Emitted output at 20.005 MHz was about 0.6 W. Lima is located near the geomagnetic equator. Quito is roughly at the same longitude as Lima, but near the geographic equator. Relationship of the probability, expressed in percentages, of signal reception at the satellite range shown in Figures 2.12 and 2.13. According to test results, the primary maximum of antipodal reception with a probability near or greater than 40 percent occurred when the artificial Earth satellite was near the perigee below $h_{max}F2$ in the evening and near-midnight zone, and the ground-based point was in the near-noon zone. A second lower maximum of antipodal reception with a probability of 20 percent occurred when the artificial Earth satellite was at an apogee above $h_{max}F2$ in the night zone (3-8 a.m.), and the ground-based point was in the daylight zone (3-8 p.m.). From analysis of the Doppler effect, the direction of signal arrival was determined. Under optimum conditions noted above, AS chiefly passed to the west of the artificial Earth satellite and consequently, to the east of the reception point on routes with low illuminance.

Test results showed that the equatorial ionospheric anomaly is extremely favorable for antipodal propagation. So, when signals were received from San Marco 1 in January, 1965 (inclination of orbit about 38°) at four ground-based stations (0-38° SLat), only ten AS were recorded. Half of these were at the equatorial station in Quito [60].

§4. Experiment on Propagation of Signals Between an Emitter and Receiver Situated in the Ionosphere

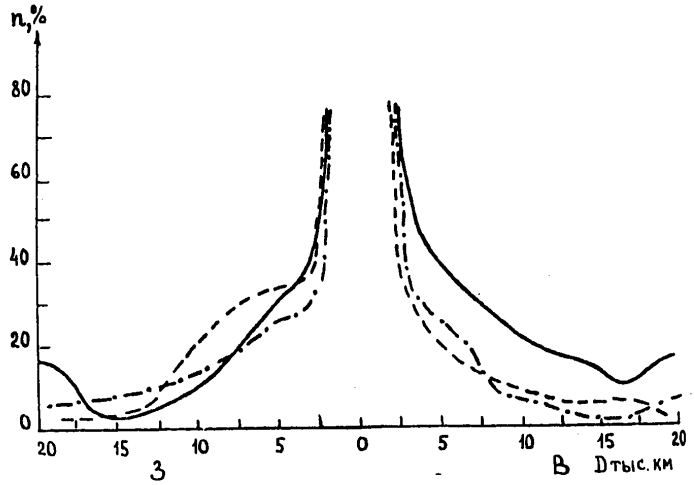

Figure 2.13 1000 km

In November-December, 1966, two satellites (OV4-1) were launched into quasi-circular orbits (apogee 300 kilometes, perigee 250 kilometers); a transmitter was installed on board one and a receiver on board the other [58]. During joint flight, the position of the satellites and range between them varied up to and including the antipodes.

Both satellites were launched on November, 3, 1966 from Cape Kennedy. The angle of orbital inclination to the equator was 30-33°. Signals were broadcasted at frequencies 20.75; 34.4; 46.8 MHz in pulsed mode with a pulse width of 1000, 100, 20 mcs successively at each working frequency. Maximum broadcasting output reached 600 W. Width of channel bandpass at each working frequency was 200 kHz. Emitting and receiving antennas were linearly polarized.

Best frequency for reception from the satellites was 34.3 MHz. In the test period (54 days), the average percentage of reception at this frequency was 63 percent.

Several cases of KS reception were recorded at a frequency of 34.3 MHz with a change in time of the circular path within 140.300 to 142.161 ms and attenuation from 3.34 to 18.22 dB.

Frequency of 20.75 MHz in signal reception from satellites was worse and was received only in two cases with a comparatively short range between satellites (angular separation 34.4° and 37.5°).

In the same cases, the frequency 46.8 MHz was received, and in three cases the angular separation of the satellites was 38.8; 75.1 and 168.8°. In most cases, apparently, the frequency 46.8 MHz was above the limiting frequency of radio wave reflection in the ionospheric duct (Chapter III, §7).

Poor passage at 20.75 MHz seems to connected with the fact that the satellite, being at altitudes of 250-300 kilometers, was usually much higher than the channel axis and conditions of input and output of energy were unfavorable. With a reduction in altitude, reception was somewhat improved, because the satellite approached the channel axis corresponding to 34.3 MHz.

Simultaneous with reception on board the artificial Earth satellite, reception at ground-based stations situated at a point of projection of the receiving satellite and the Earth, or at points closer to the transmitting satellite in the plane of the same great circle (in average points of the direct and inverse routes) was accomplished. In some cases, reception was simultaneously carried out on an aircraft flying over Florida at an altitude of about 10 kilometers.

A large number of ground-based stations participated in the experiment: Cape Kennedy (Florida), Littleton (Massachusetts), Bassenden (Australia), Bangkok (Thailand), Johnson Island, Great Bahama Island, Antigua, Asuncion, Caernarvon, Point Mugu, Hawaii. Ground-based stations measured attenuation, Doppler frequency shift, transient pulse time, and the extent of multipath emission. The best frequency in the ground-based network was 20.75 MHz.

In many cases, signals were recorded from artificial Earth satellites by other artificial Earth satellites with absolutely no reception on the ground. Although the discreteness of ground-based stations does not totally preclude skip modes which arise simultaneously with ricocheting, the results have been interpreted to be a direct experimental confirmation of artificial Earth satellite emission ricocheting, especially at 34.3 MHz.

During this period of average W, the bottom limit of f_{max} (Chapter III, §7) was about 38 MHz; thus at 46.8 MHz, in many cases, conditions could not be satisfied for radio wave reflection on the ionosphere. At 20.75 MHz, signals underwent greater absorption than at 34.3 MHz. When received on the ground, the best frequency was 20.75 MHz, because conditions for re-entry of beams to Earth were more favorable than for the higher frequencies.

Chapter III. Refraction of Radio Waves in Ionospheric Ducts

In preceding chapters, results of experimental research on ultra long-range signals and long-range signals with an emitter located in the ionosphere and some tentative results of analysis of observations, chiefly optimum conditions of propagation of radio waves, were presented. The primary task and content of the theoretical portion of this book (Chapters III and IV) is a presentation of the foundations of the extreme-parametric method of determining the characteristics of ionospheric radio ducts and some results of its utilization for analysis and derivation of theoretical estimates.

An immediate reason for early hypotheses on possible non-skip propagation of radio waves was the real difference between some characteristics of ultra long-range signals detected in the 1920s and those inherent in skip modes (propagation at frequencies much higher than standard maximum usable frequency, or muf, reduced damping, etc.). One of the first was based on observable values of KS time lags, which speculated a circular trajectory of signals at an altitude about 200 kilometers above the Earth [2]. An attempt to validate this hypothesis was made in the pre-war years by drawing upon the theory known to acoustics of an experimentally discovered "head wave", which stood over the sharp interface of two media and excited a wave inclined toward the boundary at a lesser velocity [13-14]. But in [78] it was indicated that in the actual ionosphere there are no such boundaries having an abrupt change in dielectric permeance over the expanse of the wavelength. In addition, with continuous irradiation of the Earth, a "head wave" should possess a great reserve of energy, or absorption within the ionospheric layer should be very small; in addition, a beam striking from the Earth would be unable to excite a "head wave". The limiting skip mode we can admit only in specific cases, for example, in the twilight zone (evening echo), where the increased upper limit of frequencies combines with reduced absorption.

The hypothesis of ricocheting of radio waves in the elevated ionospheric duct above the Earth, advanced in 1945 [78], provides a better explanation of test data on the passage of ultra long-range signals. The term "ricocheting" corresponds to an idealized geometric picture of beam reflection by the ionosphere similar to the "whispering gallery" known in acoustics. In the non-uniform ionosphere having smooth change of variables, beam refraction can occur leading to passage, under specific conditions, above the ground surface. It was indicated that the skip mode can shift to a ground ricochet in the twilight region, where is the layer is inclined. According to the evolved method of normal waves, the trajectory of a beam corresponds to a narrow region having finite amplitude, formed as a result of interference and dispersion of the packet of normal waves of different velocities and amplitude distribution profile along the wavefront. The probability of ricocheting increases for higher working frequencies, which can be much higher than the muf of gently-sloping beams. Furthermore, the passage of the lower boundary of beam libration above the primary absorption region of the ionosphere could qualitatively explain the low damping of ultra long-range signals. In [78-80] it was shown that it is not only the layer enclosed between two ideal boundaries, but also the medium with continously changing ε that has waveguide properties. The above-ground duct occurs when the modified index of refraction rh(r) (r is range to center of the Earth, n is index of refraction) has a peak at some intermediate level, around which may occur libration of beams. Slippage (instability with respect to refraction) was shown possible along the upper limiting boundary of beam return, and simultaneous existence of several ducts and degeneration of the above-ground waveguide is possible in the limiting case where the limits of libration merge at the highest working frequency. Beam trajectory is applicable to waveguides if the parameters of the medium slowly change along the wavelength, while the cross section of the waveguide is much longer than the wavelength in free space.

An idealized model of the modified index of refraction squared, equal to unity up to some level and then decreasing in inverse proportion to the distance to the center of the Earth cubed, was used for analytical purpses in [79].

Qualitative analysis (in general form without presumptions of the real model N(r)) of refraction conditions and rotation of beams, was done in [81], where attention was focused on the relationship of the direction of beam rotation as a function of the sign of the altitude derivative rn(r).

After the launch of the first sputnik, several features were experimentally discovered which showed the even greater role of ricochet modes in long-range radio wave propagation than when an emitter is situated on Earth. This activated theoretical research into ionospheric ducts.

The possibility of capture/escape of ricochet beams by the waveguide shown in [79] by means of horizontal ioniation gradients (ionospheric inclines) was analyzed in several studies [82-86].

A typical feature of research begun in this period is the shift from qualitative analysis to quantitative calculations for certain ionospheric models.

In the 1960s research was begun on relationships between key point parameters $r^2n^2(r)$ and N(r)—profiles [88-92] which were later used as a foundation for the extremal-parametric method of determining characteristics of ionospheric radio ducts.

In 1971, study [93] showed the possibility of qualitative study of radio wave beam trajectories in a stratified medium using the method of phase trajectories.

To account for the effect of a horizontally-irregular ionosphere on the ionospheric duct and evaluate the possibility of beam retention therein, in 1971 it was proposed to use the approximate condition of the adiabatic invariant [94]. Calculations of certain charactertistics of world-wide channels were made on that basis for an approximate model of the ionosphere which would correspond to equinox conditions of the minimum of solar activity [95, 96]. The effect of wave effects was also investigated [97, 98].

Since the early 1970s research has been active in various possible physical factors of radio wave capture/release from the ionospheric duct (see Chapter IV).

After establishing the theoretical pssibility of radio wave ricochet in ionospheric radio ducts [78], the primary task of theoretical research was the shift to quantitative analysis allowing for variations in the real ionosphere. Several methodological versions with different mathematical apparatus are possible, taking account of physical factors, initial ionospheric data, ionospheric models employed, characteristics determined, etc. For the theoretical methods designed for analysis of experiments and for prognosis, it is most important to have a combination of a comparatively simple mathematical apparatus and an adequately correct ionospheric model with availability of initial ionospheric information.

§1. Initial Assumptions of the Extremal-Parametric Method of Analysis of Characteristics of Ionospheric Ducts

Various aspects of theoretical research, whose results underly the extremal-parametric method (EPM), have been considered in several published studies [88-92, 99-104].

EPM is based on these analytical relationships: 1) key point parameters of altitude gradients of modified (allowing for sphericity of the medium) dielectric permeance $r^2\varepsilon(r)$ and electron concentration N(r); 2) the set of characteristics of radio ducts (integral, etc.) from key point parameters (extremes) $d[r\varepsilon(r)]/dr$.

The mathematical apparatus of EPM therefore permits us to determine various characteristics of radio ducts on the basis of key point parameters of the ionosphere which serve as initial ionospheric information.

Altitude variation of the modified index of refraction rn(r) and especially its extremes play an important, completely specified role in the case of refraction of radio waves and formation of ionospheric ducts. In the general case rn(r) is a non-monotonous function of altitude having extremes, as can be seen in Figure 3.1.

Thus for $u(r) = r^2n^2(r)$, we find

$$r^2n^2(r) = r^2 - \frac{r^2f_N^2(r)}{f^2},$$

where the first term smoothly increases in proportion to altitude. The non-monotonic nature occurs because of the effect of the second term which is dependent on altitude variation $f_N^2(r)$ and f--working frequency. On the other hand, with refraction of beams in a spherically-stratified medium

$$rn(r) = \frac{r_0n_0\sin\varphi_0}{\sin\varphi(r)}.$$

(The index "0" relates to the initial point of emission, φ is the angle of the beam from the vertical). After escape of a beam at angle φ_0, angle φ changes from φ_0 to a maximum value of $\varphi = \pi/2$, attained at the point of rotation. Consequently, at this point, function rn(r) acquires its smallest value in the entire interval of altitudes from the emitter to the point of rotation. The value rn(r) at this point is usually smaller than r_0n_0 and only for the angle of escape $\varphi_0 = \pi/2$ can it be $rn(r) = r_0n$. This means that rotation of upward beams can be accomplished only in a sector of decrease of function rn(r) with an increase of altitude, where $[rn(r)]'_r \leqslant 0$. In the sector of increase of function rn(r) with altitude, where $[rn(r)]'_r \geqslant 0$, rotation of downward beams is accomlished. Boundaries between sectors of rn(r) having different signs $[rn(r)]'_r$ are extremal levels of rn(r). The level r_A where rn(r) is minimum, is

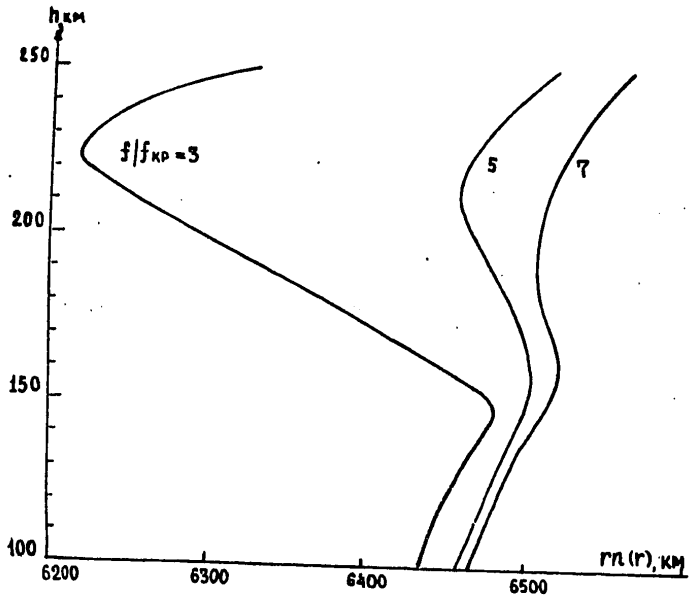

Figure 3.1

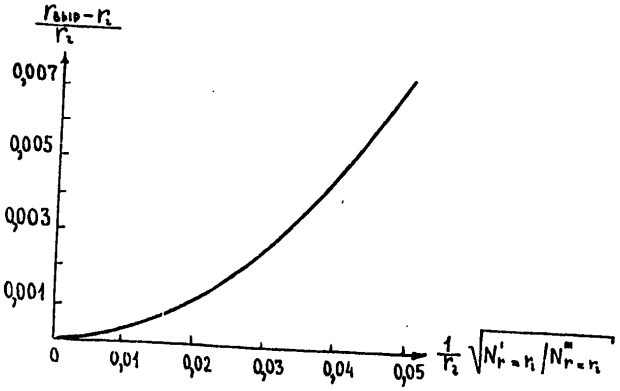

Figure 3.2

the uppermost possible boundary of the channel. The level r_B, where rn(r) is maximum, demarcates the intervals of frequencies corresponding to the upper (above r_B) and lower (below r_B) points of beam rotation. In other words, r_B is the channel axis. At this level, the angle of beams with the vertical passes through the minimum or, in other words, r_B is the geometric site of points of beam inflection. The lower boundary of low points of beam rotation r_c (lower boundary of the channel) satisfies equation $r_c n(r_c) = r_A n_A$. Since in the general case $n(r_c)$ is less than unity,

$$r_c = \frac{r_A n(r_A)}{n(r_c)} \geq r_A n_A.$$

With an increase in f, the non-monotonicity of variation in rn(r) becomes less pronounced (see Figure 3.1) and ultimately vanishes at rather high $f = f_{max}$. The minimum and maximum of rn(r) approach each other in altitude and magnitude (first drops, second rises).

In extremes u(r), the condition $u'_r(r) = 0$ is satisfied; at the level of inflection u(r), $u''_r(r) = 0$. In the limiting case of degeneration of non-monotonicity of u(r), corresponding to degeneration of the channel at the r_{degen} level, conditions of equality to zero of $u'_r(r)$ and $u''_r(r)$ should be simultaneously satisfied. These differential conditions form the initial system of expressions of the mathematical apparatus of the EPM.

An equivalent system of expressions is found after differentiation:

$$n^2(r) + \frac{r}{2}\left[n^2(r)\right]'_r = 0,$$

$$n^2(r) + 2r\left[n^2(r)\right]'_r + \frac{r^2}{2}\left[n^2(r)\right]''_r = 0,$$

$$\left[n^2(r)\right]'_r + \frac{r}{3}\left[n^2(r)\right]''_r = 0.$$

Without considering ν --the number of collisions—on the index of refraction, $n^2(r) = \varepsilon(r)$ and the equivalent system has the form:

$$\varepsilon(r) + \frac{r}{2}\,\varepsilon'_r(r) = 0,$$

$$\varepsilon(r) + 2r\,\varepsilon'_r(r) + \frac{r^2}{2}\,\varepsilon''_r(r) = 0,$$

$$\varepsilon'_r(r) + \frac{r}{3}\,\varepsilon''_r(r) = 0.$$

In the ionosphere (without considering the effect of the Earth's magnetic field)

$$\varepsilon(r) = 1 - \frac{f_N^2(r)}{f^2},$$

which permits us to write down the system in the form:

$$f_N^2(r) + \frac{r}{2}\left[f_N^2(r)\right]'_r - f^2 = 0, \tag{3.1}$$

$$\left[f_N^2(r)\right]'_r + \frac{r}{4}\left[f_N^2(r)\right]''_r - \frac{1}{2r}\left[f^2 - f_N^2(r)\right] = 0, \tag{3.2}$$

$$\left[f_N^2(r)\right]'_r + \frac{r}{3}\left[f_N^2(r)\right]''_r = 0. \tag{3.3}$$

The second expression can also be represented thus:

$$\left[f_N^2(r)\right]'_r + \frac{r}{2}\left[f_N^2(r)\right]''_r + \frac{r}{4}\frac{\left[f_N^2(r)\right]''^2_r}{\left[f^2 - f_N^2(r)\right]} = 0 . \tag{3.4}$$

From condition (3.1) we derive expressions (3.5) and 3.6) for the upper limit of frequencies of reflection in the ionosphere of a horizontal beam having initial point of escape at levels r and r_{degen}, respectively (see Chapter III, §6).

$$f_{max}(r) = \sqrt{f_N^2(r) + \frac{r}{2}\frac{d f_N^2(r)}{dr}}, \tag{3.5}$$

$$f_{max} = \sqrt{f_N^2(r_{BMP}) + \frac{r_{BMP}}{2}\frac{d f_N^2(r_{BMP})}{dr}} . \tag{3.6}$$

It follows from condition (3.4) that the level r_{degen} is located in an interval of altitudes where $[f_N^2(r)]'_r$ and $[f_N^2(r)]''_r$ have opposite signs. In other words, r_{degen} lies above r_2, corresponding to the maximum of the vertical gradient $f_N^2(r)$.

The magnitude of displacement $r_{degen} - r_2$ is determined by the expression

$$\frac{r_{skip} - r_i}{r_i} = \sqrt{1{,}2\,\frac{\left[f_N^2(r)\right]'_{r=r_i}}{\left[f_N^2(r)\right]''_{r=r_i}}\,\frac{1}{r_i^2} + 0{,}04} - 0{,}2, \qquad (3.7)$$

derived from (3.3) with approximation of variation of $f^2(r)$ in the upper vicinity of r_2 by a third-power polynomial (Figure 3.2).

An expression equivalent to (3.7) can be derived in the form:

$$\frac{r_{skip} - r_i}{r_{max} - r_i} = \sqrt{0{,}04\left(\frac{r_i}{r_{max} - r_i}\right)^2 + 0{,}6} - 0{,}2\,\frac{r_i}{r_{max} - r_i}. \qquad (3.8)$$

The difference $r_{degen} = r_2$ is usually very small (fractions and units of a kilometer), i.e., the level r_{degen} is arranged in the immediate upper vicinity of r_i.

Analysis of radio wave refraction and the effect of altitude variation rn(r) on it and its extremes showed that variation $[f_N^2(r)]'_r$ $[f_N^2(r)]''_r$ and their signs are extremely substantial in both the limiting case of degeneration and in the interval of altitudes of arrangement of channels of various frequencies. Parameters max dN/dr and the interlayer trough play an important role in shaping the qualitative and quantitative picture of radio wave propagation.

Below is presented a system of analytic relationships of parameters of extremes of the modified index of refraction from key point parameters N'(r). They include, in addition to critical frequencies f_{cr} and geometric parameters r_{max}--the geocentric range of the ionization maximum and y_m--the half-thickness of the layer, also parameters of the interlayer trough (denoted by the index M", r_M and f_M--geocentric range and plasma frequency of the minimum N in the trough) and maximum dN/dr (denoted by the index "2").

Expressions (3.9-3.12) were derived on the basis of condition (3.1) of extremes rn(r) (see Chapter III, §4.5) for combinated quadratic model N(r) (see Chapter III, §2):

$$\frac{r_A}{r_{max}} = 0{,}75 + 0{,}25\sqrt{1 - 8\,\frac{y_m^2}{r_{max}^2}\left[\left(f/f_{kp}\right)^2 - 1\right]}, \qquad (3.9)$$

$$\frac{U_A}{r_{max}^2} = \left(\frac{r_A}{r_{max}}\right)^2\left\{1 - \frac{f_{kp}^2}{f^2}\left[1 - \left(\frac{r_{max}}{y_m}\right)^2\left(1 - \frac{r_A}{r_{max}}\right)^2\right]\right\}, \qquad (3.10)$$

$$\frac{r_b}{r_M} = 0{,}75 + 0{,}25\sqrt{1 + 8p\left[\frac{f^2}{f_2^2} - \frac{f_M^2}{f_2^2}\right]}, \qquad (3.11)$$

$$r_{\max}^2 = \left(\frac{r_b}{r_M}\right)^2 \left\{1 - \frac{f_c^2}{f_b^2}\left[\left(\frac{f_M}{f_c}\right)^2 + \frac{1}{p}\left(\frac{r_b}{r_M} - 1\right)^2\right]\right\}, \tag{3.12}$$

where $$p = \frac{\left(\frac{r_c}{r_M} - 1\right)^2}{\left(1 - f_M^2/f_c^2\right)}.$$

On the basis of (3.5) and (3.6) for the same model of N(r) we find

$$\frac{f_{\max}(r)}{f_{kp}} = \sqrt{1 + \left(\frac{r_{\max}}{y_m}\right)^2 \left[3\frac{r}{r_{\max}} - 2\left(\frac{r}{r_{\max}}\right)^2 - 1\right]} \tag{3.13}$$

$$\frac{f_{\max}}{f_{kp}} = \sqrt{1 + \left(\frac{r_{\max}}{y_m}\right)^2 \left[3\frac{r_{skip}}{r_{\max}} - 2\left(\frac{r_{skip}}{r_{\max}}\right)^2 - 1\right]} \tag{3.14}$$

Analytical relationships of certain characteristics of ionospheric channels as a function of parameters of extremes of the modified index of refraction are cited in Chapter IV. To determine the integral characteristics of channels we used a combined quadratic model u(r) described in Chapter III, §3. The combined quadratic models of N(r) and u(r), as shown in §2.3 of Chapter III, take into account features of the altitude variation of these functions and their derivatives in the neighborhood of the extremes, which is necessary to derive adequately correct qualitative picture and estimates.

Therefore, the mathematical apparatus of EPM includes a series of analytical expressions making it possible to determine various characteristics of ionospheric channels as a function of key point parameters N'(r), which are initial. Among the latter are critical frequencies and geometric parameters of the F2 layer, according to which there are extremely accessible global prognostic materials constructed on the basis of years of data from the world-wide network of ionospheric stations. The EPM can be used both for analysis of experiments and for prediction in the field of long-range and ultra long-range propagation of radio waves in ionospheric ducts.

§2. Combined Quadratic Model of Altitude Variation of Electron Concentration

The distribution of electron concentration in the ionosphere N(r) directly affects refraction and various characteristics of radio wave propagation. The greatest effect on the qualitative picture and quantitative values of characteristics are exerted by key point sectors $[N(r)]'_r$, lying near the extremes and the level of inflection N(r) and containing the bulk of information on altitude variation of N(r) and its derivatives. Zero values of $[N(r)]'_r$ correspond to levels of maximum and minimum concentration, while the maximum $N_r(r)$ corresponds to the level r of inflection of N(r) (see Figure 3.3).

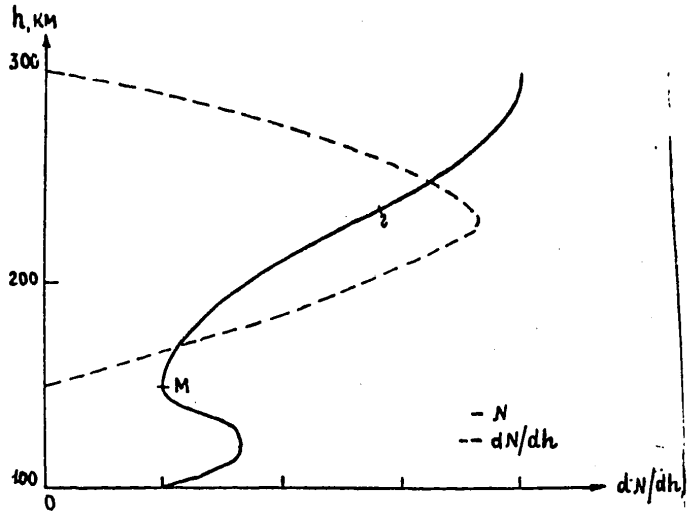

Figure 3.3

Key point parameters are initial in the system of analytic expressions for calculating various characteristics of ionospheric channels. The correct analytical model of N(r) profile should yield the correct position of the key point extremal levels $N'_r(r)$. But this requirement is not satisfied by single models of N(r) usually utilized. These single models of N(r) as linear, quasilinear, parabola, quasiparabola, exponent, etc. generally have no intermediate point of inflection at the level of r_2 corresponding to the maximum of N'_r. Other single models of N(r) have fixed position of r_2-level with respect to the apex (level of maximum N) and the origin of the layer where N = 0. So, the r_2-level is situated in the upper part of the layer of the Epstein model, in the middle of a quadratic sinusoid, and the lower part of a biparabola of the Chapman model. Indeed, as shown by analysis of measured N(r)-profiles, $r_{max} - r_2$ undergoes significant variation, roughly from 10-100 kilometers and there is no unique connection between r_2 and r_{max} and y_m. Single models of N(r) do not provide approximation of the upper part of the trough, since they do not contain f_{cr}, h_{max} and y_m, and the trough parameters do not figure in. In most single models of N(r), they are at a very low initial level of N = 0, whereas indeed the minimum of N in the trough has a finite value. These shortcomings are completely related to quasilinear and quasiparabolic models of N(r) in which it is possible to derive analytical expressions for the integral characteristics of radio wave propagation. Therefore, not one of the known idealized single models of N(r) can be given preference as most precise and universal, i.e., suited for any conditions [105].

As an illustration, let us consider the effect of a parabolic single model of N(r) on the qualitative picture and some characteristics of radio wave propagation. Altitude variation of rn(r) for this single model is shown in Figure 3.4. The highest values of rn(r) occur at the origin of the layer $r = r_{max} - y_m$ independent of f. At this level $[rn(r)'_r] \neq 0$, i.e., the condition of the maximum rn(r) is not

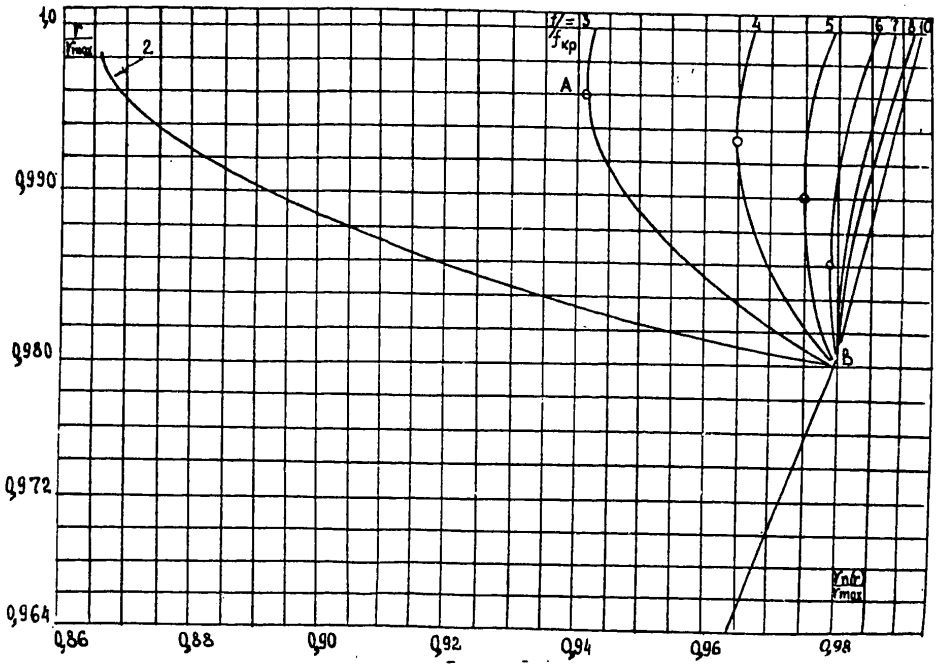

Figure 3.4

satisfied. In the upper neighborhood of the initial level, the curve has its convexity downward, not upward, as it should in the upper neighborhood of the maximum. In other words, $[rn(r)]''_r$ has a sign inverse to that which it should have. At the initial level, where N = 0, lie the points of inflection of any trajectories for different f_p. Indeed, points of beam inflection lying on the channel axis are displaced upward with an increase in f (Chapter III, §1). Angles between the beam and the channel axis are different for different f_p and can differ from theoretical values for a parabolic single model. The upper limit of frequencies of beam reflection in the channel f_{max} for this model corresponding to the origin of the layer is most often exaggerated (Chapter III, §6), because the level of degeneration lies above the origin of the layer. For a parabolic single model, the interval of beam oscillation in the ionosphere monotonically decreases as the beam approaches the initial layer level. However, as shown in Chapter IV, §3, the interval of oscillation, as the beam approaches the channel axis, must pass through an intermediate minimum and then slowly increase to its final limiting value. Similar distortions of the qualitative picture and quantitative estimates can arise not only when a parabolic single model is used, but also with other models of N(r).

Inclusion of parameters of the maximum of N'_r and the "trough" in the single model of N(r) could lead to a rise in the power of polynomials by several units and consequently, to such complication of calculations that would make them

poorly suited for practical use. It is better to reject single models and use the combined model of N(r) instead; it consists of discrete approximations above and below r_2, assuring the drop and rise of N'_r in proportion to r, respectively.

To approximate the variation of N(r) above the level of channel degeneration up to and including r_{max} of layer F, it is advantageous to use a fragment of the parabola directed with its convexity downward with its peak at the level of r_{max}

$$f_N^2(r) = f_{kp}^2 \left[1 - \frac{(r_{max} - r)^2}{y_m^2}\right], \qquad (3.15)$$

where the half-thickness of the layer y_m is a parameter inversely proportional to the root of N''_r:

$$y_m = \frac{r_{max} - r_2}{\sqrt{1 - (f_2/f_{kp})^2}} = \sqrt{2}\,\frac{\sqrt{N_{max}}}{\sqrt{[N(r)]''_{r=r_{max}}}}. \qquad (3.16)$$

The upper part of the "trough" from the r_M-level of the minimum of f_N to the r_H-level, where $f_N = f_E$, should be approximated by a fragment of an inverted (i.e., convexity upward) parabola:

$$f_N^2(r) = f_M^2 - \frac{(f_2^2 - f_M^2)}{(r_H - r_M)^2}(r - r_M)^2. \qquad (3.17)$$

In the altitude interval $[r_2, r_M]$ situated in the lower part of the F-layer, a necessary and adequate approximation is the complete third-power polynomial which, having four coefficients, assures the continuity of N(r) and $N'_r(r)$ at both ends of the interval and link-up with any approximations of N(r) in contiguous sectors

$$f_N^2(r) = f_E^2 + a(r - r_H) + \frac{(-2a - A + 3B)}{(r_2 - r_H)}(r - r_H)^2 + \frac{(a + A - 2B)}{(r_2 - r_H)}(r - r_H)^3,$$

where $a = \min [f_N^2(r)]'_r$ when $r = r_H$,

$A = \max [f_N^2(r)]'_r$ when $r = r_2$,

$B = \dfrac{f_2^2 - f^2E}{r_2 - r_H}$.

The coefficient "B" does not depend on models of N(r) in adjacent section. However, these models do affect the numerical values of the coefficients "a" and "A". Thus, in the special case where the upper segment of N(r) is approximated by a segment of a parabola with its apex at the level r_{max} of the F layer

$$A = 2\frac{(r_{max} - r_t)}{y_m^2}(f_{xp})^2 = 2\frac{(f_{xp}^2 - f_t^2)}{(r_{max} - r_t)}.$$

In approximating N(r) in the upper part of the trough by a segment of an inverted parabola with its peak at the level r_M

$$a = 2\frac{(f_t^2 - f_M^2)}{(r_t - r_M)}.$$

A significant shortcoming of the third-power polynomial is the lack of opportunity to derive formula relationships to determine channel axis variables appearing in certain waveguide characteristics, including angular characteristics of capture and release.

Thus a quadratic model of N(r) below r_2 should be used to guarantee satisfaction of the primary condition: an increase in N'_r in proportion to r.

This model can be a segment of the inverted parabola with its peak at the r_M level

$$f_N^2(r) = f_M^2 + \frac{(f_t^2 - f_M^2)}{(r_t - r_M)^2}(r - r_M)^2. \qquad (3.18)$$

In this combined model, both parabolas have the necessary opposing signs of curvature above and below the r_2 level of maximum of $N'_r(r)$.

Reciprocally inverted quasiparabolas, convenient for calculating integral characteristics of radio wave propagation, can also be utilized

$$f_N^2(r) = f_{xp}^2\left[1 - \frac{(r_{max} - r)^2}{y_m^2} \cdot \frac{(r_{max} - y_m)^2}{r^2}\right], \qquad (3.19)$$

$$f_N^2(r) = f_M^2 + (f_t^2 - f_M^2)\frac{(r - r_M)^2}{(r_t - r_M)^2} \cdot \left(\frac{r_t}{r}\right)^2. \qquad (3.20)$$

To derive analytical relationships of parameters of the extremes of rn(r) from key point parameters of N(r), we use the aforementioned combined model of N(r) consisting of segments of reciprocally inverted parabvolas. Therefore, key point parameters $[N(r)]'_r$ are initial for calculation of various characerstics of ionospheric channels defined by the EPM. Thus the study of the entire set of

key point parameters of $[N(r)]'_r$ is a vital problem.

Variations in critical frequencies of ionosphere layers and geometric parameters of the F2-layer based on analysis of many years of observations in the world-wide network of ionospheric stations, have been studied the most thoroughly [70]. Data on variations of parameters of the N'_r maximum of the interlayer F/E-region can be derived on the basis of analysis of N(r)-profiles recorded by methods of airborne measurement, non-coherent scattering, etc., and in the future, obtained from vertical probing ionograms based on solution of the inverse problem.

From the condition of continuity of $f_N^2(r)$ and $[f_N^2(r)]'_r$, appearing in the combined model, at the r_2-level max $[f_N^2(r)]'_r$ we find:

$$r_1 = r_{max} - \frac{y_m^2}{(r_{max} - r_M)}\left(1 - \frac{f_M^2}{f_{kp}^2}\right), \tag{3.21}$$

$$\frac{f_1^2}{f_{kp}^2} = 1 - \frac{y_m^2}{(r_{max} - r_M)^2}\left(1 - \frac{f_M^2}{f_{kp}^2}\right)^2, \tag{3.22}$$

$$\left[f_N^2(r)\right]'_{r=r_1} = \frac{2 f_{kp}^2\left(1 - \frac{f_M^2}{f_{kp}^2}\right)}{(r_{max} - r_M)}. \tag{3.23}$$

These formulas allow us to determine parameters of the maximum vertical ionization gradients in terms of known parameters of the prime maximum of ionization and the interlayer minimum (trough).

§3. Combined Quadratic Model of Altitude Variation of Modified Dielectric Permeance

The qualitative picture of radio wave propagation and validity of quantitative estimates of their characteristics can be assured only if we consider actual altitude variation $u(r) = r^2n^2(r)$. Consideration of the signs of $u''_r(r)$ in intervals of altitudes limited by extremes and points of inflection of u(r) corresponding to the real variation of u(r) is very important, as is a precise definition of the position of these levels and their appropriate magnitudes. Thus, variation u(r) governs all integrals of characteristics of radio wave propagation, because u(r) appears in subintegral expressions and determines the limits of integration.

The combined quadratic model of u(r) is more advantageous to use than the quasiparabolic models $f_N^2(r)$ to determine integral characteristics (intervals of beam oscillation, etc.) and derive analytic expressions. Parameters of the quadratic model are altitude and magnitudes of extremes and points of inflection of u(r). The combined model includes several models, each of which approximates a specific altitude interval, within which u(r) has monotonic variation and $u''_r(r)$ retains its sign [99].

For example, in the interval $[r_A, r_п]$

$$u(r) = u_A + (u_п - u_A)\frac{(r_A - r)^2}{(r_A - r_п)^2}, \tag{3.24}$$

in the interval $[r_п, r_B]$

$$u(r) = u_б - (u_б - u_п)\frac{(r - r_б)^2}{(r_п - r_б)^2}, \tag{3.25}$$

in the interval $(r_B, r_п1)$

$$u(r) = u_б - (u_б - u_{п1})\frac{(r_б - r)^2}{(r_б - r_{п1})^2}. \tag{3.26}$$

The indexes п and п1 correspond to points of inflection of u(r) above and below the level of the channel axis r_B, respectively. At altitudes where n^2 is approximately equal to unity, for example below 100 kilometers, $u(r) = r^2$ can be taken.

With this approach, the integral characteristics are expressed as the sum of integrals for the corresponding intervals of altitudes.

The quadratic nature of the model u(r) makes it possible to reduce integrals to tabular form and derive analytic expressions for the integral characteristics. Theoretical formulas are simpler and contain less parameters (e.g., f does not appear in them in manifest form) than when using models of N(r).

Expressions for altitudes of rotation of beams necessary when calculating specific integrals can be found by using the condiition of rotation u(r) = V, where $V = r_0^2 n_0^2 \sin^2 \varphi_0$ (index '0' corresponds to initial point of beam escape).

For the upper point of rotation

$$r_б = r_A - (r_A - r_п)\sqrt{\frac{V - u_A}{u_п - u_A}} \tag{3.27}$$

where $u_A \leq V \leq u$, when $r_B \geq r$.

For more gently sloping beams reflected below $r_п$ where $u_п \leq V \leq u_B$

$$r_б = r_B + (r_п - r_B)\sqrt{\frac{u_б - V}{u_б - u_п}}. \tag{3.28}$$

The position of lower points of rotation is defined by the expression

$$r_н = r_б - (r_б - r_м)\frac{\sqrt{u_б - V}}{\sqrt{u_б - u_м}} \qquad (3.29)$$

where $V \geq u_M$.

The index "M" corresponds to the level of minimum f^2_N of the trough or (with some exaggeration) to the level of inflection $r_{п1}$, lying on its lower branch.

At point $r_п$ of inflection u(r)

$$u''_r(r) = 0$$

or

$$\left[f^2_N(r)\right]'_r + \frac{r}{2}\left[f^2_N(r)\right]''_r + \frac{r}{4}\frac{\left[f^2_N(r)\right]'^2_r}{\left[f^2 - f^2_N(r)\right]} = 0. \qquad (3.4)$$

In the section of monotonic increase of $f^2_N(r)$, as r increases the first and third terms of this equation have positive signs; consequently, at the $r_п$-level the second term should be negative. In the interval of altitudes $[r_M, r_з]$, this condition is not satisfied. The condition is satisfied only in the neighborhood of $r_з$, lying above this level, i.e., $r_п > r_з$. The level $r_п$ is constrained on top by the r_{degen} level of degeneration of extremes of u(r). Thus the level $r_з$ approximately (with some underestimation) can be taken as $r_п$.

The combined model of u(r) is equivalent to the combined model of $f^2_N(r)$.

In the interval $[r_п, r_B]$

$$u(r) = r^2\left[1 - \frac{f^2_N(r)}{f^2}\right] = u_б - (u_б - u_п)\frac{(r - r_б)^2}{(r_п - r_б)^2},$$

$$f^2_{N\,зкв}(r) = f^2\left\{1 - \left[\frac{u_б}{r^2} - \frac{(u_б - u_п)}{r^2}\frac{(r - r_б)^2}{(r_п - r_б)^2}\right]\right\}.$$

In other words, f^2_N eq(r) is approximated above and below $r_п$ by the quasi-parabolas

$$f^2_{N\,зкв}(r) = A + \frac{B}{r} + \frac{C}{r^2}.$$

The level of $r_A(f)$ is the upper limit of the interval of altitudes for $f^2eq(r)$ at a given f; $r_B(f)$ is the lower limit.

Comparison of equivalent models of u(r) of quasiparabolas $f^2_Neq(r)$ with initial parabolas of $f^2(r)$ showed that at key point extreme levels r_A, r_B, $r_п \approx r_э$, both models yield completely coinciding values of f^2_N. The greatest differences in the middle part of these intervals of altitudes do not exceed 0.1 percent of the greatest values of f^2_N in the interval of altitudes; in most cases they lie within about 0.01 to 0.1 percent and monotonically decrease in inverse proportion to working frequencies, near the limiting working frequencies of channel degeneration, they reach zero values. $\Delta f^2_N = f^2_Neq - f^2_N$ are positive above $r_п$ and decrease in direct proportion to y_m.

Therefore, the quadratic model of u(r) is adequately valid, and also permits us to derive analytic expressions for the set of integral refraction characteristics of radio wave propagation.

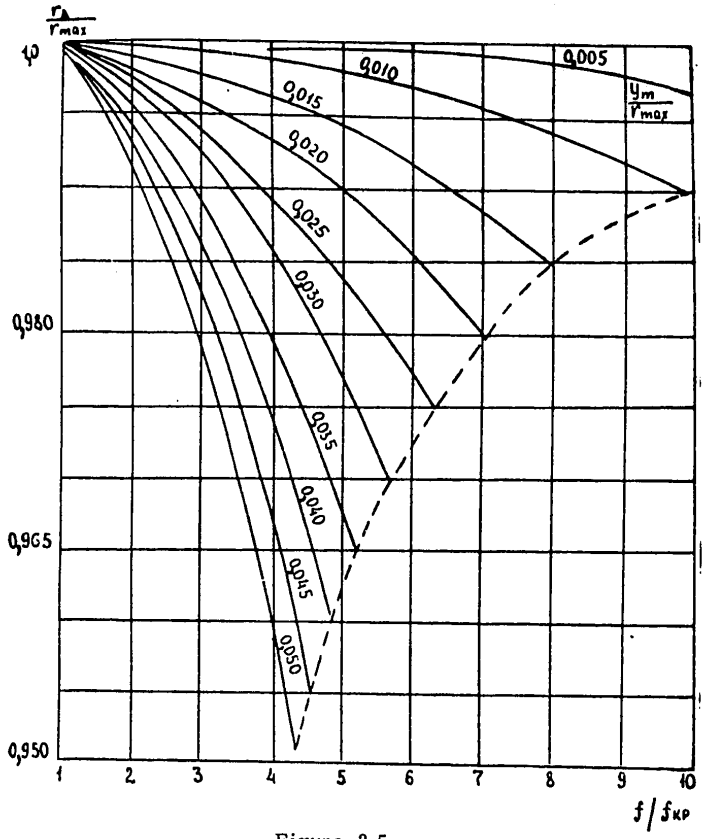

Figure 3.5

§4. Limiting Boundaries of Channels. Magnitudes of Minimum of Modified Index of Refraction

The upper limiting boundary of the ionospheric channel is the r_A-level, corresponding to the minimum of rn(r) [88].

Using condition (3.1) of the extreme of rn(r), cited in §1 of Chapter II and the parabolic model of N(r) in the altitude interval $[r_{max}, r_2]$ (Chapter II, §2), we find expression (3.9):

$$\frac{r_A}{r_{max}} = 0.75 + 0.25 \sqrt{1 - 8 \frac{y_m^2}{r_{max}^2} \left[(f/f_{kp})^2 - 1 \right]} . \qquad (3.9)$$

This relationship is shown graphically in Figure 3.5. The ratio of $r_A : r_{max}$ decreases in indirect proportion to f/f_{cr} and y_m/r_{max}.

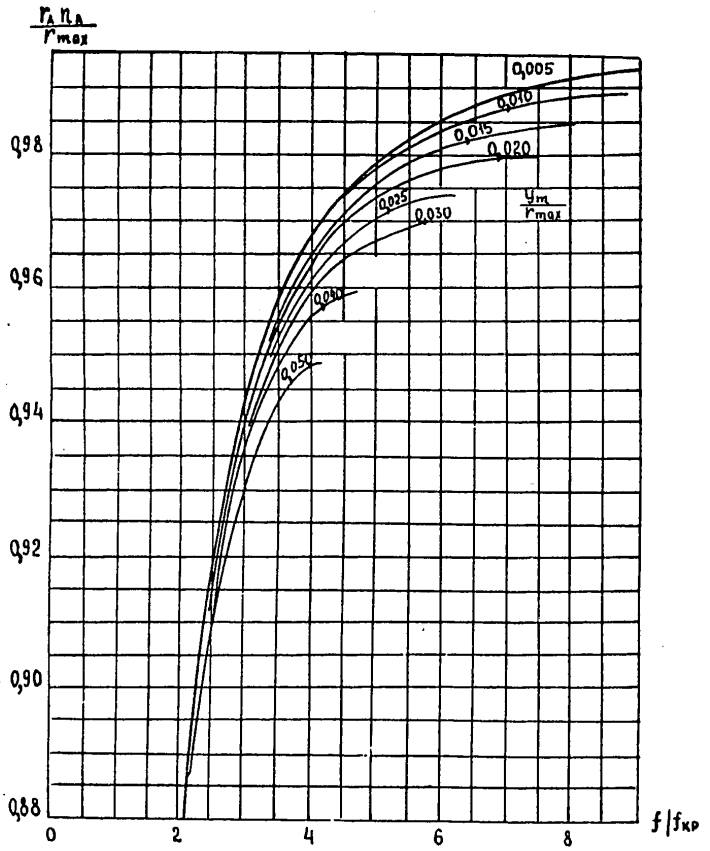

Figure 3.6

The lower limiting boundary of the ionospheric channel is the level r_c, which lies below the r_B-level of the maximum of rn(r), in which $r_c n_c = r_A n_A$. At the level r_c, the limiting, steepest beam should be reflected, having an upper point of rotation at the r_A-level.

$$r_c = \frac{r_A n_A}{n_c} .$$

For beams whose lower points of rotation are at levels where n is approximately equal to unity (e.g., at low N at h less than 100 kilometers), $r_c \simeq r_A n_A$.

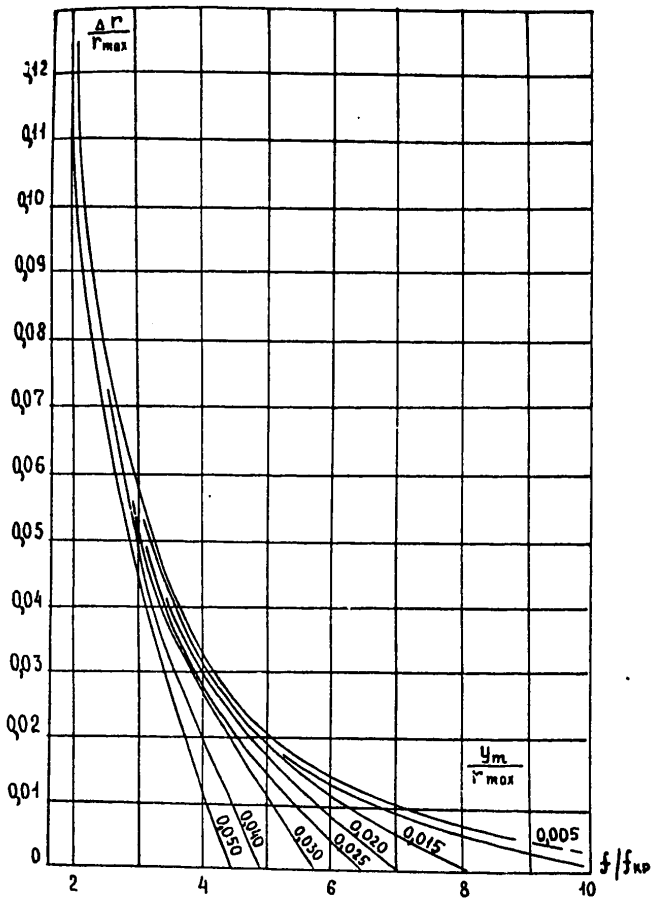

Figure 3.7

In cases where the low points of rotation are displaced toward levels having great N in proportion to an increase in f_p, n_c becomes slightly less than unity. If we take $n_c = 1$ in these cases, i.e., $r_c = r_A n_A$, we find the lower boundary of the channel with slight underestimation. Therefore, the quantity $\sqrt{u_A} = r_A n_A$ generally yields the limiting lower level for the lower boundary of the channel. For the same parabolic model of N(r), we find

$$n_A = \sqrt{1 - \frac{f_{kp}^2}{f^2}\left[1 - \left(\frac{r_{max}}{y_m}\right)^2\left(1 - \frac{r_A}{r_{max}}\right)^2\right]}$$

and the analytical expression (3.10) to determine $r_A n_A / r_{max}$.

The relationship is graphically shown in Figure 3.6 ($r_A n_A / r_{max}$ as a function of f/f_{cr} and y_m/r_{max}).

As f/f_{cr} increases, the quantity $r_A n_A / r_{max}$ increases.

The limiting upper magnitude for the vertical dimension of the channel is determined by the difference

$$\Delta r = r_A - r_A n_A.$$

The relationship of $\Delta r/r_{max}$ as a function of f/f_{cr} and y_m/r_{max} is graphically shown in Figure 3.7. With a fixed value of f, Δr decreases in direct proportion to f_{cr} and inverse proportion to y_m. At fixed ionospheric parameters, Δr decreases in inverse proportion to f_p, striving toward zero when f approaches f_{max}.

As a function of the initial conditions of beam escape, the vertical range between the upper and lower envelopes of trajectory can, to some extent, be less than the specific dimensions of the channel.

So, in the case of adequately gently-sloping trajectories, the cross section of the channel is

$$\delta r = \sqrt{u_b - V}\left[\frac{(r_n - r_b)}{\sqrt{u_b - u_n}} + \frac{(r_b - r_M)}{\sqrt{u_b - u_M}}\right]. \qquad (3.30)$$

§5. Axes of Ionospheric Ducts. Magnitudes of Maximum of Modified Index of Refraction.

The axes of channels corresponding to the r_B-level of the maximum of rn(r) play an important role in refraction of beams in the ionosphere. Libration of beams takes place on both side of the axis; the upper and lower points of beam rotation

are arranged above and below the axis, respectively. The level r_B is, for all trajectories at a fiven f_p, the geometric locus of points of inflection, displaced along the axis as a function of initial conditions. The quantity $r_B n_B$ of the maximum of rn(r) and its level appear in analytic expressions for defining many characteristics of ionospheric ducts, including the refraction key point characteristics of capture/escape and integral ones considered in Chapter IV. Hence it follows that r_B and $r_B n_B$ are parameters which have to be defined to allow for various ionospheric conditions and working frequencies [91, 100].

The lower limiting boundary for r_B-levels is the r_M-level of the minimum of N in the interlayer E/F-region [90].

Using condition (3.1) of the extreme of rn(r) and approximating the upper part of the trough by a segment of the inverted parabola (i.e., convexity directed downward) with its peak at the r_M-level

$$f_N^2(r) = f_M^2 + \frac{(f_E^2 - f_M^2)}{(r_H - r_M)^2}(r - r_M)^2 \quad , \tag{3.17}$$

(the index "H" corresponds to the upper point of the trough, where $f_N = f_E$) we find an analytical expression for radio wave reflection on the F-layer:

$$\frac{r_B}{r_M} = 0{,}75 + 0{,}25\sqrt{1 + 8K\left[\frac{f^2}{f_E^2} - \frac{f_M^2}{f_E^2}\right]} \quad , \tag{3.31}$$

where

$$K = \left(\frac{r_H}{r_M} - 1\right)^2 \frac{1}{1 - f_M^2/f_E^2} \quad .$$

For this same model of $f_N^2(r)$, the expression for the index of refraction n_B at the r_B-level is derived in the form

$$n_B = \sqrt{1 - \frac{1}{(f/f_E)^2}\left[\left(\frac{f_M}{f_E}\right)^2 + \frac{1}{K}\left(\frac{r_B}{r_M} - 1\right)^2\right]} \quad .$$

The expression for estimating the upper limit of frequencies f of upper radio waves for which the axes r_B of ducts pass in the trough if derived under the assumption in (3.31) that $r_B = r_H$:

$$\frac{f_{\text{верхн}}}{f_E} = \sqrt{\frac{1}{8K}\left[\left(\frac{r_H/r_M - 0.75}{0{,}25}\right)^2 - 1\right] + \frac{N_M}{N_E}} \quad . \tag{3.32}$$

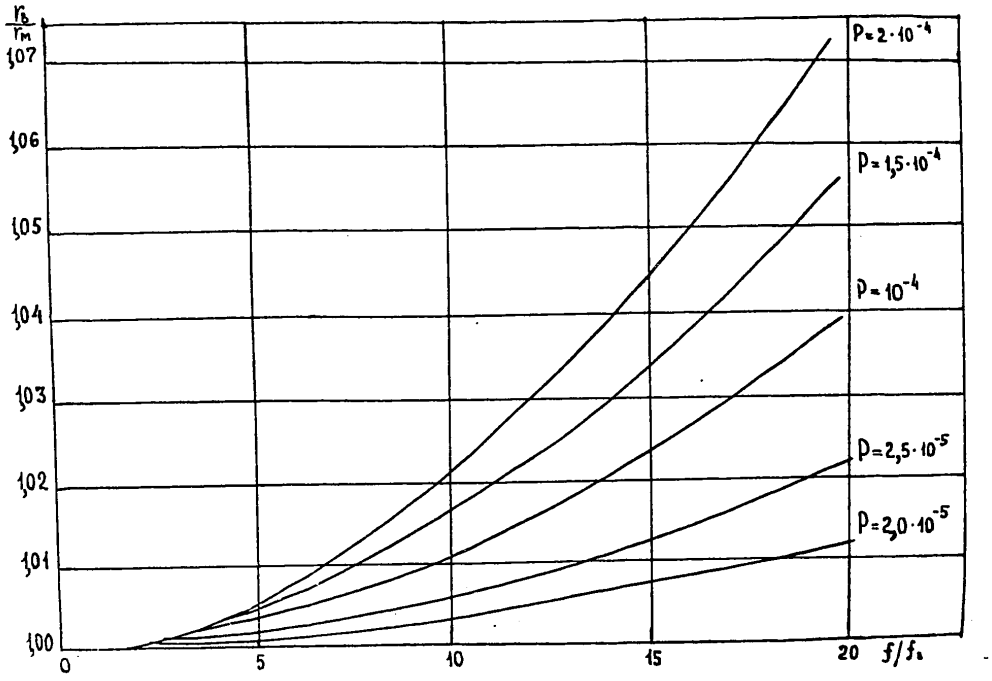

Figure 3.8

As working frequencies increase, $f_p \geq f_{up}$-levels of r_B are displaced into the F-region up to and including the level r_{degen} (degeneration of waveguides), lying somewhat higher than the r -level of the maximum of N'_r. For analysis of variations in r_B and $r_B n_B$ in the F-region in the altitude interval $[r_H, r_\tau]$, condition (3.1) of the extreme of rn(r) can be used as well as the model approximating the variation of N(r) in this interval. By using the complete third-power polynomial with its four coefficients assuring increase in $N'_r(r)$ in direct proportion to r and the continuity of N(r) and $N'_r(r)$ at ends of the interval (a fit with any superincumbent or subincumbent segments of N(r)), we find the complete third-power equation which is satisfied by the r_B-level. The great shortcoming of this apprxoimation is the impossibility of deriving clear formula relationships for r_B and $r_B n_B$. We thus use the model of N(r) in the form of an inverted parabola with its apex at the level r_M, passing through the r_τ-level, assuring satisfaction of the prime condition: increase in $N'_r(r)$ in direct proportion to r. For this model we find that

$$n_B = \sqrt{1 - \frac{1}{(f/f_1)^2}\left[\left(\frac{f_M}{f_1}\right)^2 + \frac{1}{p}\left(\frac{r_B}{r_M} - 1\right)^2\right]},$$

where

$$\frac{r_B}{r_M} = 0{,}75 + 0{,}25\sqrt{1 + 8p\left[f^2/f_t^2 - f_M^2/f_t^2\right]}, \qquad (3.11)$$

$$p = \left(\frac{r_t}{r_M} - 1\right)\frac{1}{1 - f_M^2/f_t^2}$$

The relationships r_B/r_M and $r_B n_B/r_M$ as a function of f/f_τ for different p are graphically illustrated in Figures 3.8 and 3.9.

The formula and graphic relationships of r_B and $r_B n_B$ as a function of key point parameters $N'_r(r)$ and f may be utilized in solving various problems of radio wave refraction of radio waves in the ionosphere.

§6. Upper Limit of Frequencies of Reflection of Radio Waves in the Ionosphere

The upper limit of frequencies of reflection of radio waves in the ionosphere depends on the N(r)-profile and initial conditions of beam escape. Using the law of refraction in a spherically symmetric medium:

$$r n(r) \sin\varphi = r_0 n_0 \sin\varphi_0,$$

$$f(r) = f_N(r)\sqrt{\frac{1 - \frac{f_0^2}{f_N^2(r)}\frac{r_0^2}{r^2}\sin^2\varphi_0}{1 - \frac{r_0^2}{r^2}\sin^2\varphi_0}},$$

where f_N and f_0 are frequencies of ionospheric plasma at the point of rotation and near the emitter, respectively.

In the case of a ground-based transmitter ($r_0 = a$, $f_0 = 0$) and emission at angle ψ to the Earth's surface

$$f(r) = f_N(r)\sqrt{\frac{1}{1 - \frac{a^2}{r^2}\cos^2\psi}},$$

or

$$\text{muf} = \max f(r)$$

$$\text{МПЧ} = \max_{\text{muf}}\left[f_N(r)\sqrt{\frac{1}{1 - \frac{a^2}{r^2}\cos^2\psi}}\right],$$

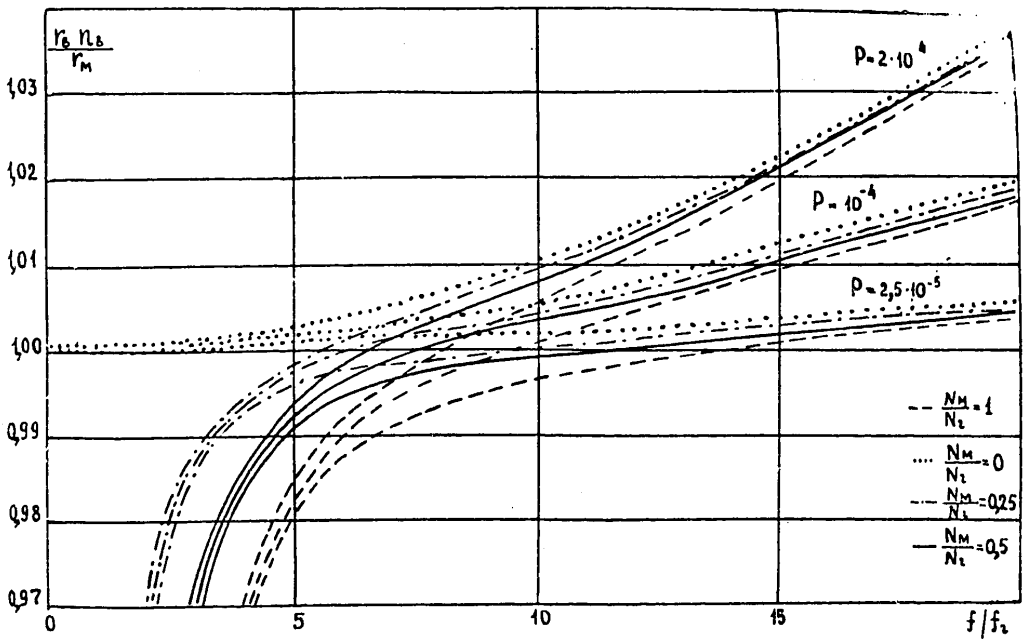

Figure 3.9

the level of rotation r satisfies the condition of the extreme

$$\frac{d}{dr}\left[f_N^2(r)\sqrt{\frac{1}{1-\frac{a^2}{r^2}\cos^2\psi}}\right]=0,$$

$$\left[f_N^2(r)\right]'_r\left[1-\frac{a^2\cos^2\psi}{r^2}\right]-\left[f_N^2(r)\right]2\frac{a^2\cos^2\psi}{r^2}=0.$$

For a parabolic model of the layer, we find the complete fourth-power equation with respect to r/r_{max}:

$$\left(1-\frac{r}{r_{max}}\right)\frac{r}{r_{max}}\left(1-\frac{\frac{a^2\cos^2\psi}{r^2_{max}}}{\left(\frac{r}{r_{max}}\right)^2}\right)+\left(1-\frac{r}{r_{max}}\right)^2\frac{\frac{a^2\cos^2\psi}{r^2_{max}}}{\left(\frac{r}{r_{max}}\right)^2}-$$

$$-\frac{\frac{a^2\cos^2\psi}{r^2_{max}}}{\left(\frac{r}{r_{max}}\right)^2}\left(\frac{y_m}{r_{max}}\right)^2=0,$$

$$\frac{muf}{f_{KP}} = \sqrt{\frac{1-\left(\frac{r_{max}}{y_m}\right)^2\left(1-\frac{r}{r_{max}}\right)^2}{1-\frac{a^2\cos^2\Psi}{r^2_{max}}\left(\frac{r}{r_{max}}\right)^2}},$$

Muf / f_{cr} also satisfies the condition of the minimum of rn(r)

$$\frac{a\cos\Psi}{r_{max}} = \frac{r_A}{r_{max}}\sqrt{1-\frac{f_{KP}^2}{(muf)^2}\left[1-\left(\frac{r_{max}}{y_m}\right)^2\left(1-\frac{r_A}{r_{max}}\right)^2\right]}.$$

Hence

$$\frac{muf}{f_{KP}} = \sqrt{\frac{1-\left(\frac{r_{max}}{y_m}\right)^2\left(1-\frac{r_A}{r_{max}}\right)^2}{1-\frac{a^2\cos^2\Psi}{r^2_{max}}\left(\frac{r_A}{r_{max}}\right)^2}}. \qquad (3.33)$$

That is, the maximum of the product

$$f_N(r)\sqrt{\frac{1}{1-\frac{a^2}{r^2}\cos^2\Psi}}$$

corresponds to $r = r_A$.

The relationship of muf/f_{cr} as a function of $a\cos\Psi/r_{max}$ and y_m/r_{max} is graphically illustrated in Figure 3.10. In the general case of an emitter located in the ionospheric plasma, the expression for f_{max} of a horizontal beam escaping at level r_0 can be derived by means of the limiting transition

$$f_{max} = \lim_{r\to r_0,\ \varphi_0\to\frac{\pi}{2}} f(r).$$

By transition to the limit of the ratio of the first derivatives of the numerator and demonator of the expression for $f^2(r)$, we find

$$f_{max} = \sqrt{f_N^2(r_0) + \frac{r_0}{2}\frac{d}{dr}f_N^2(r_0)}. \qquad (3.5)$$

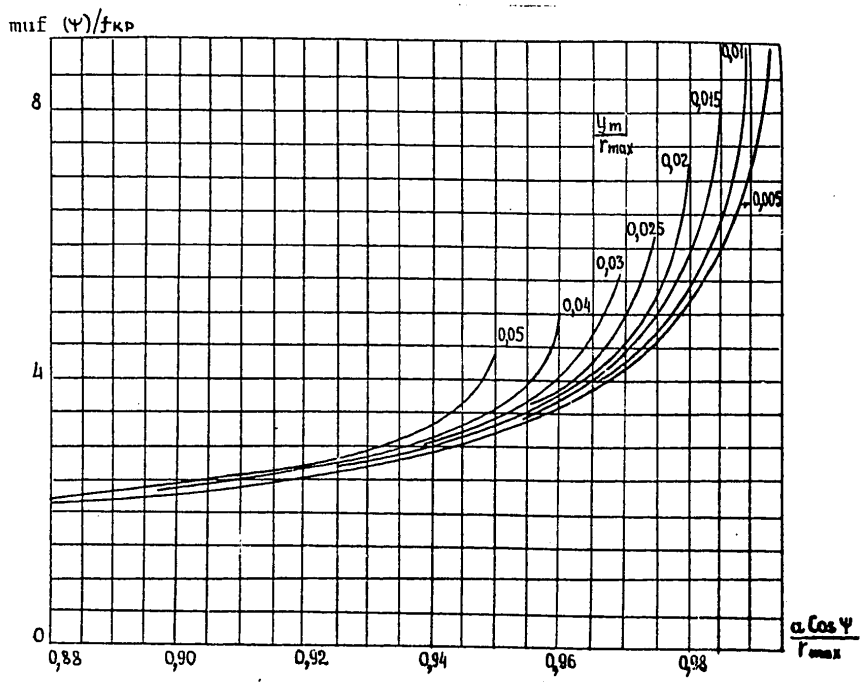

Figure 3.10

The expression for f_{max} can also be derived from the condition

$$r_A(f_{max}) = r_0 ,$$

because when r_A approaches r_0 and φ_0 approaches $\pi/2$, i.e., all beams entering the upper emission hemisphere cease being reflected in the ionosphere, starting with some frequency f_{max}.

After performing a differentiation of the left side of the condition of extreme levels of rn(r)

$$n(r) + r\frac{dn(r)}{dr} = 0,$$

we find the following equivalent condition

$$f^2 = f_N^2(r) + \frac{r}{2}\frac{d f_N^2(r)}{dr} , \qquad (3.34)$$

is valid for $r = r_A$.

When $r = r_A = r_o$, it follows that $f = f_{max}$; f_{max} therefore depends on the altitude of the emitter of the vertical variation of electron concentration $f^2(r)$. The expression for f_{max} can be derived for any analytic model of $f^2(r)$ [89, 92].

For example, using the parabolic model of the layer represented in the form:

$$f_N^2(r) = f_{KP}^2 \left[1 - \left(\frac{r_{max}}{y_m}\right)^2 \left(1 - \frac{r}{r_{max}}\right)^2\right].$$

for which

$$\frac{d f_N^2(r)}{dr} = 2 f_{KP}^2 \left(\frac{r_{max}}{y_m}\right)^2 \left(1 - \frac{r}{r_{max}}\right) \frac{1}{r_{max}},$$

we find

$$f_{max} = f_{KP} \sqrt{\left\{1 + \left(\frac{r_{max}}{y_m}\right)^2 \left[3 \frac{r_o}{r_{max}} - 2\left(\frac{r_o}{r_{max}}\right)^2 - 1\right]\right\}}. \qquad (3.35)$$

This relationship is graphically illustrated in Figure 3.11. The highest value of f_{max} is found at the level of the origin of the parabolic layer where $r_o = r_{max} - y_m$

$$f_{max} = f_{KP} \sqrt{\frac{r_{max}}{y_m} - 1},$$

f_{max} varies widely as a function of the altitude of the emitter and the parameters of the layer.

When the emitter is located near r_{max}, it follows that $f_{max} \simeq f_0F2$. With a reduction in r_o, f_{max} approaches muf_o and $f_{max} = \mathrm{muf}_o$ at the level $r_o = r_A$ (muf_o). When r_o is less than r_A(muf_o), f_{max} is greater than muf_o.

The highest value of f_{max} for the given ionospheric conditions is achieved when the emitter is located at the level of degeneration r_{degen} of the extremes of rn(r). The expression which is satisfied by r_{degen} can be derived from the condition of the maximum of f^2_{max}

$$\left.\begin{aligned} &\frac{d f^2_{max}(r)}{dr} = 0, \\ &\frac{d f_N^2(r)}{dr} + \frac{r}{3} \frac{d^2 f_N^2(r)}{dr} = 0. \end{aligned}\right\} \qquad (3.3)$$

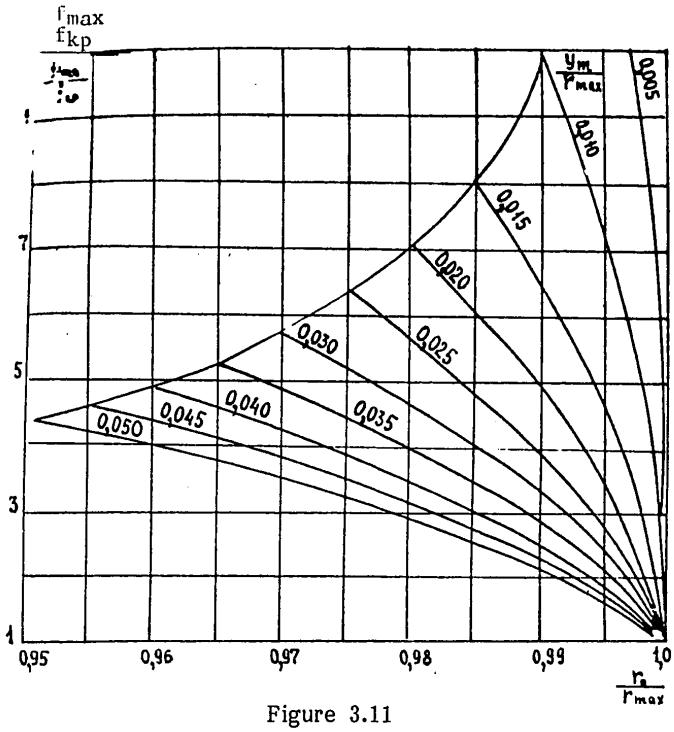

Figure 3.11

The level r_{degen} lies above the $r\zeta$-level of the maximum of $\text{grad}f_N^2$ and even higher than the origin of the parabolic layer.

When $\varphi = \pi/2$, the level of rotation r satisfies condition $rn(r) = r_0 n_0$. As long as the emitter continues to remain above the Earth, f_{max} is greater than muf_0.

In the limit where the transmitter reaches the Earth's surface, f_{max} is less than or equal to muf_0.

From the condition $r_A(f)$ and $n_A(f) = a\cos\Psi$, it is possible to graphically derive relationships for the parabolic model of the layer (Fig. 3.10)

of muf_0/f_{cr} as a function of y_m/r_{max} and $a\cos\Psi/r_{max}$.

It follows from Figure. 3.11 that f_{max} can be several times greater than muf_0, especially for small y_m/r_{max}.

Idealized models are unsuitable for estimating f_{max}, however. For that purpose it is necessary to utilize existing data on N(r)-profiles under diverse conditions derived by experimental means. In a non-monotonic profile of N(r), where there exist several layers each of which has an f_{max}. In the general case, they are

not equal and the greatest of them yields the limiting f_{max} for reflection in the entire thickness of the ionosphere. In other words, as working frequency increases there may be successive degeneration of channels located below N_{max} of various layers. In extensive routes, the actual upper limit of frequencies is constrained by the minimum of f_{max} in the route.

Additional constraints may be imposed by the following factors: the limited nature of the upper limit of frequencies of receiving and transmitting equipment, location of the artificial Earth satellite below or above r_{degen}.

In ground-based reception, because of the need to guarantee re-entry of beams, the measured upper limit fo frequencies can be much lower than f_{max} near the artificial Earth satellite and even the minimum value of f_{max} on the route. So, the re-entry of ricocheting beams to Earth because of refraction is assured at working frequencies, primarily not exceeding muf near the receiver. The latter constraint plays no role if the receiver is located on board the artificial Earth satellite near the waveguide.

§7. Limiting Frequencies of Degeneration of Ionospheric Ducts

One of the important characteristics of conditions of ricocheting of radio waves in the ionospheric duct is the limiting working frequency f_{max}, a point at which the channel degenerates. Variations in f_{max} in various sections of a horizontally-heterogeneous ionosphere at various times result from fluctuations in N(r)-profiles. The formula for calculation of f_{max} contains a level of r_{degen} of degeneration, $f_N^2(r_{degen})$ and $[f_N^2(r)]'_r = r_{degen}$ which satisfy the condition (3.3).

For estimates of f_{max}, we can also use parameters of the maximum N'_r appearing in the formula

$$f_{max} \simeq \sqrt{\frac{N(r_1)}{1.24 \cdot 10^4} + \frac{r_1}{2} \cdot \frac{1}{1.24 \cdot 10^4} \cdot \left[\frac{dN(r)}{dr}\right]_{r=r_1}}. \qquad (3.36)$$

This considers that the level r_{degen} is usually close to the r_η-level of the maximum of N'_r and somewhat lower than the first subradical term because $N(r_\eta)$ is less than $N(r_{degen})$. The first multiplier of the second term ($r_\eta < r_{degen}$) is neutralized by the higher value of N'_r at the level r_η than at the level r_{degen}.

Some results of calculation of f_{max} and f_{max}/f_0F2 on the basis of N(r)-profiles derived in recent years by various experimental methods are cited below (measurements using noncoherent scattering, etc.).

According to the set of theoretical estimates [92, 105], both f_{max} and f_{max}/f_0F2 fluctuate widely, undergoing latitudinal, seasonal, diurnal, cyclical

(according to W) and other variations. The greatest values of f_{max} about 90 MHz and f_{max}/f_0F2 about 10 were derived at W_{max} in the winter, about noon, in middle latitudes. In other words, f_{max} may be almost four times greater than m_uf under the same ionospheric conditions. The smallest values of f_{max} roughly equal to 12 MHz (or less) and f_{max}/f_0F2 roughly equal to 3 were obtained for high-latitude regions during intensive ionospheric and magnetic perturbation. In the highest auroral activity, according to data of the high-latitude station Chatanik (Alaska), during August 4-9, 1972 there can be degeneration of the maximum of N at altitudes in the F-region (i.e., monotonic drop in N in inverse proportion to altitudes); in conseqence, there is, in effect, complete degeneration of the ionospheric duct over the entire range of working frequencies [107]. Calculations made for other ionospheric conditions yield values of f_{max} and f_{max}/f_0F2 which lie between those mentioned above. So, at middle latitutdes during periods of average and low W for two seasons, the absolute values of f_{max} varied from 60-20 MHz, reaching the highest values in winter (about noon) and summer (during the night) in the period of average W. The ratio of f_{max}/f_0F2 varied from 5 to 10. The highest values were attained at night. The amplitude of diurnal variations is much greater in summer than in winter [105]. (Figs. 3.12, 3.13).

At low W in winter (at midnight) over all geomagnetic latitudes (0-75° NLat), f_{max} is about 18-22 MHz, while at noon f_{max} ranges from 37 (at Φ = 0 and 75°) to 49 MHz (at Φ = 50°).

At high W, the ratio of f_{max}/f_0F2 ranges from 3.5 to 5 in summer and from 4.5 to 7.5 in winter [92].

Calculations for a high-latitude point, according to measurements of N(r)-profiles in 1971-1973 yielded values of f_{max} which fluctuated widely from 12 to 71 MHz and f_{max}/f_0F2 from 3.12 to 8.7. There is a well-expressed tendency toward a reduction in these quantities with increase in auroral activity and ionospheric magnetic perturbation. Under comparatively calm and mildly perturbed conditions, f_{max} is roughly equal to 71-17 MHz and f_{max}/f_0F2 is roughly equal to 8.7 to 4.0. In periods of intense perturbation, from August 4-9, 1972, f_{max} and f_{max}/f_0F2 dropped, fluctuating from 44-121 MHz and 6.88-3.12, respectively.

In recent years there has been an increase in the amount of ionospheric information obtained by various methods. For some periods, positive results have been achieved in developing global models of the ionosphere. This made it possible to plotting global distribution charts of f_{max}. Because the N(r)-profile, especially in the portion adjoining the bottom of $h_{max}F$, undergoes longitudinal geomagnetic effects, in some measure this affect f_{max} as well. Therefore, an adequate form of the global representation of f_{max} may be the isolines on the world maps for fixed physical points in time. However, allowing for today's availability of ionospheric data, the global distributions can be roughly represented as a relationship of f_{max} as a function of local time. An example of this map for the minimum of W in equinox with unperturbed ionospheric conditions is given in Figure 3.14 [106].

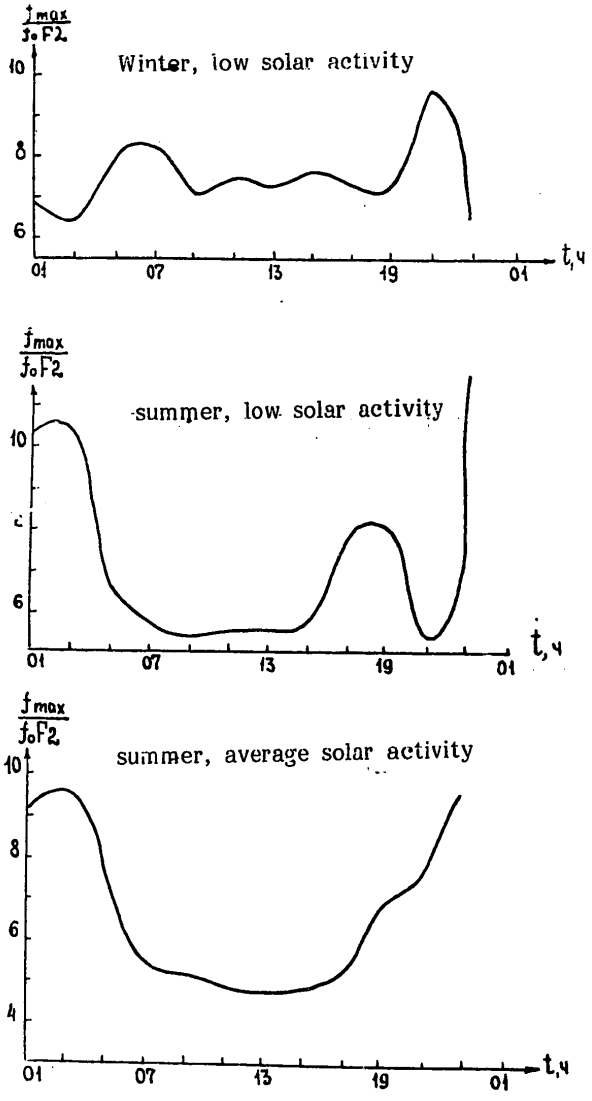

Figure 3.12

In general, f_{max} fluctuates between 20 and 80 MHz, undergoing significant latitude and diurnal variations, reaching its highest values in the near-equatorial region during transition from daylight conditions to night (in the twilight zone). Asymmetry with respect to noon occurs for the equatorial region, where during transition from night to day, the values of f_{max} are much lower (on the order

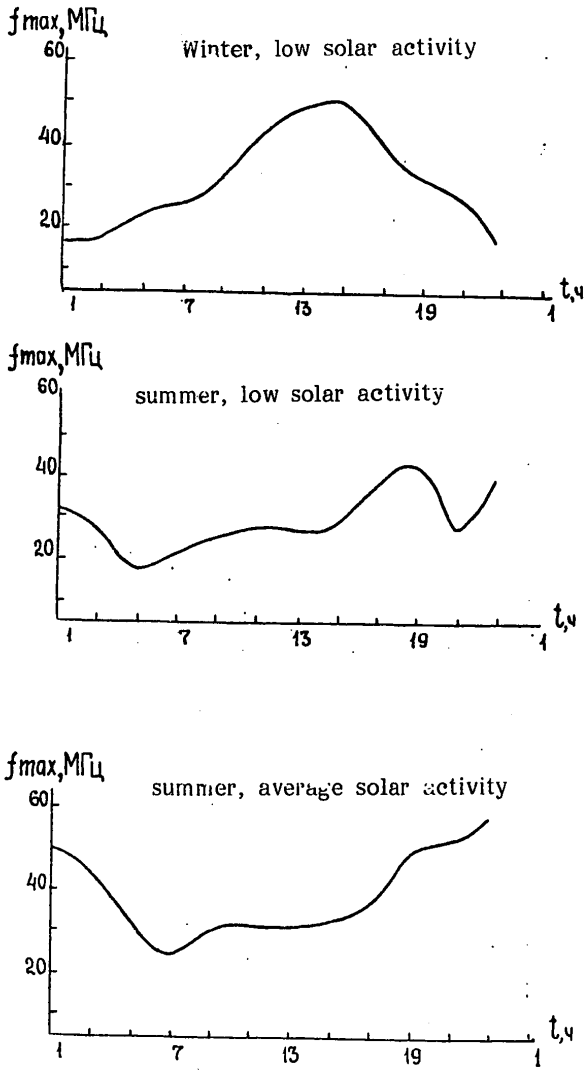

Figure 3.13

of 20-40 MHz). This characteristic takes on extremely low values in the midnight period in auroral regions of the northern and southern hemisphere.

With increased W from 10-100, f_{max} can increase by more than 10 MHz.

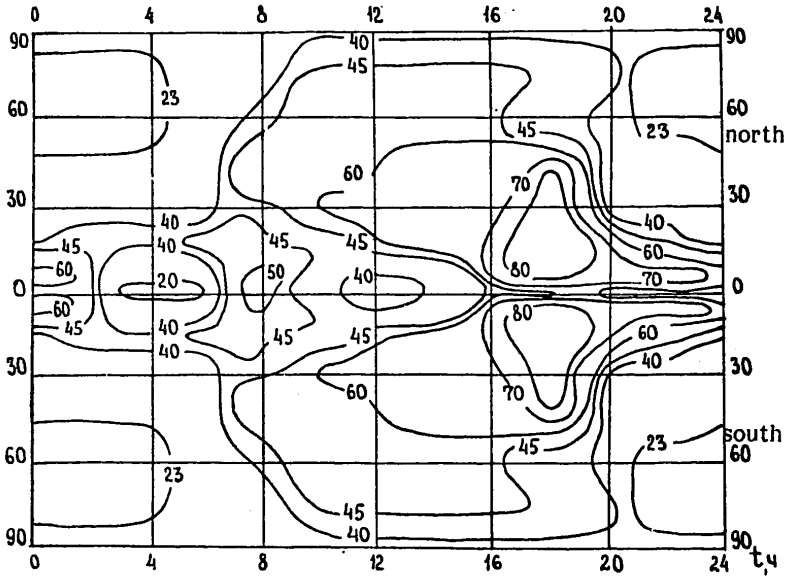

Figure 3.14

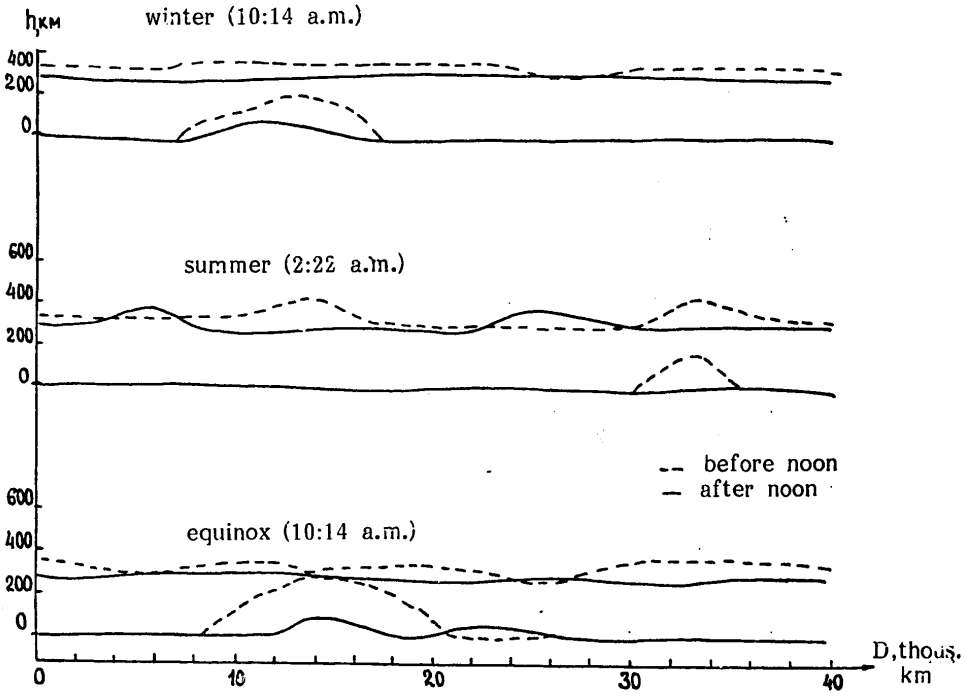

Figure 3.15

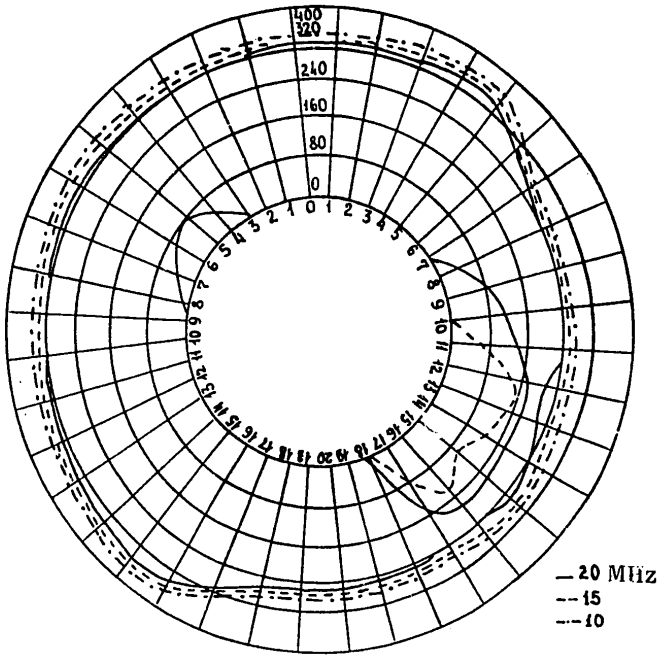

Figure 3.16

These global distributions are of particular interest in analysis and prognosis of conditions of long-range super-refraction of radio waves when the emitter and receiver are located on Earth, and even more so in the ionosphere. The upper limit of frequencies of radio wave reflection on the ionosphere in a horizontally heterogeneous route can not be higher than the minimum value.

Figure 3.16 corresponds to the great circle passing through the middle-latitude point of azimuth 160° for June, 1970 at 4:30 p.m., local daylight-saving time. At frequencies 20 and 15 MHz, the channel is ground-to-ground; at 10 MHz, it is completely ground-based [92].

Chapter IV

Some Characteristics of Ionospheric Channels

Theoretical analysis of characteristics of ionospheric channels using computer is continued in this chapter. Refraction angular characteristics of capture of radio waves by ionospheric channels is considered (as well as their escape) when an emitter is located on the Earth's surface or in the ionosphere.

Several studies have been devoted to investigating various physical causes of capture/escape in order to gain practical application of the merits of the duct mechanism of propagation. Study is continuing of the horizontal gradient of electron concentration [79, 82-85] by one of the first possible causes of of capture/escape indicated in the literature. In the 1970s, it was found possible to have refractory geometric-optical capture/escape even without horizontal gradients or localized heterogeneities of ionization because of horizontal gradients in the magnetic field H and the effective number of collisions ν_{eff} leading to horizontal gradients in the index of refraction of radio waves in the ionosphere [108]. Analysis was started of conditions of capture with the aid of heterogeneity artificially created by the emitted wave per se or another wave [94]. It was shown that the parameters of duct channels corresponding to different magnetic ion components can generally be extremely different [109, 110]. It was shown possible to excite a horizontally heterogeneous channel with a Pedersen beam slipping along its upper boundary [111, 112]. Other possible causes of capture which might be different irregularities of the ionosphere were also studied: small-scale [113], undulating ionospheric perturbations (VIV)[108, 115], large-scale [116], and others. The following possible causes of capture have been specified: horizontal gradient, large (as compared to wavelength) localized heterogeneity, periodic or random distributed heterogeneity, artificial heterogeneity. Study was begun into perturbations in the ionosphere formed by the motion of the solar terminator [116].

The possible capture (extraction) by the ionospheric channel of radio waves scattered by meteor traces was examined in studies [117, 118]. The level of the meteor signal, all other things being equal, is commensurate with the signal level from the regular ionosphere in single-skip propagation and is almost two orders greater than the level of ionospheric scattering of radio waves. A positive factor is the possibility of reflection by meteor traces of radio waves of extremely high frequencies; this should not reduce the upper limit of the frequency range of super-refraction of radio waves.

In [118], it was experimentally proven possible to extract radio waves from ionospheric channels by scattering on meteor traces in the absence of conditions of extraction due to ionospheric inclines.

In addition to the refraction characteristics of capture/escape, we shall take a look at the integral characteristics of ionospheric channels below (parameters of beam oscillation, cluster and phase paths, absorption, etc.).

§1. Refraction Characteristics of Capture and Re-entry of Radio Waves by Ionospheric Ducts

Let us consider the angular and frequency characteristics of capture of emission by the ionospheric channel defined by conditions of beam refraction in the ionosphere.

In the region outside of the duct, at levels below its rn(r) less than $r_A n_A$ and above the duct rn(r) greater than $r_A n_A$.

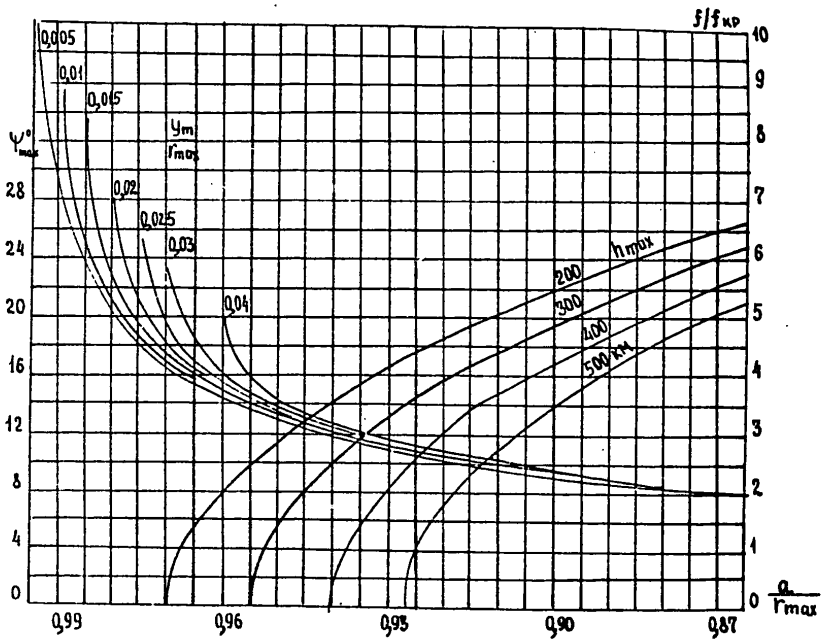

Figure 4.1

In the first case (ground-based emitter), any beam, regardless of its origin and bearing, by undergoing only ordinary refraction in a spherically-symmetric medium, intersects the duct and exits into the exterior region of the ionosphere. In the second case (aerospace emitter), the most gently sloping beams (rn sin φ greater than or equal to $r_A n_A$) will be reflected above r_A into the exterior region, while steeper beams (rn sin les than $r_A n_A$) will intersect the duct and fall to Earth.

In other words, the potential possibility of capture and escape occurs when a deflecting factor of some physical nature is located within the duct. When the deflecting factor is outside the channel, the required deflection of the refracted beam for channel-capture can be diminished somewhat. One of the refractory characteristics of channel-capture is the angle of beam escape Ψ above the Earth's surface at which the beam can be reflected at the upper channel boundary level, i.e., not emerge from it while still in the initial section.

Another important characteristic of capture is the minimally necessary angle δ of deflection of a beam toward the horizontal from the direction of ordinary refraction, i.e., additional rotation at which it will be retained in the channel.

In considering refraction in a spherically-symmetric section of the ionosphere, we find that [101]: Ψ = arc cos $r_A n_A/a$, where a is the Earth's radius. Because $r_A n_A$ increases in direct proportion to f_w, then Ψ monotonically rises. At a fixed f_w, Ψ depends on f_{cr}, h_{max}, y_m, i.e., on N(r)-profile which undergoes significant changes. The relationship of Ψ as a function of these parameters is graphically illustrated in Figure 4.1.

For the required angle of additional rotation of the refracted beam at any level r within the duct, we find the expression

$$\delta_p(r,f) = \arcsin \frac{r_A n_A}{r n(r)} - \arcsin \frac{r_0 n_0 \sin \varphi_0}{r n(r)}. \qquad (4.1)$$

The index "0" correspond to initial conditions of emission. Thus, $r_0 n_0 \sin \varphi_0 = a$ for a beam escaping tangentially toward the Earth's surface. The index "p" denotes ricocheting. For a fixed f-post., the quantity $\delta p(r)$ is a non-monotonic function of altitude. On the axis of the channel, $\delta(r)$ passes through the minimum, while at the boundaries (where $rn(r) = r_A n_A$), it passes through the maximums:

$$(\delta_p)_{min} = \arcsin \frac{r_A n_A}{r_B n_B} - \arcsin \frac{r_0 n_0 \sin \varphi_0}{r_B n_B}, \qquad (4.2)$$

$$(\delta_p)_{max} = \arccos \frac{r_0 n_0 \sin \varphi_0}{r_A n_A}. \qquad (4.3)$$

For the case of radio wave slippage along the r_B-level, allowing for the fact that the refracted beam intersecting this level at some angle must be deflected from the horizontal, we find that

$$\delta_c = \arccos (r_0 n_0 \sin \varphi_0 / r_B n_B). \qquad (4.4)$$

Examples of the calculated graphic relationships of $(\delta p)_{max}$ and δ_c as a function of key point parameters of the N(r)-profile, initial conditions of emission and working frequencies are shown in Figures 4.2 and 4.3.

Figure 4.2 corresponds to $r_0 n_0 \sin \varphi_0 = a$, i.e., tangential to the Earth's surface from a ground-based transmitter or the angle φ_0 = arc sin $(a/r_0 n_0)$, if the transmitter is located above the surface.

Figure 4.3 shows the relationship of δ_c as a function of $f/f_{\text{л}}$, p and $f_M/f_{\text{л}}$, where $p = (r_{\text{л}}/r_M - 1)^2/(1 - f^2_M/f^2_{\text{л}})$. In a concrete example, $r_0 n_0 \sin \varphi_0 = 0.976$ r_M, which corresponds to $r_0 n_0 \sin \varphi_0 = a$ where h_M = 150 kilometers.

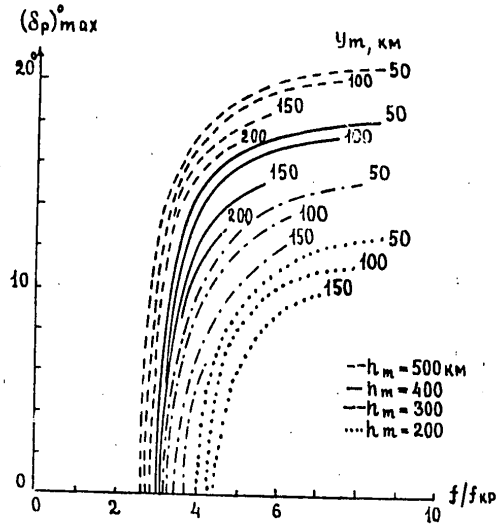

Figure 4.2

The necessary angles of additional rotation calculated according to the formulas cited above often greatly exceed the angles of regular ionospheric inclines, especially at high working frequencies. This indicates the important role of physical factors in realization of capture. For cases where capture factors (e.g., ionospheric heterogeneity) can be viewed as equivalent to some plane screen inserted into the ionosphere and reflecting incident beams, we find the following expressions for estimating the angles of the screen with the horizontal, assuring capture in the channel

$$\Delta_p(r, f) = 0.5 \arccos \frac{r_0 n_0 \sin \varphi_0}{r n(r)} + 0.5 \arccos \frac{r_A n_A}{r n(r)}, \qquad (4.5)$$

$$\Delta_c(f) = 0.5 \arccos \left(r_0 n_0 \sin \varphi_0 / r_b n_b\right). \qquad (4.6)$$

Expression (4.5) corresponds to ricocheting, (4.6)—to slippage along the channel axis. The physical nature of this equivalent plane screen can be extremely diverse. For example, it may be ionization heterogeneities oriented along magnetic force lines; ionized meteor traces; undulating ionospheric disturbances forming periodic or quasi-periodic spatial structures, etc. The angular refraction and frequency characteristics of emission capture by the ionospheric duct have mainly been defined by the parameters and latter's configuration, which results from the space-time global distribution of electron concentration. Relationships derived on the basis of analysis can be utilized for estimating capture in the channel using some physical factor with known angular, frequency and other characteristics. Analysis of test data on KS (Chapter I, §4) showed that under optimum conditions of KS reception near the point of emission and reception,

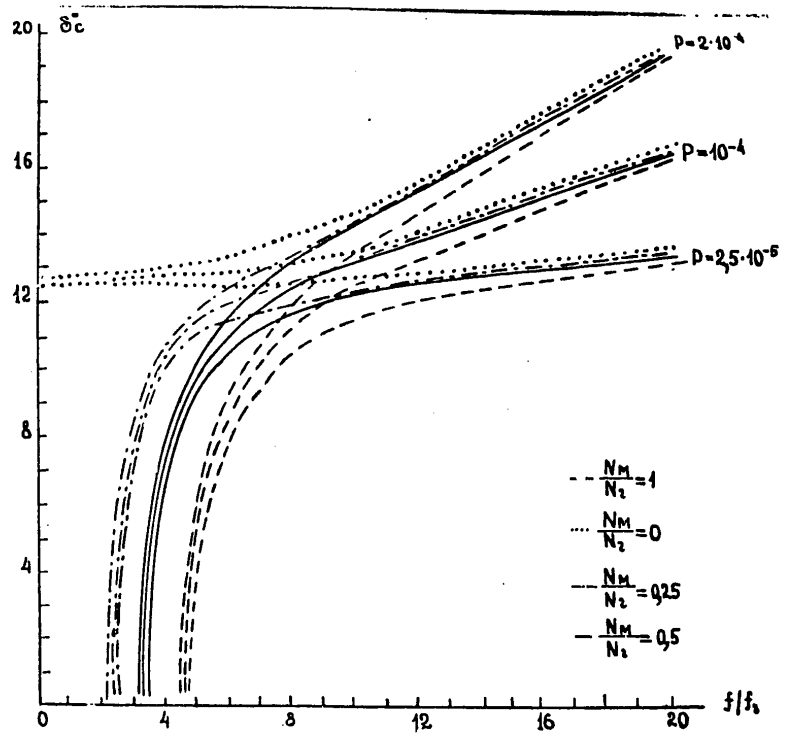

Figure 4.3

f_0F2 were higher, f_0E were lower, and there were no substantial ionospheric layer inclines ($\partial f_0F2/\partial D$ less than 0.5 MHz/1,000 kilometers)[38]. This confirms the functional relationship derived for angles of additional rotation as a function of f_0F2 and indicates the possibility of capture not only due to horizontal gradients of H. The qualitative evaluation suggests that the horizontal gradient can play the role of a capture factor if it has the proper sign: N at a fixed level decreases toward the receiver. Fulfillment of this condition depends both on the ordinarily complex global distribution of N which undergoes time variations as well as on the bearing of the route and position of the end points. Hence it follows that the space-time variations of the capture factor and its relative significance can be considerable under specific conditions. A positive aspect of this factor is that it is purely refractive and is not associated with additional energy losses. However its appearance is restricted because of the aforementioned conditions as well as the comparatively small magnitudes of the regular gradients (angles of incline of levels of equal N on the order of several degrees).

Irregular heterogeneities of the ionosphere are a different type can also promote capture and re-entry, although with greater energy losses than because of gradients in the index of refraction.

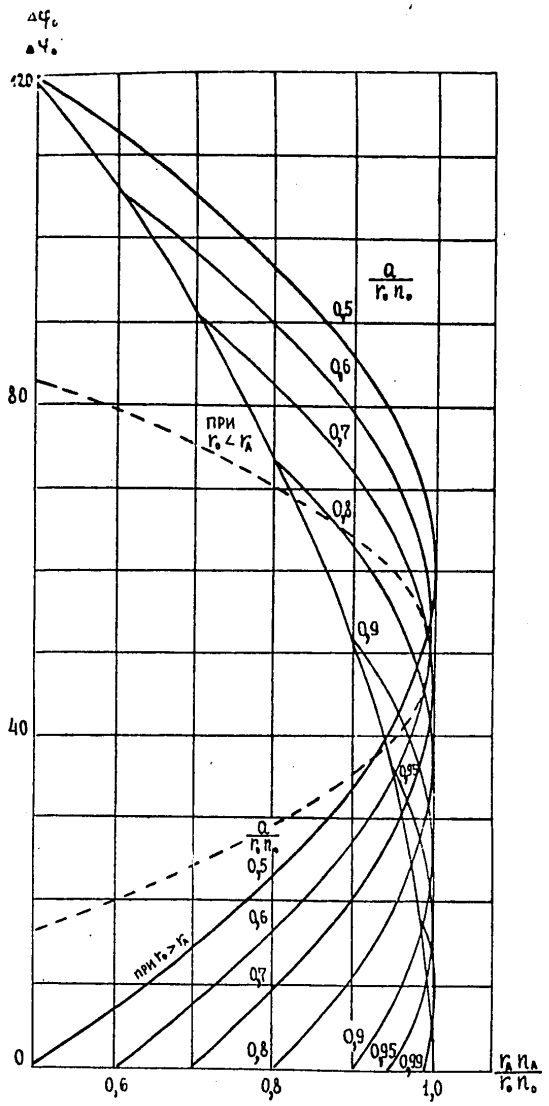

Figure 4.4

Realization of capture (escape) can be promoted by a whole series of factors of different physical nature, having different space-time variations, energy and other characteristics.

The relative significance and role of various physical factors of capture under differing conditions can change greatly. Under specific conditions, any of the factors plays a dominant role, ir their effect is comparable.

Combined capture is possible because of the simultaneous appearance of factors of different physical nature at the same or different sections of the route, as well as situations of reciprocal intensification of effect of different factors with the coincidence, for example, of the signs of the horizontal gradient of N and its equivalents, because of gradients of H, ν_{eff}, etc.; and, on the contrary, attenuation of effect with opposition of signs. Further study of each of these factors and their quantitative mathematical analysis is necessary. Particular attention is merited by factors with small energy losses, having the most likely appearance under natural conditions or with artifical effects. To realize this mathematical apparatus, fuller knowledge of variations in the regular world-wide ionosphere and its subtleties is necessary, including VIV. As a result of theoretical estimates, data can be derived on optimum conditions of capture in a specific route, including the position of the ground-based emitter, its frequency and angular characteristics of emission combined with the creation of the needed type of irregularities in the ionosphere via powerful emissions from Earth.

It is impossible to draw an unambiguous conclusion on the substantive predominance of any physical factor under any and all conditions. Thus it would be more expedient to continue research on all these factors of capture and their set of complex characteristics, which in the final analysis will permit us to determine regions of the most efficient appearance of each mechanism of capture of different physical nature.

In optimum bearings of ultra long-range and long-range propagation of radio waves, with ground-based emitter and aerospace emitter, respectively, favorable conditions of refraction in the channel and in the capture/re-entry sections are combined. Necessary conditions are defined by refraction, and adequate ones are defined by the set of energy factors assuring a signal level above the threshold at a given working frequency.

§2. Some Refraction Characteristics for Ionosphere-Based Emitters

Initial conditions near the emitter (altitude, plasma frequency, working frequency, N(r)-profile of the ionosphere) have a great effect on refraction of radio waves and relative efficiency of omnidirectional satellite broadcasting. We will make a distinction between the upper and lower hemispheres of emission lying above and below the plane in which the satellite is located. When the artificial Earth satellite is below the level $r_A(f)$, corresponding to the minimum of [rn(r)], the portion of emission not screened on top escapes into the outer ionosphere and consequently, does not participate in further propagation. When the artificial Earth satellite is above the level $r_A(f)$, beams from the upper hemisphere do not participate in long-range propagation, as well as some beams from the lower hemisphere which are screened below by the F2 layer. Thus in any satellite position, the lower hemisphere of emission is more efficient than the upper one. Let us define the K-ratio of the portion of satellite emission remaining or escaping into outer regions of the ionosphere to all emission (assuming it isotropic and the initial section of the ionosphere to be spherically-symmetric).[71]

Using an expression of the angle of the limiting screened beam with the vertical

$$\varphi_{0\,min} = \arcsin (r_A n_A / r_0 n_0)$$

("0" is an index corresponding to the position of an artificial Earth satellite), we find:

where r_0 is greater than $r_A(f)$ $\quad K = 1 - \frac{1}{\pi} \arcsin (r_A n_A / r_0 n_0)$,

where r_0 is less than $r_A(f)$ $\quad K = \frac{1}{\pi} \arcsin (r_A n_A / r_0 n_0)$.

The relationship of K as a function of $r_A n_A / r_0 n_0$ is shown by the dotted line in Figure 4.4. When r_0 is greater than r_A, K is greater than 0.5 and increases monotonically in proportion to r_0, asymptotically approaching unity. When $r_0 = r_A$, K = 0.5. When r_0 is less than r_A, K is less than 0.5 and falls monotonically to K_{min}, corresponding to artificial Earth satellite position on the channel axis (where rn(r) is max), i.e., $r_0 = r_B$. K_{min} depends on the N(r)-profile and f_w. As f_w increases because of the rise in $r_A n_A$ at fixed r_0 less than r_A, K increases and then falls when r_0 is greater than r_A. As f_w increases, K_{min} increases because of the rise in $r_A n_A / r_B n_B$, striving toward unity at the maximum frequency of channel degeneration. The maximum value of K_{min} = 0.5.

If we shift to consideration of ricocheting beams, we must exclude part of the lower hemisphere emission from artificial Earth satellite emission which strikes Earth immediately in the zone of direct radio line-of-sight of the artificial Earth satellite. The lower boundary of the sector of ground-based beams is defined by the expression φ_0 = arc sin $(a/r_0 n_0)$. (a is the Earth's radius).

Expressions for determination of the width of the initial sector of ground-based beams (in one of two opposite directions) have the following form:

$$\Delta\varphi_0 = \arccos(a/r_0 n_0) + \arccos(r_A n_A / r_0 n_0) \text{ при } r_0 < r_A(f),$$

$$\Delta\varphi_0 = \arccos(a/r_0 n_0) - \arccos(r_A n_A / r_0 n_0) \text{ при } r_0 > r_A(f).$$

The relationship of $\Delta\varphi_0$ as a function of $r_A n_A / r_0 n_0$ at various $a/r_0 n_0$ is graphically illustrated in Figure 4.4. As a function of artificial Earth satellite position and ionospheric conditions, differences in sector width of ground-based beams can be significant. When the artificial Earth satellite is situated above $h_{max}F2$ at a considerable altitude, the sector width can decrease to units of degrees. As a result of one of the consequences of the law of refraction, we find the expression

$$\Psi_{min} = \arccos \left(\frac{r_0}{a} \sqrt{1 - (fN)_0^2 / f^2} \right), \qquad (4.7)$$

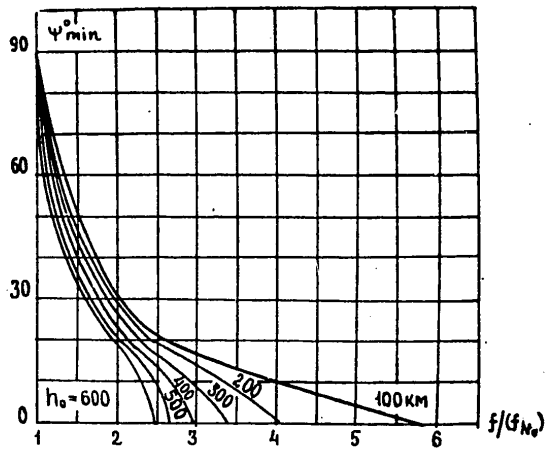

Figure 4.5

where Ψ_{min} is the smallest angle (above the Earth's surface) of beam arrival to Earth for various working frequencies. The relationship of Ψ_{min} as a function of h_0 (satellite altitude) and $f/(f_N)_0$ is graphically illustrated in Figure 4.5

Another consequence of the law of refraction [56] is expression

$$f_{min} = \frac{(fN)_0}{\sqrt{1-\left(\frac{a\cos\Psi}{r_0}\right)^2}}, \qquad (4.8)$$

where f_{min} is the lower limit of beam frequencies able to strike the Earth at a desired angle Ψ (Fig. 4.6).

We can derive an expression to define the greatest vertical angle of beam arrival to Earth Ψ_{max} after reflection in the ionosphere from the condition $r_A n_A = a \cos \Psi_{max}$. In fact, when a beam is reflected at lower levels than r_A, at the point of rotation rn(r) greater than $r_A n_A$ and consequently, Ψ is less than Ψ_{max},

$$\Psi_{max} = \arccos \frac{(r_A n_A / r_{max})}{(a / r_{max})}. \qquad (4.9)$$

The relationship of Ψ_{max} as a function of f/f_{cr}, y_m/r_{max} and h_{max} is graphically illustrated in Figure 4.1.

The angular refraction characteristics of ionospheric-channel emission capture examined in the preceeding section are applicable not only to a ground-based emitter, but also to an on-board satellite emitter.

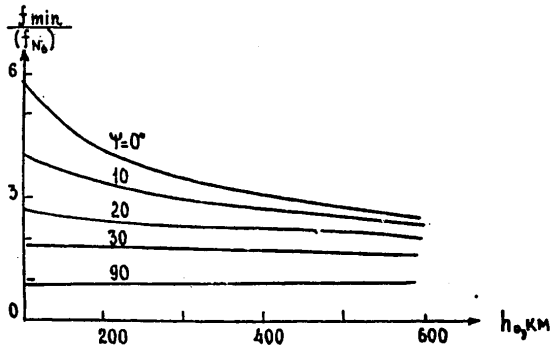

Figure 4.6

Angles of additional rotation of refracted beams required for capture become smaller as the channel-external emitter approaches the channel boundary.

When the emitter enters inside the channel because of ordinary refraction, some beams in a certain sector are restrained by the channel in its initial sector. The most optimum conditions for channel capture of artificial Earth satellite emission are created when the artificial Earth satellite is located near the channel axis and the opportunity arises for refraction of beams in the immediate proximity of the axis under extremely favorable damping conditions.

When the artificial Earth satellite moves upward or downward away from the channel axis, or escapes from the channel, for example above $h_{max}F2$, conditions of channel-capture of emission deteriorate. There is an increase in the role of ionospheric incline as a possible capture factor, when the level of equal electron concentration N rises toward the receiver. When the emitter is located on board an artificial Earth satellite in the ionosphere, conditions of emission capture by the ionospheric channel are much better than in the case of the ground-based transmitter.

Further refraction of beams captured by the channel in its initial sector, their possible retention in the channel and escape to Earth are extremely dependent on the distribution of electron concentration in the horizontally-heterogeneous route.

Each vertical section of the route (viewed as piecewise-uniform) has a limiting minimum angle of the beam with the vertical on the r_B-axis of the channel at which the beam can be reflected against the ionosphere and be retained in the channel

$$\varphi_{min}\,\beta = \arcsin(r_A n_A / r_B n_B). \qquad (4.10)$$

In a horizontally-heterogeneous ionosphere, the values of $r_A n_A$ and $r_B n_B$ fluctuate along the route, giving rise to corresponding changes in $\varphi_{min B}$.

With an increase in $r_A n_A / r_B n_B$ toward the receiver, $\varphi_{min B}$ rises. There is then a reduction in the angular width of the packet of beams able to reflect against the ionosphere. With a reduction in the initial angle of escape of beams and rise in working frequencies (when the sector of captured beams narrows), the conditions of reflection deteriorate in such routes. Consequently, the probability of retention by the channel of nascent ricocheting beams is slight. In particular, position of the ricochet mechanism above $r_A(f)$ is unfavorable in such routes. According to conditions of ordinary refraction in the ionosphere, after rotating, beams passing below r_A again escape into the outer region of the ionosphere without being captured by the channel. Only because of scattering effects (e.g., from the Earth) is it possible for more gently sloping beams than the incident ones to intersect the r_B-level at angle φ greater than $\varphi_{min B}$. Therefore, in routes having an increase in $r_A n_A / r_B n_B$ toward the receiver, conditions of reflection in the ionosphere of nascent ricocheting beams is extremely unfavorable.

On the other hand, however, with a reduction in $r_A n_A / r_B n_B$ toward the receiver, $\varphi_{min B}$ decreases and correspondingly, the angular width of the packet of beams able to reflect against the ionosphere increases. Such routes have the most favorable conditions for reflection of ricocheting beams in the ionosphere. In these routes, it also becomes possible to have reflection in the ionosphere by means of ordinary reflection of beams passing below r_A, when the artificial Earth satellite is located above this level. The most favorable routes are those with monotonic reduction in $r_A n_A / r_B n_B$ toward the receiver. In the presence of an intermediate maximum of $r_A n_A / r_B n_B$, escape of some radio waves in the corresponding sector into the outer region of the ionosphere is possible. The intermediate minimum of $r_A n_A / r_B n_B$ in the route is less favorable. Though absolute values of $r_A n_A / r_B n_B$ increase in proportion to working frequencies, the nature of change of $r_A n_A / r_B n_B$ is identical for various working frequencies and is defined by $N(r, \theta)$. This is also true for $r_A n_A$, whose variation along the route yields the lower limiting boundary of the channel at a given f_w. If this boundary reaches the Earth's surface, re-entry of ricocheting beams is possible. Thus a gradual drop in the altitude of the low points of rotation of a beam occurs in a horizontally-heterogeneous medium with the gradual reduction of $r_A n_A$ toward the receiver.

In the initial point of escape of the ricocheting beam $r_0 n_0 \sin \varphi_0$ is greater than a. When the beam intersects several successive vertical sections of the horizontally-heterogeneous route at levels r and at angles φ, $rn \sin \varphi$ changes and can reach values which, under specific conditions, are equal to or less than a (Earth's radius), where it becomes possible to have beam re-entry to Earth near the receiver or at the intermediate point of the route. Conditions of re-entry of ricocheting beams to Earth are quite similar to those of direct re-entry of artificial Earth satellite transmissions, when r_0 and φ_0 are known. In this case, r and φ at intermediate points of trajectory are not assigned, which makes the problem more complex.

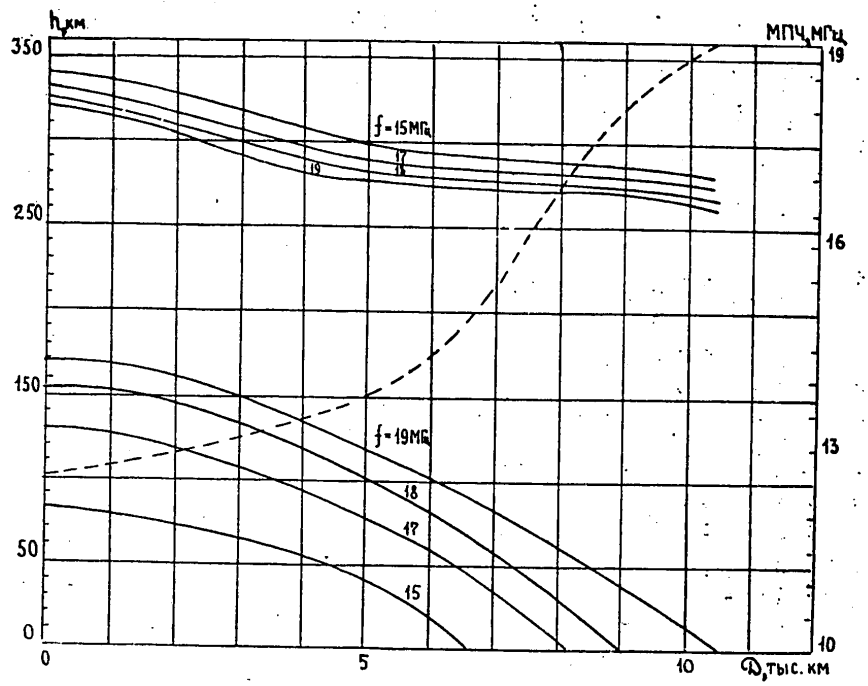

Figure 4.7

In each vertical section of the route, there is a point below $r_{max}F2$ at which $r_A n_A$ = a at f_1 = muf where muf corresponds to tangential incidence to Earth in the corresponding sector of the route. If a beam of frequency f_1 passes through the section with rotation at level $r_A(f)$, it can re-enter to Earth in the next sector of the route. Because $r_A n_A$ increases in direct proportion to f_w for the same route cross section, for any r_{refl} situated below r_A, it follows that rn(r) is greater than a when f_2 is greater than f_1. Thus the condition of rotation with subsequent re-entry for radio waves of frequencies greater than f_1 is not satisfied. In other words, the point where muf = f_1 is the origin of the interval of rotation points with possible subsequent re-entry to the beam for frequency f_1. Some additional rise in frequencies of radio waves capable of reflection on Earth after rotation is possible if the ionosphere is inclined in the re-entry sector. This incline is equivalent to increasing the angle of arrival, where it becomes possible to have beam incidence onto the Earth along a tangential line, which has passed above the Earth's surface without an incline. For this beam at the point of rotation $r_A n_A$ is greater than a at frequency f_2 greater than muf, since at frequencies lower than f_2, $r_A n_A$ takes smaller values. According to [86], because of the incline an increase in muf by about 10 percent is possible. This means that radio waves can re-enter at a frequency 10 percent greater than muf at the rotation point. This frequency is near muf above the point of incidence of the beam to Earth. Thus, routes having monotonic rise in muf toward the receiver are extremely favorable for

re-entry of ricocheting beams to Earth at f_w not in excess of muf at the receiving point.

An example of upper and lower channel boundaries calculated along the horizontally-heterogeneous route is given in Figure. 4.7 for several fixed working frequencies (solid lines) and the muf (dotted line).

Re-entry of radio waves at various frequencies occurs at points in the route with the corresponding values of muf. With a rise in f_w, the distance of the re-entry point to the emitter increases. Less favorable are routes with disturbance of monotonicity of muf increasing toward the receiver. In the presence of an intermediate maximum of muf, the latter limits some of the route where beam ricocheting and re-entry to Earth is possible. The intermediate minimum of muf can aggravate conditions of reflection of ricocheting beams in the ionosphere.

As the above suggests, conditions of reflection of ricocheting beams in the ionosphere are defined by the variation of $r_A n_A / r_B n_B$, and their conditions of re-entry to Earth by variation in $r_A n_A$, closely connected to variation of muf. Routes with a rise in N (muf) toward the receiver in most instances correspond to a decrease in both $r_A n_A / r_B n_B$ and $r_A n_A$, i.e., the most favorable conditions are established there for reflection in the ionosphere and re-entry to Earth of ricocheting beams with the emitter located below and above the r_A-level; this conclusion agrees with the results of experimental research of long-range signals from artificial Earth satellites cited in §2 of Chapter II.

§3. Some Characteristics of Radio Wave Oscillation in Ionosphere Channels

Analytical relationships for some integral characteristics of waveguides (intervals of oscillation of beams ricocheting in the channel, etc.) can be derived by using the combined quadratic model of altitude variation of the modified index of refraction squared $u(r) = r^2 n^2(r)$ (§3, Chapter III). The corresponding integrals are reduced to tabular form.

The integral which expresses the interval of oscillation of ricocheting beams

$$\theta = \sqrt{V} \int_{r_{\text{отр}}}^{} \frac{dr}{r\sqrt{u(r) - V}}$$

is equivalent to the sum of integrals for several altitude intervals, limited by the upper and lower levels of rotation and inflection of trajectory on the axis r_B of the channel, as well as by levels r_n of inflection of u(r). Formulas are cited below for intervals of oscillation of beams in the altitude interval from r_B to the r_B-upper point of rotation [99].

For gently sloping beams reflected below r_n, where u_n is less than V is less than u_B, we find the following expression

$$\theta = \sqrt{\frac{\beta_B}{\alpha_1 + \beta_B - 1}} \quad \text{arc Cos} \sqrt{\frac{1-\beta_B}{\alpha_1}} \quad , \tag{4.11}$$

where

$$\alpha_1 = \frac{1 - \frac{u_n}{u_B}}{\left(\frac{r_n}{r_B} - 1\right)^2} , \qquad \beta_B = \frac{V}{u_B} = \sin^2 \varphi_B$$

(φ_B is the angle of the beam with the vertical at level r_B).

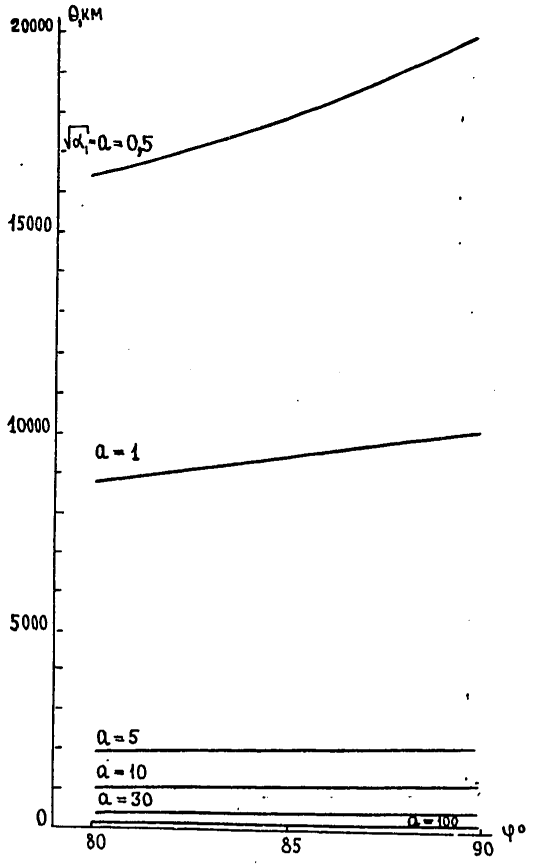

Figure 4.8

This relationship is graphically illustrated in Figures 4.8 and 4.9. The limiting case of gently sloping beams with great $v = u_B \sin^2 \varphi_B$ is a slipping beam with $\varphi_B = \pi/2$.

Where $\beta_B = 1$, we find

$$\theta = \frac{\pi}{2} \frac{1}{\sqrt{\alpha_1}}. \tag{4.12}$$

For steeper beams reflected above r_η (or approximately above r_ζ—the level of the maximum of N'_r), i.e. where $u_A < v \ll u$, we have the following expression

$$\theta = \frac{\sqrt{\beta}}{\sqrt{\frac{r_A^2}{r_\eta^2}\alpha - \left(\beta - \frac{u_A}{u_\eta}\right)}} \ln \left[\sqrt{\frac{r_A^2 (1-\beta)}{r_\eta^2 \left(\beta - \frac{u_A}{u_\eta}\right)}} - \frac{(1-\beta)}{\alpha} + \frac{r_A}{r_\eta} \frac{\sqrt{1-\frac{u_A}{u_\eta}}}{\sqrt{\beta - \frac{u_A}{u_\eta}}} - \right.$$

$$\left. - \frac{\sqrt{\beta - \frac{u_A}{u_\eta}}}{\sqrt{\alpha}} \right] + \frac{\sqrt{\beta_b}}{\sqrt{\alpha_1 + \beta_b - 1}} \arcsin \left[\frac{\sqrt{1-\beta_b}}{\sqrt{\alpha_1}} \frac{r_\eta}{r_b} + \frac{\sqrt{\alpha_1}\left(\frac{r_\eta}{r_b} - 1\right)}{\sqrt{1-\beta_b}\,\frac{r_\eta}{r_b}} \right] -$$

$$- \frac{\sqrt{\beta_b}}{\sqrt{\alpha_1 + \beta_b - 1}} \arcsin \frac{\sqrt{1-\beta_b}}{\sqrt{\alpha_1}}, \tag{4.13}$$

where

$$\alpha = \frac{\left(1 - \frac{u_A}{u_\eta}\right)}{\left(\frac{r_A}{r_\eta} - 1\right)^2}, \quad \beta = \frac{v}{u_\eta} = \sin^2 \varphi_\eta.$$

An example of calculation according to formulas (4.11; 4.13) of relationships of $\theta(\varphi_B)$ for average models of the daytime and nighttime ionosphere for several working frequencies is given in Figure 4.10. Under fixed ionospheric conditions and at angle φ_B of beam escape, the interval of oscillation increases in proportion to working frequencies.

For the model u(r) with $u''_r > 0$, the tabular integral is reduced to a logarithmic function which decreases in proportion to the initial angle φ_B of beam escape. For the model of u(r) with $u''_r < 0$, the tabular integral reduces to an arccosine function which increases in proportion to φ_B. Consequently, the signs of $u''_r(r)$ have a great effect on the qualitative picture of unknown relationships of θ as a function of initial data. In the general case $\theta(\varphi_B)$ is a nonmonotonic function with two maximums, corresponding to the limiting, steepest and most gently sloping slipping beam and an intermediate minimum corresponding to a beam reflected slightly above the r_ζ-level. The first maximum corresponding to the Pedersen limiting beam is much greater than the second. The intermediate

minimum is usually very wide. For adequately gently sloping beams, the interval of oscillation θ increases very slowly in proportion to the angle φ_B. Small dθ /d φ_B of gently sloping beams indicate the increased probability of their longitudinal focusing on the channel axis and improvement of energy characteristics.

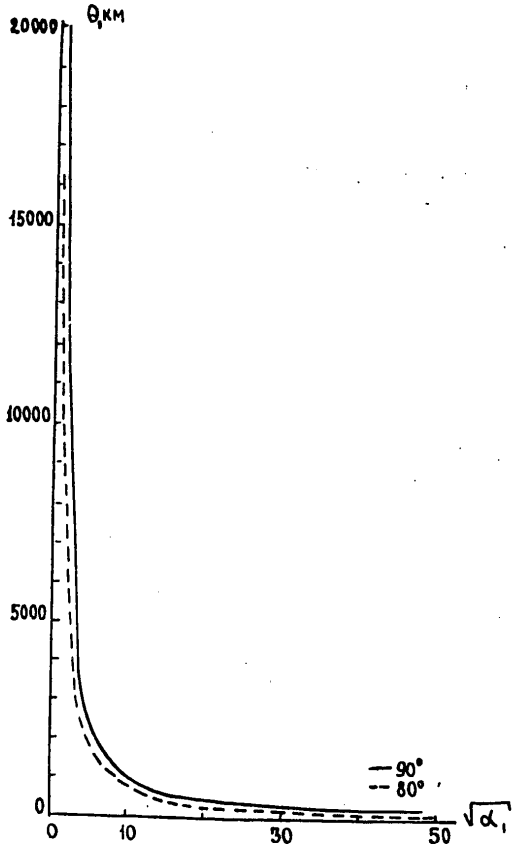

Figure 4.9

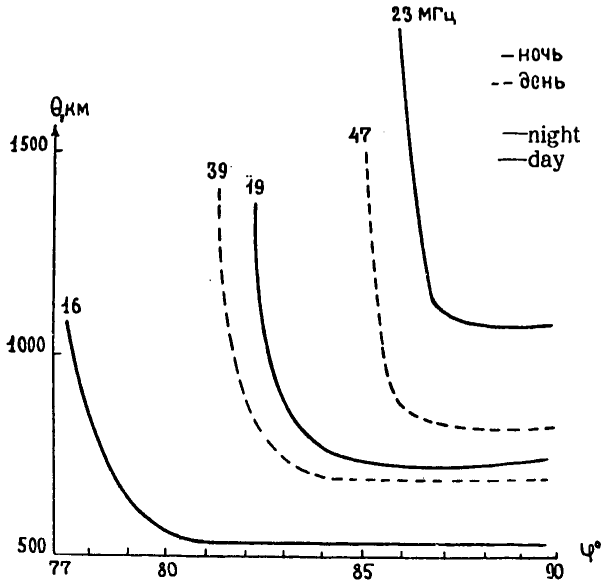

Figure 4.10

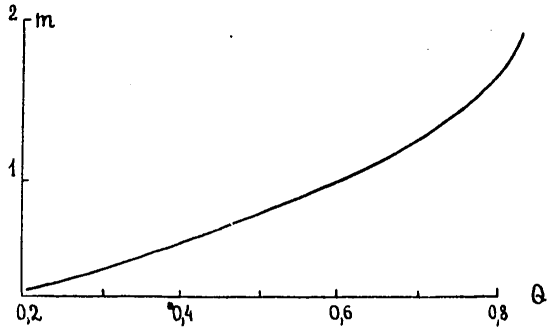

Figure 4.11

A correct qualitative relationship of $\theta(\varphi_B)$ can be derived when using the combined model of N(r) consisting of a quasiparabola above r_2 and an inverted quasiparabola below r_2 (Chapter III, §2). But in this case, the formula for θ is more complicated and contains a large number of parameters including working frequencies.

Calculations of intervals of oscillation based on the quadratic combined model of u(r) are possible are various ionospheric and initial conditions. If the position of the emitter does not coincide with the channel axis, one of the limits of integration becomes the level r_0 of the emitter itself, which is located, for example, on board an artificial Earth satellite.

In the presence of substantial horizontal heterogeneity of the ionosphere. channel configurations for fixed working frequency defined by the upper and lower boundaries, axis and transverse dimensions change in various sectors of the route.

Variation of different waveguide parameters along the route can be calculated on the basis of EPM materials (Chapter III, §4-6) in terms of the prescribed variation of key point parameters of the ionosphere.

Parameters of trajectories of a beam oscillating in the channel (interval of oscillation, position of points of rotation, etc.) in the general case must differ from the same parameters calculated according to formulas for a spherically-symmetric medium.

Let us use the integral equation

$$u(r_0\theta_0) = V + \int_{\theta_0}^{\theta} \frac{\partial u(r,\theta)}{\partial \theta}\, d\theta \,, \qquad (4.14)$$

corresponding to the classic principle of Fermat as applied to the point of beam rotation $r_0\theta_0$, where $\sin^2 \varphi = 1$.

Let us transform (4.14) by using analytical models of u(r) with coefficients dependent on θ. Variables r and θ are separated:

$$u(r,\theta) = u_b - C(r - r_b)^2 ,$$

$$C = \frac{(u_b - u_n)}{(r_n - r_b)^2} = -\frac{1}{2} u''_r .$$

Let us say that C is a linear function of θ; $C = C_1 + C'_0\theta$. Variation of trajectory $r(\theta)$ is approximated by a fourth-power polynomial which satisfies the necessary conditions at the initial point of escape and point of rotation of a beam for r, r'_θ, r''_θ:

$$r(\theta) = r_b + (r_0 - r_b)\left[m\frac{\theta}{\theta_0} + (4-3m)\left(\frac{\theta}{\theta_0}\right)^3 + (2m-3)\left(\frac{\theta}{\theta_0}\right)^4\right],$$

$$m = (\theta_0 r_b \operatorname{ctg}\varphi_1)/(r_0 - r_b) \qquad (4.15)$$

(φ_1 is the initial angle of beam escape).

After performing integration and necessary substitions, we find an equation equivalent to the integral one, in the form

$$Q = 0{,}714286m - 0{,}088095m^2 - 0{,}030159m^3,$$

where

$$Q = \frac{c_1 r_b \operatorname{ctg}\varphi_1}{c_0'(r_0 - r_b)}\left[\frac{(r_{0\partial H} - r_b)}{(r_0 - r_b)^2} - 1\right] \qquad (4.16)$$

($r_0\partial_H$-level of rotation of beam in a spherically-symmetric medium).

From the condition of rotation at the upper point $r''_\theta < 0$, it follows that $m < 2$, $Q < 0.834$. The relationship Q(m) is graphically illustrated in Figure 4.11.

These expressions indicate the important role of quantities and signs of $u''_r(\theta)$ and $du''_r(\theta)/dQ$ in shaping trajectory characteristics in a horizontally-heterogeneous ionosphere.

Let us examine the possibilities of analytical representation of integral equations based on the EPM

$$J = \int^{r_A} \sqrt{u(r) - u_A}\, dr,$$

$$J_0 = \int^{r_{отр}} \sqrt{u(r) - V}\, dr,$$

corresponding to the use of the approximate condition of the adiabatic invariant for a horizontally-heterogeneous ionosphere. [94]. The limiting maximum value yields the integral of J. By using the combined quadratic model of u(r), let us find the following analytical expressions for the tabular integrals of J and J_0:

$$J = \frac{(r_n - r_b)}{\sqrt{u_b - u_n}}\frac{1}{2}\left[\sqrt{u_b - u_n}\cdot\sqrt{u_n - u_A} + (u_b - u_A)\arcsin\frac{\sqrt{u_b - u_n}}{\sqrt{u_b - u_A}}\right] +$$

$$+ \frac{1}{2}(r_A - r_n)\sqrt{u_n - u_A}. \qquad (4.17)$$

When $v < u_п$

$$J_0 = \frac{(r_п - r_в)}{\sqrt{u_в - u_п}} \cdot \frac{1}{2}\left[\sqrt{u_в - u_п}\,\sqrt{u_п - V} + (u_в - V)\arcsin\sqrt{\frac{u_в - u_п}{u_в - u_A}}\right] + \frac{(r_A - r_в)}{\sqrt{u_п - u_A}} \cdot$$

$$\cdot \left\{(V - u_A)\ln\sqrt{V - u_п} + \sqrt{u_п - u_A}\,\sqrt{u_п - V} - (V - u_A)\ln\left[\sqrt{u_п - u_A} + (u_п - V)\right]\right\}. \tag{4.18}$$

When $v \geq u_п$ (for more gently sloping beams)

$$J_0 = \frac{\pi}{4}\,\frac{(r_п - r_в)}{\sqrt{u_в - u_п}}\,\sqrt{u_в - V}\ . \tag{4.19}$$

In a horizontally-heterogeneous ionosphere, limiting values of the integral J fluctuate in different sections of the route.

Using (4.19), let us find the analytical expression for analysis of the initial angle of escape of the limiting beam retained by the channel (when $J_0 = \min J$ in the route)

$$V_0 = (u_в)_0 - \frac{16}{\pi^2}\left[\frac{(u_в - u_п)}{(r_п - r_в)^2}\right]_0 J_0^2\ , \tag{4.20}$$

where $V_0 = (u_в)_0 \sin^2(\varphi_в)_0$.

In horizontally-heterogeneous ionospheric channels, beams oscillate about the axis $r_B(\theta)$ of the channel in which are arranged the points of inflection of all trajectories of a given working frequency, corresponding to minimum values of the angle of the beam with the vertical. Its maximum values, equal $\pi/2$, are attained at the upper and lower points of rotation of beams whose position in the channel depends on initial conditions of escape and the distribution of u(r, θ).

§4. Cluster and Phase Paths

Integrals which express L_{cl}—the cluster path and L_{ph}—the phase path,

$$L_{cl} = \int^{r_{max}} \frac{r\,dr}{\sqrt{u(r) - V}}\ ,$$

$$L_{ph} = \int^{r_{max}} \frac{u(r)\,dr}{r\sqrt{u(r) - V}}\ ;$$

we will reduce to tabular form using the quadratic models of $u(r) = ar^2 + br + c$. Here, L_{ph} can be represented as the sum:

$$L_\varphi = a L_{1p} + \frac{c}{\sqrt{V}}\theta + b\int_{r_{refl}}^{r_{tp}} \frac{dr}{\sqrt{u(r)-V}}.$$

These analytical expressions for L_{cl} and L_{ph} are cited below. For rather gently sloping beams ($r_{refl} < r_\Pi$, $v > u_\Pi$)

$$L_{2p} = \frac{\pi}{2}\frac{r_b(r_n-r_b)}{\sqrt{u_b-u_n}} + \frac{(r_n-r_b)^2\sqrt{u_b-V}}{(u_b-u_n)}, \tag{4.21}$$

where $v = u_\Pi$

$$L_{2p\,max} = \frac{\pi}{2}\frac{r_b(r_n-r_b)+(r_n-r_b)^2}{\sqrt{u_b-u_n}}, \tag{4.22}$$

where $v = u_B$

$$L_{2p\,min} = \frac{\pi}{2}\frac{r_b(r_n-r_b)}{\sqrt{u_b-u_n}}. \tag{4.23}$$

For steeper beams ($r_{refl} > r$, $v < u_\Pi$)

$$L_{2p} = \frac{(r_n-r_b)^2\sqrt{u_b-V}-\sqrt{u_n-V}}{(u_b-u_n)} - \frac{\sqrt{u_n-V}(r_A-r_n)^2}{(u_n-u_A)} + \\ + \frac{r_b(r_n-r_b)}{\sqrt{u_b-u_n}}\arcsin\frac{\sqrt{u_b-u_n}}{\sqrt{u_b-V}} - \frac{r_A(r_A-r_n)}{\sqrt{u_n-u_A}}\ln\left[\frac{\sqrt{V-u_A}}{\sqrt{u_n-u_A}-\sqrt{u_n-V}}\right]. \tag{4.24}$$

Phase paths are expressed by the following formulas.

In the case of gently sloping beams

$$L_\varphi = \frac{1}{\sqrt{V}}\left[u_b - \frac{(u_b-u_n)r_b^2}{(r_n-r_b)^2}\right]\theta + \pi\frac{r_b\sqrt{u_b-u_n}}{(r_n-r_b)} - \frac{(u_b-u_n)}{(r_n-r_b)^2}L_{2p}. \tag{4.25}$$

In the case of steep beams

$$L_\varphi = \frac{\left[u_b - \frac{(u_b-u_n)r_b^2}{(r_n-r_b)^2}\right]}{\sqrt{\frac{(u_b-u_n)r_b^2}{(r_n-r_b)^2} - (u_b-V)}} \left\{ \arcsin \frac{(u_b-V)(r_n-r_b)+(u_b-u_n)r_b}{r_n\sqrt{u_b-u_n}\sqrt{u_b-V}} - \right.$$

$$\left. - \arcsin \frac{\sqrt{u_b-V}\,(r_n-r_b)}{r_b\sqrt{u_b-u_n}} \right\} + \frac{r_b\sqrt{u_b-u_n}}{(r_n-r_b)} \arcsin \frac{\sqrt{u_b-u_n}}{\sqrt{u_b-V}} +$$

$$+ \frac{\left[u_A + \frac{(u_n-u_A)r_A^2}{(r_A-r_n)^2}\right]}{\sqrt{\frac{(u_n-u_A)r_A^2}{(r_A-r_n)^2} - (V-u_A)}} \ln \frac{\sqrt{\frac{(u_n-u_A)r_A^2}{(r_A-r_n)^2} - (V-u_A)}\sqrt{u_n-V} + \frac{(u_n-u_A)r_A}{(r_A-r_n)} - (V-u_A)}{r_n\sqrt{\frac{(u_n-u_A)r_A^2}{(r_A-r_n)^2} - (V-u_A)}} + \frac{r_n r_A(u_n-u_A)}{(r_A-r_n)^2}$$

$$+ \frac{r_A\sqrt{u_n-u_A}}{(r_A-r_n)} \ln \frac{\sqrt{u_n-u_A} - \sqrt{u_n-V}}{\sqrt{V-u_A}} - \sqrt{u_b-V}\,. \qquad (4.26)$$

Using the above formulas for cluster paths, relationships were calculated for L_{cl} as a function of the initial angle of beam escape from the channel axis t several working frequencies for average models of daytime and nighttime ionosphere (Figure 4.12).

These relationships have an intermediate maximum which corresponds to a beam reflected near r 2. On both sides of the maximum of L_{cl} with spacing of the beams r_{refl} from r 2, delays increase. When it approaches the channel axis, the smallest value of L_{cl} is achieved.

To shift from estimates of L_{cl} related to part of the interval of beam oscillation (from the point of escape to the point of rotation) to cluster delays per unit path length L_{cl}/θ, let us consider the relationship $\theta(\varphi)$ for the same models of the ionosphere and working frequencies considered in §3 of Chapter IV. With an increase in φ, the interval of oscillation θ rapidly falls to its minimum and then undergoes little change with rather gently sloping beams.

The relationship of L_{cl}/θ as a function of φ (Figure 4.13) has the same qualitative nature as L_{cl}. Because of the rapid increase in θ with change in φ, L_{cl}/θ decreases much faster than L_{cl}.

Figure 4.13 indicates several typical features of angular and frequency relationships L_{cl}/θ. There are rather wide intervals of angles of escape of beams for each working frequency, correponding to the small change of L_{cl}/θ. For 16 MHz at night, limiting angles of the interval 82-88°; for 19 MHz, 85-89°. In the daytime, for 47 MHz, 87-89°. In the interval of the most gently sloping beams near slippage along the axis of the channel, where $\varphi \approx$ 87-90°, we find the smallest absolute values and a difference in L/θ which corresponds to the day, night and different working frequencies.

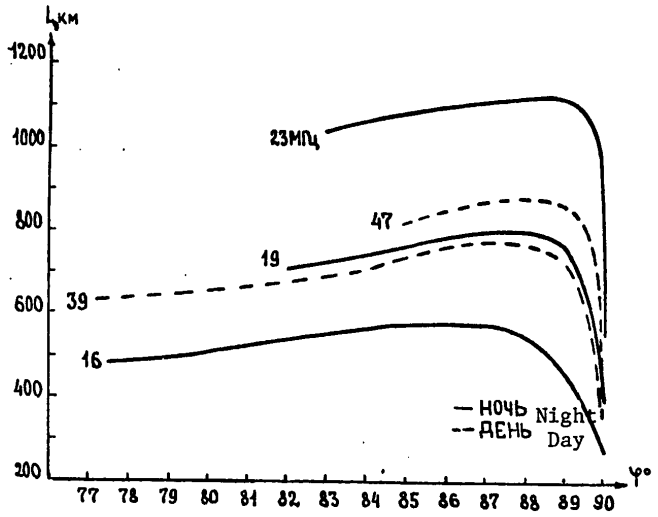

Figure 4.12

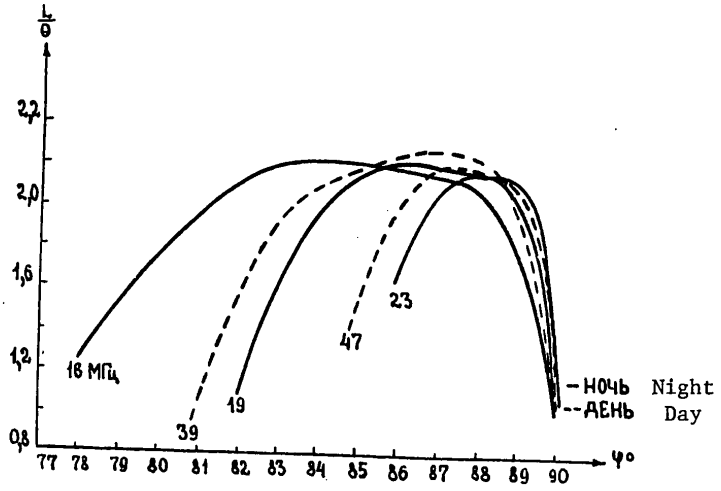

Figure 4.13

Maximum L_{cl} and L_{cl}/θ correspond to steeper beams reflected at levels near max N'_r. With further increase of beam curvature, absolute values decrease, but there is an increase in the difference in L_{cl}/θ under different conditions.

Magnitudes of time of around-the-world signals can be assessed by the formula

$$\tau_{кс} = \frac{40 \text{ тыс. км}}{c} \frac{L_{гр}}{\theta} = 0{,}134 \frac{L_{гр}}{\theta} \text{ с}$$

Because observable $\tau \geq 0.138$ seconds, the most likely average L_{cl}/θ are equal to or greater than 1.03, which corresponds to rather gently sloping beams retained by the channel. According to theoretical estimates of signal delays in propagation in the ionospheric duct, they should be smaller (per unit path length) and more stable than in skip modes. This conclusion agrees with measured results. The high stability of the time of rounding-the-globe and smaller delay per unit path length than in inverse signals observed in world-wide signals (ratio equals 0.996219 according to [25]) indicate the important role of ionospheric channels in world-wide propagation.

Analysis confirms the important role of the maximum of N'_r in shaping the qualitative picture of ionospheric propagation of radio waves and the need to consider its parameters in quantitative estimates of cluster delays of signals and other characterstics. The results can be utilized to interpret measurements of signal time delays.

§5. Absorption of Radio Waves in Ionospheric Channels

The energy characteristics of signals greatly depends on absorption of radio waves in the ionosphere. When radio waves are propagated in ionospheric channels, as in the case of skip modes, absorption Γ at fixed working frequencies is defined by the altitude variation of $f^2(r)$ and $\nu(r)$-effective number of collisions:

$$\Gamma = \frac{1}{c} \int \frac{\nu(r) \cdot r f_N^2(r) dr}{f^2 \sqrt{u(r) - V}}.$$

In the subintegral expression, let us substitute

$$\frac{f_N^2(r)}{f^2} = 1 - \frac{u(r)}{r^2},$$

because

$$u(r) = r^2 \left(1 - \frac{f_N^2(r)}{f^2}\right).$$

Let us represent the expression for Γ in the form of the difference of two integrals:

$$\Gamma = \frac{1}{c}\int \frac{\nu(r)\,r\,dr}{\sqrt{u(r)-V}} - \frac{1}{c}\int \frac{\nu(r)u(r)\,dr}{r\sqrt{u(r)-V}}\,.$$

Let us consider that in the Γ-region, ν fluctuates little with altitude in the interval of channel altitudes (decreases in inverse proportion to working frequencies).

We then find

$$\frac{c\Gamma}{\nu} = L_{zp} - L_{\varphi}. \qquad (4.27)$$

Analytical expressions for analysis of the integral absorption of radio waves in the ionospheric channel under different inital conditions of beam escape can be derived using formulas for L_{cl} and L_{ph} cited in §4, Chapter IV.

Thus for gently slopiong beams ($r_{refl} < r_{\Pi}$, $v > u_{\Pi}$)

$$\frac{c\Gamma}{\nu} = \left[1+\frac{(u_B-u_\Pi)}{(r_\Pi-r_B)^2}\right]L_{zp} - \frac{1}{\sqrt{V}}\left[u_B - \frac{(u_B-u_\Pi)r_B^2}{(r_\Pi-r_B)^2}\right]\theta - \pi\frac{r_B\sqrt{u_B-u_\Pi}}{(r_\Pi-r_B)}, \qquad (4.28)$$

where

$$L_{zp} = \frac{\pi}{2}\frac{r_B(r_\Pi-r_B)}{\sqrt{u_B-u_\Pi}} + \frac{(r_\Pi-r_B)^2\sqrt{u_B-V}}{(u_B-u_\Pi)},$$

$$\theta = \frac{\sqrt{V}}{\frac{\sqrt{u_B-u_\Pi}\,r_B}{(r_\Pi-r_B)} - (u_B-V)}\,\arccos\frac{(r_\Pi-r_B)\sqrt{u_B-V}}{r_B\sqrt{u_B-u_\Pi}}$$

(see §§3, 4, Chapter IV).

In the limiting case of a beam slipping along the channel axis ($v = u_B$)

$$\frac{c\Gamma}{\nu} = \frac{\pi}{2}\frac{(r_\Pi-r_B)(r_B^2-u_B)}{r_B\sqrt{u_B-u_\Pi}} \qquad (4.29)$$

and

$$\frac{c\Gamma/\nu}{\theta} = \frac{r_B^2-u_B}{\sqrt{u_B}}. \qquad (4.30)$$

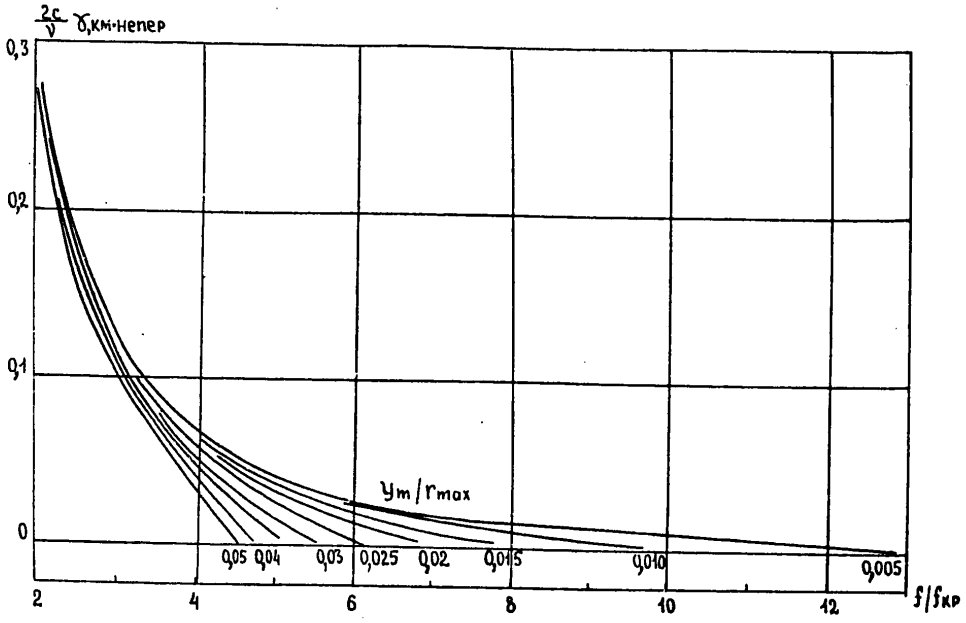

Figure 4.14

Let us consider the frequency dependence of radio wave absorption in ionospheric channels in limiting cases of propagation near the upper boundary r_A of the channel (steepest beams retained by it) and along the axis r_B of the channel [102]. Formulas of the frequency dependence of absorption can be derived on the basis of the EPM using analytical expressions for $r_A(f)$ and $r_B(f)$ (§§4, 5, Chapter III). Let us substitute them in the formula of the coefficient of absorption γ per unit length, whose frequency dependence is completely defined by the right side of the expression

$$\frac{2c}{v}\gamma(f)=\frac{f_N^2(r(f))/f^2}{\sqrt{1-f_N^2(r(f))/f^2}}.$$

As a result we find $(2c/v)\gamma_A$ as a function of f/f_{cr}, y_m/r_{max} and $(2c/v)\gamma_B$ as a function of f/f_M

$$q=pf_M^2/f_t^2=\left(\frac{r_t}{r_M}-1\right)^2\Big/\left(\frac{f_t^2}{f_M^2}-1\right).$$

Calculated frequency dependencies of absorption for several values of key point parameters of the ionosphere are presented in Figures 4.14 and 4.15. The nature of the frequency dependence of absorption at the boundary (Figure 4.14) and the axis (Figure 4.15) of the channel are very different. Absorption on the channel boundary monotonically decreases in inverse proportion to working frequency to

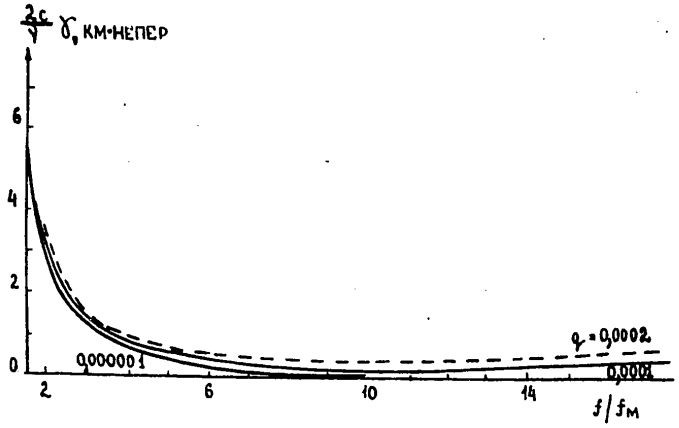

Figure 4.15

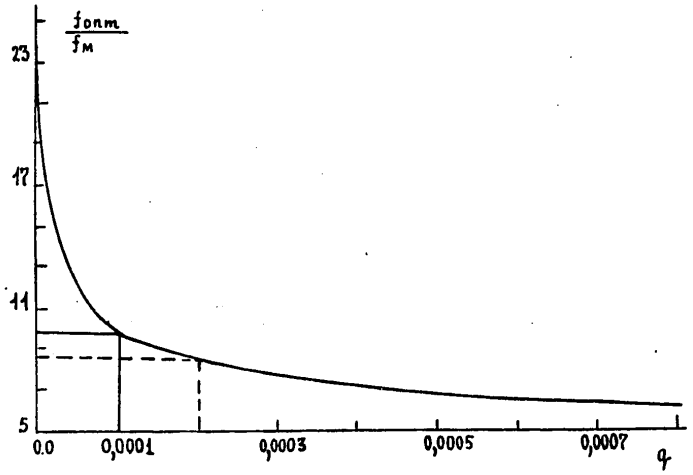

Figure 4.16

its final minimum values corresponding to the limiting frequency of channel degeneration. Absorption on the channel axis at first decreases in inverse proportion to working frequency and, after passing through the minimum for real q, slowly increases, fluctuating within comparatively small limits. In terms of absolute value, absorption along the axis is many times less than along the boundary of the channel. The substantive qualitative difference in the frequency variation of absorption at both levels is the result of the opposing nature of displacement with increase of f of the level r_A, which drops to altitudes with smaller f^2_N, and the level r_B which rises to altitudes with greater f^2_N. In the second case there is a compensating effect, wherein the ratio of $f^2_N(r_B(f))/f^2$ fluctuates slowly. In calculating the possible change of ν with altitude, the curves can change slightly because $\gamma(f) \sim \nu(r(f))$. With more likely increase

of ν with altitude, γ_A will be inversely proportion to f and consequently, the drop in $\gamma_A(f)$ will be somewhat accelerated. Because of the increase in ν_B in proportion to frequency, $\gamma_B(f)$ will fall somewhat more slowly at low f and rise more quickly at high frequencies. The qualitative distinction of the frequency dependence of absorption at the boundary and axis of the channel are retained in this case as well.

Estimates of actual values of q can be made for existing N(r)-profiles. In Figure 4.15, the solid line roughly corresponds to the upper limit of q for middle latitudes (values of q indicated above for dotted line are not probable). For twilight conditions, the values are q are extremely low; this involves a reduction in absorption along the channel axis. In a horizontally-heterogeneous route in different sectors, values of q can differ, but the resultant frequency dependence of integral absorption must retain a qualitative nature.

From the condition of the minimum of absorption at optimum frequencies f_{opt}

$$\frac{d}{df}\gamma(n_1(f))=0$$

we find the formula

$$\frac{f_{опт}}{f_м}=\sqrt[4]{1+\frac{1}{q}}, \qquad (4.31)$$

The calculated relationship of f_{opt}/f_M as a function of q is shown in figure 4.16. As q increases there takes place a monotonic drop in f_{opt}/f_M. Optimum frequencies greatly depend on the quantity min N in the trough; they are also affected by other parameters of the trough and maximum of N'_r.

In a horizontally-heterogeneous route, the resulting optimum frequency can be roughly represented by the expression

$$f_{опт}=\frac{1}{n}\sum_{n=1}^{n}(f_м)_n\sqrt[4]{1+\frac{1}{q_n}}, \qquad (4.32)$$

where n is the number of discrete points in the route.

The weakly expressed frequency dependence of absorption along the channel axis and values of f_{opt} for actual q and f_M correspond to observed aspects of damping of ultra long-range signals. They usually have weakly expressed frequency dependence, reduced absolute values with minimum above standard (§3, Chapter I). The observable characteristics differ considerably from the usually well expressed frequency dependence of damping of skip modes with

minimum below MPCh [37].

Theoretical estimates confirm the assumption of largely super-refraction of ultra long-range signals and indicate their tendency to pass near the channel axis over much of the route.

§6. Spatial Damping of Radio Waves in Ionospheric Channels

The significant difference between spatial damping of energy flux density and spherical divergence in free space becomes even clearer when there is more heterogeneity of the medium and refraction and smaller altitude dimensions of the region of radio wave propagation. This region, in the case of ionospheric radio ducts, at very high working frequencies, is much less than in skip modes.

Based on radiation concepts of energy flux density of a refracted, reflected and focused beam in conjunction with the mathematical apparatus of EPM, we can find analytical expressions to determine spatial damping of the electrical fields of radio waves in channels.

In general form, the factor of longitudinal focusing of energy flux density in the plane of propagation of radio waves

$$\frac{\sin \varphi_0(r_0)}{\cos \varphi(r)} \cdot \frac{1}{d\theta(\varphi_0)/d\varphi_0},$$

where $\varphi_0(r_0)$ is the initial angle of beam escape at level r_0 of the emitter, $\varphi(r)$ is the angle of the beam with the vertical at level r of the receiver; θ is the interval of oscillation.

In a spherically-symmetric medium

$$\frac{\sin \varphi_0(r_0)}{\cos \varphi(r)} = \frac{1}{\sqrt{\operatorname{cosec}^2 \varphi_0(r_0) - \frac{u(r_0)}{u(r)}}} \qquad (4.33)$$

because $u(r)\sin^2 \varphi(r) = u(r_0)\sin^2 \varphi_0(r_0)$.

For any emitter and receiver height $u(r_0)$ and $u(r)$ can be derived by using analytical quadratic models of u(r) (Chapter III, §3-5). At levels below 100 kilometers, $n \simeq 1$ and $u(r) = r^2$. On the Earth's surface $u(r) = d^2$, where d is the Earth's radius. When an emitter and receiver are situated at the same level $r_0 = r$, we find $u(r_0) = u(r)$ and $\sin \varphi_0/\cos \varphi = \tan \varphi_0$. In the general case, we use models u(r) corresponding to intervals of altitudes in which the emitter and receiver are found. These cases are possible: 1) emitter in interval $[r_B, r_\pi]$, receiver at $[r_n, r_A]$; 2) emitter in interval $[r_n, r_A]$, receiver at $[r_B, r_n]$; 3) emitter and receiver both in interval $[r_B, r_n]$; 4) emitter and receiver in interval $[r_\pi, r_A]$; 5) emitter and receiver in interval of altitudes below 100 kilometers, e.g. on Earth's surface.

Using the appropriate models of u(r), we find analytical expressions for the multiplier $\sin\varphi_0/\cos\varphi(r)$ for any position of emitter and receiver.

Analytical expressions for $d\theta(\varphi_0)/d\varphi_0$ can be found by differentiating with respect to φ_0 the expressions of $\theta(\varphi_0)$ from §3, Chapter IV.

For gently sloping beams reflected below $r_п$, we find:

$$\frac{d\theta(\varphi_0)}{d\varphi_0} = \frac{\sin^2\varphi_0}{(\alpha_1-\cos^2\varphi_0)} - \frac{(1-\alpha_1)\cos\varphi_0}{(\alpha_1-\cos^2\varphi_0)^{3/2}} \arccos\left[\frac{\cos\varphi_0}{\sqrt{\alpha_1}}\right]. \qquad (4.34)$$

Gently sloping beams oscillating near the channel axis are most important, because as φ_0 decreases, the probability of beam retention by the channel over most of its expanse also decreases.

Allowing for the factor of longitudinal focusing , electrical field strength is represented in the general form

$$E(r,\theta) = \frac{173\sqrt{P_{изл}}}{r\sqrt{\sin\theta}} \sqrt{\frac{\sin\varphi_0}{\cos\varphi(r)}} \frac{1}{\sqrt{d\theta(\varphi_0)/d\varphi_0}}.$$

Here P_{em} is emitted output.

The multiplier $1/\sqrt{\sin\theta}$ considers the sphericity-induced divergence of beams where $0 < \theta < \pi/2$ and convergence (focusing) right down to the antipode where $\pi/2 < \theta < \pi$ in bearings transverse to the plane of propagation of the radio waves.

Analytical expressions for $E(r, \theta)$ can be found by substituting the corresponding formulas for $\sin\varphi_0/\cos\varphi(r)$ and $d\theta(\varphi_0)/d\varphi_0$ corresponding to various altitudes of emitter and receiver and ranges of beam escape angles φ_0.

For example, for gently sloping beams, when the emitter is located on the channel axis and the receiver its in its upper vicinity in the interval $[r_B, r\ ]$, we find:

$$E(r,\theta) = \frac{173\sqrt{P_{изл}}}{r\sqrt{\sin\theta}} \frac{1}{\sqrt[4]{\operatorname{cosec}^2\varphi_0 - \frac{u_в}{u_в-(u_в-u_п)(r-r_в)^2/(r_п-r_в)^2}}} \cdot \frac{1}{\sqrt{\frac{\sin^2\varphi_0}{(\alpha_1-\cos^2\varphi_0)} - \frac{(1-\alpha_1)\cos\varphi_0}{(\alpha_1-\cos^2\varphi_0)^{3/2}} \arccos\left[\frac{\cos\varphi_0}{\sqrt{\alpha_1}}\right]}} \qquad (4.35)$$

When the emitter and receiver are at a single level, the factor of longitudinal focusing of the field

$$F = \frac{\sqrt{tg\,\varphi_0}}{\sqrt{d\theta(\varphi_0)/d\varphi_0}}.$$

Let us cite several numerical estimates of $F(\alpha, \varphi_0)$ corresponding to the position of the emitter and receiver on the channel axis and range of angles of escape of gently sloping beams. Calculated relationships of $F(\varphi_0)$ for several fixed values of

$$\alpha_1 = \left(1 - \frac{U_n}{U_b}\right) \Big/ \left(\frac{r_n}{r_b} - 1\right)^2$$

are shown in Figure 4.17.

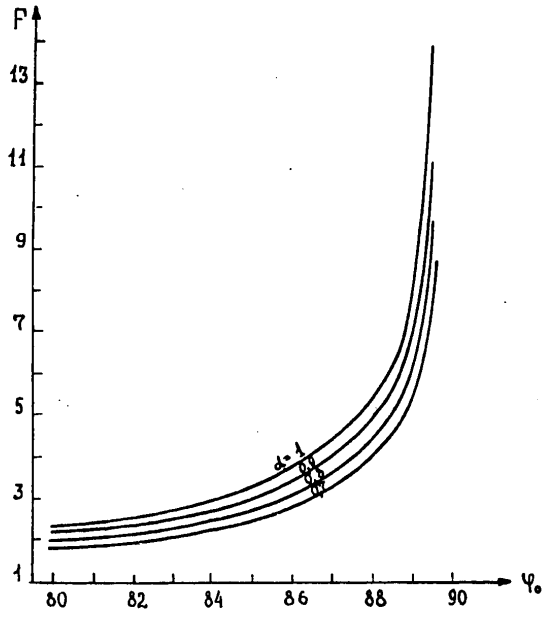

Figure 4.17

With an increase in φ_0 and α, the focusing factor increases monotonically. In particular, F increases rapidly in direct proportion to φ_0 as the beams approach the channel axis and values of α_1 near unity. When $\alpha_1 = 1$ we find that $F = \sqrt{\tan \varphi_0}$. In the range of angles $\varphi_0 = 80\text{-}89.5^\circ$, $F \simeq 2\text{-}10$. The focusing factor is much less dependent on α_1, i.e., changes in ionosphere parameters and working frequency affect it less. The altitude distribution of the field in the channel is defined by several factors. The field near the channel axis reaches a maximum which corresponds to a slipping beam ($\varphi_0 = \pi/2$) and rather small values of $d\theta/d\varphi_0$.

On the upper boundary of the channel, the field reaches a zero value because for the limiting steep beam

$$d\theta(\varphi_0)/d\varphi_0 = \infty.$$

Spatial damping of radio waves in ionospheric channels can also be affected by horizontal heterogeneities of the ionosphere. Their effect on skip modes was examined in [86]. Sectors of the route with reduced electron concentration N in the direction of radio wave propagation lead to additional longitudinal focusing, while with an increase in N there is defocusing (by about 10-20 percent). Sectors of the route with increased N on both sides of the route plane, i.e., in a direction transverse to it, produce transverse focusing of the beam. On the other hand, when N is reduced on both sides of the route plane, there is defocusing. Transverse focusing is greater on meridional routes passing near the terminator.

Qualitative manifestations of focusing and defocusing effects similar to skip modes must be present in ionospheric radio ducts as well. But their quantitative contribution may differ.

In any mode, the factor of transverse focusing deviates from the relationship $1/\sin\theta$ under the influence of transverse gradients of ionization; and the field maximum is, to some degree, displaced from the geometric antipode of the emitter. In various sectors of the route, longitudinal and transverse gradients of ionization may have different signs. As a result, there may be cases of integral accumulation or partial compensation of focusing and defocusing effects which influence the absolute values of propagation damping of radio waves.

We should also bear in mind the possible effect of various physical factors of capture (extraction) of radio waves by ionospheric channels on the integral damping of radio waves in the route as a whole. The corresponding additional damping depends on frequency and, together with absorption and spatial damping in the channel itself, affects the frequency dependence of integral damping and the optimum frequencies of super-refraction of radio waves in the ionosphere which correspond to its minimum.

Bibliography

1. Quack, E. JAHRB. DRAHT. TEL., 1926, 28, p. 177.
2. Quack, E. Mogel, E., Proc. IRE, 1929, 17, p. 791.
3. Mogel, H. TELEFUNKEN ZEITUNG, 1934, 67, p. 23.
4. Taylor, A.H., Young, L.C., Proc. IRE, 1928, 16, p. 561.
5. Stormer, C., NATURE, 1928, 122, p. 681.
6. Vander Pol., NATURE, 1928, 122, p. 878.
7. Appleton, E.V., NATURE, 1928, 122, p. 879.
8. Stormer, C., NATURE, 1929, 123, p. 16.
9. Pedersen, P.O., PIRE, 1929, 17, N. 10, p. 1750.
10. Galle, J.B., ONDE ELEC. 1930, 9, p. 257.
11. Galle, J.B., Talon, G., Ferrie, M.G., C.R. ACAD. SCI. 1930, 190, p. 48.
12. Appleton, E.V., WORLD RADIO, 1934, 18, p. 633.
13. Schmidt, O., PHYS. Z. 1938, 39, p. 868.
14. Burkard, O., HOCHFREQ. TECHN. UND ELEKTRO AKUST. 1940, 56, H. 4, p. 41.
15. Hess, H.A., PROC. IRE, 1948, 36, p. 981.
16. Hess, H.A., PROC. IRE, 1949, 37, p. 986.
17. Hess, H.A., PROC. IRE, 1952, 40, p. 1065.
18. Jsted, G.A., Electromagnetic Wave Propagation, N.Y. 1960, p. 515.
19. Budden, K.G., Yates, G.G., JATP, 1952, 2, N. 5, p. 272.
20. Ortner, J., J. GEOPHYS. RES., 1959, 64, N. 12, p. 2464.
21. Fenwick, R.B., Round-the-World High-frequency propagation. Techn. rep. 71. Radio Lab. Stanford Univ., 1963.
22. Fenwick, R.B., Villard, O.G., J. GEOPHYS. RES., 1963, 68, p. 5659.
23. Bubenik, D.M., Fraser-Smith, A.S., Sweeney, L.E., Villard, O.G., J. GEOPHYS. RES., 1971, 76, N. 4, p. 1088.
24. Kosikov, K. M., ELEKTROSVYAZ', 1959, No. 7.
25. Golyan, S.F., Shlionskiy, A.G., GEOMAGNETIZM I AERONOMIYA, 1971, 11, No. 1, p. 98.
26. Golyan, S.F., in: Voprosy rasprostraneniya KV (Questions of propagation of short waves), Moscow, Izmiran, 1974, part 2, p. 31.
27. Ostrovskiy, I. Ya., Shlionskiy, A.G., in: Ibid., p. 52.
28. Ostrovskiy, I. Ya., Shlionskiy, A.G., in: Ionosfernoye rasprostraneniye KV (Ionospheric propagation of short waves), Moscow, Izmiran, 1975, p. 76.
29. Prasolov, A.S., Shlionskiy, A.G., in: Rasprostraneniye dekametrovykh radiovoln (Propagation of decameter radio waves), Moscow, Izmiran, 1978, p. 36.
30. Agaryshev, A.I., Unuchkov, V. Ye., GEOMAGNETIZM I AERONOMIYA, 1975, 15, No. 4, p. 754.
31. Verdiyanis, D., Bocharov, V.I., Lobachevskiy, L.A, Martines, R., Suarez, J., Tushentsova, I.A., GEOMAGNETIZM I AERONOMIYA, 1975, 15, No. 1, p. 163.
32. Ostrovskiy, I. Ya., in: Voprosy rasprostraneniya KV (op. cit.), p. 61.
33. Svistov, N.K., VESTNIK EKSP. I TEOR. ELEKTROTEKHNIKI, 1930, 1, p. 26.
34. Bubnov, V.A., Rumyantsev, G.A., IZV. VUZOV, RADIOFIZIKA, 1957,

18, No. 4, p. 527.
35. Bubnov, V.A., Rumyantsev, G.A., IZV. VUZOV, RADIOFIZIKA, 1975, 18, No. 9, p. 1383.
36. Bukin, G.V., Karavanov, V.S., Matyugin, S.N., Uryadov, V.P., GEOMAGNETIZM I AERONOMIYA, 1975, 15, No. 3, p. 467.
37. Bubnov, V.A., Golyan, S.F., Shlionskiy, A.G., in: Ionosfernoye rasprostraneniye KV (op. cit.), p. 90.
38. Ostrovskiy, I. Ya., Shlionskiy, A.G., in: Voprosy rasprostraneniya KV (op. cit.) p. 65.
39. Shlionskiy, A.G., Ionosfernoye rasprostraneniye KV (op. cit.), p. 107.
40. Shlionskiy, A.G., RADIO, 1957, No. 5, p. 40.
41. Gerson, N.G., Henger, J.G., Pipp, P.M., Webster, J.B., CANAD. J. PHYS., 1969, 47, p. 2143.
42. Hevolin, T.N., Shlionskiy, A.G., in: Issledovaniya rasprostraneniya KV (Studies of short wave propagation), Moscow, Nauka, 1973, p. 56.
43. Dellinger, J.H., Q.S.T., 1970, 54, p. 34.
44. Villard, O.G., Graf, C.R., Lomasney, J.M., Q.S.T., 1969, 53, p. 38.
45. Villard, O.G., Graf, C.R., Lomasney, J.M., Q.S.T., 1970, 54, p. 30.
46. Grawford, F.W., Sears, D.M., Bruce, R.L., J.G.R., 1970, 75, N. 34, p. 7326.
47. Manczarski, S., ACTA GEOPHYSICA, POLONICA, 1961, 9, N 1/2, p. 82.
48. Shlionskiy, A.G., in: Rasprostraneniye dekametrovykh radiovoln (op. (cit.), p. 118.
49. Gershman, B.N., Krupina, A. Ye., Yashin, Yu. Ya., IZV. VUZOV, RADIOFIZIKA, 1974, 17, No. 10, p. 1461.
50. Shlionskiy, A.G., yashin, Yu. Ya., GEOMAGNETIZM I AERONOMIYA, 1979, 19, No. 2, p. 214.
51. Kazantsev, A.N., Romanova, T.S., Klementenko, A.N., RADIOTEKHNIKA I ELEKTRONIKA, 1958, 3 No. 9, p. 1107.
52. Kuperov, L.P., in: Issledovaniya rasprostraneniya KV (op. cit.), p. 208.
53. Berbasov, F.I., Kerblay, T.S., Kovalevskaya, Ye. M., Lyakhova, L.N., in: Issledovaniya kosmicheskogo prostranstva (Studies of outer space), Moscow, Nauka, 1965, p. 220.
54. Mullen, J.R., Allen, R.S., RADIO SCI., 1966, 1 (New Ser.), N. 10, p. 1225.
55. Basu, S., Sarkar, S., Ibid, p. 1223.
56. Carrara, N., De Giorgio, M.T., Pellegrini, P.F., SPACE SCI. REV., 1970, 11, p. 555.
57. Barker, J.I., Grossi, M.D., RADIO SCI., 1966, 1 (New Ser.), No. 10, p. 1229.
58. Barker, J.I., Grossi, M.D., RADIO SCI, 1970, 5, N. 6, p. 983.
59. Beni, P., Pellegrini, P.F., S. MARCO PROJECT REP., 1969, N. 21, p.3
60. Beni, P. Checcacci, P.F., Pellegrini, P.F., S. MARCO PROJECT REP., 1971, N. 22, p. 3.
61. Mullen, J.R., Zuckerman, L.H., RADIO SCI., 1970, 5, N. 6, p. 997.
62. Benediktov, Ye. A., Bukin, G.V., Kushnerevskiy, Yu. V., Matyugin, S.N., Mozerov, N.P., Perekhvatov, Yu. K., Fligel', M.D., KOSMICHESKIYE

ISSLEDOVANIYA (Aerospace Research), 1972, 10, No. 2, p. 302.
63. Kuperov, L.P., in: Iskusstvennyye sputniki Zemli (Artificial Earth satellites), Moscow, Nauka, 1960, 5, p. 66.
64. Ivanov, Yu. G., Kuperov, L.P., Solodovnikov, G.K., Chalay, M. N., KOSMICHESKIYE ISSLEDOVANIYA, 1974, 12, No. 3, p. 387.
65. Buchatskaya, G.B., ELEKTROSVYAZ', 1972, 11p. 36.
66. Al'pert, Ya. L., Chudesenko, E.F., Shapiro, B.S., in: Predvaritel'nyye itogi issledovaniy s pomosh'yu pervykh sovetskikh ISZ i raket (Tentative results of research using the first Soviet artificial Earth Satellites and rockets), Izd-vo AN SSSR, 1958, p. 40.
67. Al'pert, Ya. L., UFN, 1960, 71, No. 3, p. 369.
68. Kryazhev, V.A., Cheremnyy, V.A., Shchegol'kova, N.G., Kosolapenko, V.I., 3-ya nauchno-tekhnicheskaya konferentsiya po kosmicheskoy radiosvyazi. Tezisy dokl. (Third scientific and technical conference on aerospace radio communications. Report abstracts), Moscow, Sov. radio, 1975, p. 8.
69. Panchenko, V.A., Shlionskiy, A.G., in: Difraktsionnyye effekty rasprostraneniya dekametrovykh radiovoln v ionosfere (Diffraction effects of propagation of decameter radio waves in the ionosphere), Moscow, Nauka, 1977, p. 76.
70. T. A. Anufriyeva, B.S. Shapiro. Geometricheskiye parametry sloya F2 ionosfery (Geometric parameters of the ionospheric F2 layer), Moscow, Nauka, 1976.
71. Shlionskiy, A.G., in: Rasprostraneniye dekametrovykh radiovoln (op. cit.) p. 107.
72. Rozin, V.L., Shlionskiy, A.G., in: Issledovaniya rasprostraneniya KV (op. cit). p. 56.
73. Wells, H.W., Proc. IRE, 1958, 46, N. 3, p. 610.
74. Garriott, O.K., Villard, O.G., Proc. IRE, 1958, 46, N. 12, p. 1950.
75. Jsted, G.A., Proc. IRE, 1958, 105 B, Supp., N. 8, p. 27.
76. Hess, H.A., NACHRICHTEN TECHN Z., 1958, 11, N. 7, p. 347.
77. Ikeda, H., Ichida, T., Shibata, H., Mambo, M., REPT. JONOS. RES. JAP., 1958, 12, N. 1, p. 37.
78. Krasnushkin, P. Ye., Metod normal'nykh voln v primenenii k volnovodam i ikh algebraicheskim proobrazom (Method of normal waves in application to waveguides and their algebraic prototype) (Doctoral dissertation), 1945, Moscow State University imeni Lomonosov.
79. Krasnushkin, P. Ye., Metod normal'nykh voln v primenenii k probleme dal'nikh radiosvyazey (Method of normal waves in application to the problem of long-range radio communications), Moscow, Izd-vo MGU, 1947.
80. Krasnushkin, P. Ye., ZHURN. TEKHN. FIZIKI, 1948, 18, No. 4, p. 431.
81. Bremmer, H., Terrestrial Radio Waves, N.Y., 1949.
82. Stein, S., J. GEOPHYS. RES., 1958, 63, N. 1, p. 217.
83. Mancharski, S., ACTA GEOPHYS. POL., 1961, 8, N 1/2, p. 91.
84. Woyk (Chvojkova), BULL. ASTRON. INST. CSL. 1951, 12, N. 1, p. 1.
85. Kerblay, T.S., GEOMAGNETIZM I AERONOMIYA, 1963, 3, N. 4, p. 772.
86. Kerblay, T.S., Kovalevskaya, Ye. M., O trayektoriyakh korotkikh radio-

voln v ionosfere (On trajectories of short radio waves in the ionosphere) Moscow, Nauka, 1974.
87. Kazantsev, A.N., Lukin, D.S., KOSMICHESKIYE ISSLEDOVANIYA, 1966, 4, No. 2, p. 238.
88. Shlionskiy, A.G., GEOMAGNETIZM I AERONOMIYA, 1965, 5, No 6, p. 1052.
89. Shlionskiy, A.G., Ibid, p. 1061.
90. Shlionskiy, A.G., Ibid, 8, No. 3, p. 595.
91. Shlionskiy, A.G., Ibid, 10, No 1, p. 147.
92. Shlionskiy, A.G., O maksimal'nykh chastotakh otrazheniya radiovoln pri nadzemnom rasprostranenii v ionosfere (On maximum frequencies of reflection of radio waves in suprsurface propagation in the ionosphere), Izmiran Preprint, No. 12, Moscow, 1971.
93. Krasnushkin, P. Ye., DAN SSSR (MAT. FIZIKA), 1971, 200, No 6, p. 1313.
94. Gurevich, A.V., GEOMAGNETIZM I AERONOMIYA, 1971, 11, No. 6, p. 961.
95. Gurevich, A.V., Tsedilina, Ye. Ye., GEOMAGNETIZM I AERONOMIYA, 1973, 13 No 1, p. 283.
96. Tushentsova, I.A., Fishchuk, D.I., Tsedilina, Ye. Ye., GEOMAGNETIZM I AERONOMIYA, 1975, 15, No 1, p. 78.
97. Chang, H.T., RADIO SCI., 1971, 6, N. 4, p. 475.
98. Borisov, N.D., GEOMAGNETIZM I AERONOMIYA, 1975, 15, No 6, p. 1086.
99. Shlionskiy, A.G., in: Voprosy rasprostraneniya KV (op. cit.), p. 77.
100. Shlionskiy, A.G., in: Ibid, p. 88.
101. Shlionskiy, A.G., in: Ibid, p. 95.
102. Shlionskiy, A.G., in: Metody issledovaniya zakonomernostey rasprostraneniya radiovoln (Methods of studying patterns of propagation of radiowaves), Moscow, Nauka, 1977, p. 45.
103. Shlionskiy, A.G., in: Rasprostraneniye radiovoln v ionosfere (Propagation of radiowaves in the ionosphere), Moscow, Izmiran, 1978, p. 37.
104. Shlionskiy, A.G., in: Ibid, p. 47.
105. Shlionskiy, A.G., in: Ionosfernyye issledovaniya (Ionospheric research), Moscow, Sovetskoye radio, 1978, No. 26, p.80.
106. Kadukhin, G.F., Soboleva, T.N., Shlionskiy, A.G., in: Trayektornyye kharakteristiki korotkikh radiovoln (Trajectory characterstics of short radio waves), Moscow, Izmiran, 1978, p. 111.
107. Fatkullin, M.N., Shlionskiy, A.G., in: Difraktsionnyye effekty rasprostraneniya dekametrovykh radiovoln v ionosere (op. cit.) p. 161.
108. Bochkarev, G.S., Cherkashin, Yu. N., in: Rasprostraneniye dekametrovykh voln, Moscow, Nauka, 1975, p. 21.
109. Kim, V. Y. in: Issledovaniya po geomagnetizmu, aeronomii i fizike Solntsa, Moscow, Nauka, 1972, 25, p. 131.
110. Kim, V. Yu., in: Voprosy rasprostraneniya KV (op. cit.) p. 124.
111. Tinin, M.V., IZV. VUZOV, RADIOFIZIKA, 1973, 16, No 10, p. 1613.
112. Sazhin, V.I., Tinin, M.V., IZV. VUZOV, RADIOFIZIKA, 1975, 18, No 9 p. 1389.
113. Gurevich, A.V., Kim, V. Yu., in: Rasprostraneniye dekametrovykh radiovoln (op. cit.), p. 5.

114. Sazhin, V.I. in: Issledovaniya po geomagnetizmu, aeronomii i fizike Solntsa, Moscow, Nauka, 1976, 38, p. 186.
115. Baranov, V.A., Popov, A.V., Cherkashin, Yu. N., in: Difraktsionnyye effekty rasprostraneniya dekametrovykh radiovoln v ionosfere (op. cit.) p 43.
116. Somsikov, V.M., Troitskiy, B.V., GEOMAGNETIZM I AERONOMIYA, 1975, 15, No 5, p. 856.
117. Vever, A.S., Danilova, T.P., Shlionskiy, A.G., GEOMAGNETIZM I AERONOMIYA, 1978, 18, No 3, p. 456.
118. Bubnov, V.A., Shlionskiy, A.G., in: Rasprostraneniye dekametrovykh radiovoln (op. cit). p. 44.

8617
CSO: 8144/217

END